

7-2-2011

Assessment of the biocompatibility, stability, and suitability of novel thermoresponsive films for the rapid generation of cellular constructs

Jamie Reed

Follow this and additional works at: https://digitalrepository.unm.edu/cbe_etds

Recommended Citation

Reed, Jamie. "Assessment of the biocompatibility, stability, and suitability of novel thermoresponsive films for the rapid generation of cellular constructs." (2011). https://digitalrepository.unm.edu/cbe_etds/13

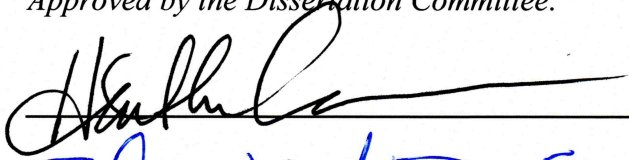
This Dissertation is brought to you for free and open access by the Engineering ETDs at UNM Digital Repository. It has been accepted for inclusion in Chemical and Biological Engineering ETDs by an authorized administrator of UNM Digital Repository. For more information, please contact disc@unm.edu.

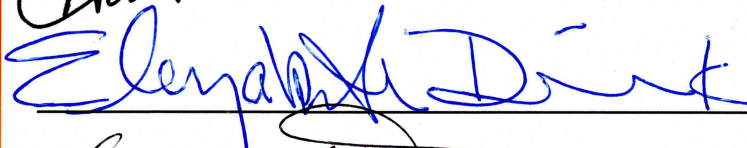
Jamie A. Reed
Candidate

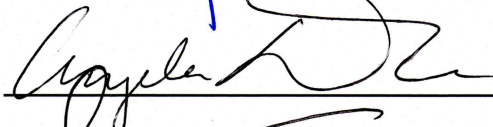
Chemical & Nuclear Engineering
Department

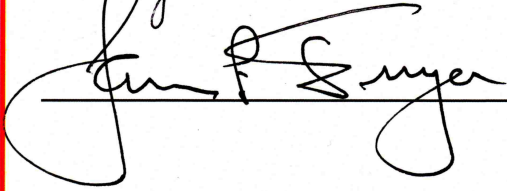
This dissertation is approved, and it is acceptable in quality
and form for publication:

Approved by the Dissertation Committee:

 _____, Chairperson

 _____

 _____

 _____

**ASSESSMENT OF THE BIOCOMPATIBILITY, STABILITY,
AND SUITABILITY OF NOVEL THERMORESPONSIVE
FILMS FOR THE RAPID GENERATION OF CELLULAR
CONSTRUCTS**

BY

JAMIE A. REED

B.S., Chemical Engineering, University of New Mexico, 2005

DISSERTATION

Submitted in Partial Fulfillment of the
Requirements for the Degree of

**Doctor of Philosophy
Engineering**

The University of New Mexico
Albuquerque, New Mexico

May, 2011

DEDICATION

For my loving and supportive parents, James and Judy Reed, who initiated my love of learning, believed in me when no else did, and encouraged me to do what makes me happy.

Yes.

This is your fault.

ACKNOWLEDGMENTS

I would like to express my deepest gratitude to my advisor and Dissertation committee chair, Prof. Heather Canavan, for her guidance and support. Besides being forensically trained and a lyrical genius, she is a dedicated mentor who has influenced me tremendously and been invaluable in my development as a graduate student. Her humor, optimism, kindness, and honesty are rare attributes that made working for her a unique, unforgettable, and enjoyable experience.

I wish to thank my Dissertation committee, which consists of Prof. Canavan, Prof. Elizabeth Hedberg-Dirk, Prof. Angela Wandinger-Ness, and Prof. Jim Freyer, for the guidance necessary to complete this work. In addition, I wish to thank Prof. Gabriel Lopez, who was a member of my committee of studies prior to his departure from UNM to Duke University, and who provided a great deal of expertise and support throughout my career at UNM.

I have been fortunate to receive excellent training and would like to specifically thank Elsa Romero, Linnea Ista, Rhutesh Shah, Thomas Angelini, and Prof. David Weitz for their patience and for sharing their experience.

Data presented in this work was obtained by a number of people. I would like to thank Lara Gamble, Jim Hull, and Megan Grobman from NESAC/BIO at the University of Washington for obtaining XPS and ToF-SIMS. From the University of Minnesota, I'd like to thank our collaborators Prof. Christy Haynes

and Sara Love, for obtaining amperometry data. At UNM, I would like to express my gratitude to Brett Andrzejewski for AFM, Kateryna Artyushkova for PCA, and Kirsten Cicotte for IR and SEM.

I've also had the extreme pleasure of working with some outstanding students in the Canavan Lab, including Blake Bluestein, Steven Candelaria, Marta Cooperstein, Jacqueline DeLora, Vanessa Eriacho, Adrienne Lucero, Laura Pawlikowski, Brissa Ponce, and Kristin Wilde. Your assistance and enthusiasm in the lab has always been appreciated. Specifically, I'd like to thank Kristin Wilde for her support and patience during the last year of my Dissertation work. Thank you for reminding me to breathe, and encouraging me to find my seal!

I would like to take this opportunity to thank Kirsten Cicotte, Adrienne Lucero, and Rosalba Rincon. You have been my classmates, encouraging me to study harder. You have been my lab mates, inspiring new directions for my research. Most importantly, you have been my best friends, making my life more interesting! And for that I am eternally grateful.

My desire for learning is the result of time spent with some phenomenal teachers. I'd like to thank Robert Benjamin, James Reed, and Judy Reed for teaching me to never give up and to follow my dreams. Your guidance has been invaluable.

Finally, and most importantly, I would like to thank my family, for their encouragement, love, and support. I'd like to thank my sister, Jade Reed, for reminding me to laugh and to fight for what I believe in. And I'd like to thank my

parents, James and Judy Reed, for whom this work is dedicated to, for being my most loyal fans. For reading papers, listening to presentations, and cheering for me every step of the way. I could not have succeeded without you.

Funding for this work was provided by: NSF PREM, NSF IGERT CORE, NSF GRFP, NIH NRSA, CBME, OGS, RAC, 3M, and SURP.

**ASSESSMENT OF THE BIOCOMPATIBILITY, STABILITY,
AND SUITABILITY OF NOVEL THERMORESPONSIVE
FILMS FOR THE RAPID GENERATION OF CELLULAR
CONSTRUCTS**

BY

JAMIE A. REED

ABSTRACT OF DISSERTATION

Submitted in Partial Fulfillment of the
Requirements for the Degree of

**Doctor of Philosophy
Engineering**

The University of New Mexico
Albuquerque, New Mexico

May, 2011

**ASSESSMENT OF THE BIOCOMPATIBILITY, STABILITY, AND
SUITABILITY OF NOVEL THERMORESPONSIVE FILMS FOR THE RAPID
GENERATION OF CELLULAR CONSTRUCTS**

By

Jamie A. Reed

**B.S., Chemical Engineering, University of New Mexico, 2005
Ph.D., Chemical Engineering, University of New Mexico, 2011**

ABSTRACT

Stimuli responsive polymers (SRP) are of great interest in the bioengineering community due to their use in applications such as drug delivery and tissue engineering. One example of an SRP is poly(*N*-isopropyl acrylamide) or pNIPAM. This SRP has the capability of changing its conformation with a slight temperature change: adherent mammalian cells spontaneously release as a confluent cell sheet, which can be harvested for cell sheet engineering purposes. Since its initial use in 1968, many researchers have used pNIPAM to obtain a cell sheet composed of their cell type of interest. The differing protocols used for these diverse cell types, such as the conditions used for cell detachment, and the varying methods used for derivatizing substrates with pNIPAM have all led to conflicting reports on the utility of pNIPAM for cell sheet engineering purposes, as well as the relative cytotoxicity of the polymer.

In this work, some of the key inconsistencies in the literature and previously

unaddressed challenges when utilizing pNIPAM films are overcome for the purpose of rapid generation of cellular constructs, specifically spheroids. Pertinent characteristics of low temperature detachment are investigated for their effect on the kinetics of cell detachment. In addition, a novel, inexpensive method for obtaining pNIPAM films for mammalian cell detachment, combining pNIPAM with a sol-gel, was optimized and compared to plasma polymerization deposition. Furthermore, proper storage conditions (e.g. temperature and relative humidity) for these films were investigated to increase stability of the films for using tissue culture conditions. To increase the speed of generation of cell sheets, electrospun mats and hydrogels with a high surface area-to-volume ratio were developed. The result is a platform appropriate for the rapid formation of cellular constructs, such as engineered tissues and spheroids for cancer cell research.

Table of Contents

CHAPTER 1. INTRODUCTION	1
1.1 IMPACT OF CANCER	1
1.2 TRADITIONAL METHODS FOR STUDYING CANCER THERAPEUTICS.....	1
1.2.1 <i>Characteristics of cancer</i>	1
1.2.2 <i>2D in vitro models to study cancer therapeutics</i>	3
1.2.3 <i>In vivo models to study cancer therapeutics</i>	7
1.2.4 <i>3D in vitro models to study cancer therapeutics</i>	11
1.3 SPHEROIDS FOR STUDYING CANCER THERAPEUTICS	12
1.3.1 <i>Relevance of spheroids</i>	12
1.3.2 <i>Current methods to obtain spheroids</i>	14
1.3.3 <i>Forming spheroids using pNIPAM</i>	16
1.4 SUMMARY	18
CHAPTER 2. EXPERIMENTAL METHODS	20
2.1 PNIPAM.....	20
2.1.1 <i>Characteristics and applications</i>	20
2.1.2 <i>Deposition methods</i>	21
2.2 PNIPAM PROCESSING FOR MAMMALIAN CELL APPLICATIONS	22
2.2.1 <i>Surface preparation</i>	22
2.2.2 <i>spNIPAM</i>	23
2.2.3 <i>ppNIPAM</i>	24
2.2.4 <i>espNIPAM</i>	26
2.2.5 <i>hpNIPAM</i>	29
2.3 SURFACE ANALYSIS	30
2.3.1 <i>XPS</i>	30
2.3.2 <i>ToF-SIMS</i>	33

2.3.3 PCA.....	36
2.3.4 Contact Angle.....	37
2.3.5 AFM.....	39
2.4 CELL CULTURE.....	42
2.4.1 General cell harvest.....	42
2.4.2 BAECs.....	43
2.4.3 MC-3T3E1.....	44
2.4.4 EMT6.....	44
2.5 CELL DETACHMENT.....	45
2.5.1 Cell detachment methods.....	45
2.5.2 Unassisted detachment.....	45
2.5.3 Assisted detachment.....	46
2.6 CELL ANALYSIS.....	48
2.6.1 Cytotoxicity.....	48
2.6.2 Biocompatibility.....	49
2.6.3 CellTracker TM	50
CHAPTER 3. THE EFFECTS OF CELL CULTURE PARAMETERS ON CELL RELEASE	
KINETICS FROM THERMORESPONSIVE SURFACES.....	53
3.1 INTRODUCTION.....	53
3.2 EXPERIMENTAL METHODS.....	55
3.2.1 Cell detachment parameters.....	56
3.3 RESULTS.....	56
3.3.1 Surface analysis.....	56
3.3.2 Kinetics of BAEC release.....	60
3.4 CONCLUSIONS.....	65
CHAPTER 4: A LOW-COST, RAPID DEPOSITION METHOD FOR “SMART” FILMS:	
APPLICATIONS IN MAMMALIAN CELL RELEASE.....	67

4.1 INTRODUCTION	67
4.2 EXPERIMENTAL METHODS	68
4.2.1 <i>Sol-gel and pNIPAM preparation</i>	69
4.2.2 <i>Sol and pNIPAM deposition</i>	69
4.3 RESULTS AND DISCUSSION.....	69
4.3.1 <i>Characterization of surfaces</i>	69
4.3.2 <i>Cellular response</i>	72
4.4 CONCLUSIONS	76
CHAPTER 5: EFFECT OF POLYMER DEPOSITION METHOD ON THERMORESPONSIVE POLYMER FILMS AND RESULTING CELLULAR BEHAVIOR.....	77
5.1 INTRODUCTION	77
5.2 EXPERIMENTAL METHODS	78
5.2.1 <i>MAMC cell culture</i>	78
5.2.2 <i>Carbon-fiber Microelectrode Amperometry (CFMA)</i>	79
5.3 RESULTS AND DISCUSSION.....	83
5.3.1 <i>Surface characterization</i>	84
5.3.2 <i>Thermoresponse</i>	87
5.3.3 <i>Mammalian Cell Culture</i>	90
5.3.4 <i>CFMA Exocytosis Response</i>	91
5.4 CONCLUSIONS	94
CHAPTER 6: EFFECT OF SUBSTRATE STORAGE CONDITIONS ON THE STABILITY OF “SMART” FILMS USED FOR MAMMALIAN CELL APPLICATIONS	96
6.1 INTRODUCTION	96
6.2 EXPERIMENTAL METHODS	98
6.2.1 <i>Storage of surfaces</i>	98
6.2.2 <i>Delamination study</i>	99
6.3 RESULTS AND DISCUSSIONS	99

6.3.1 Initial conditions	99
6.3.2 Surface stability	104
6.3.3 Cell adhesion.....	106
6.3.4 Cytotoxicity.....	109
6.3.5 Biocompatibility.....	110
6.4 CONCLUSIONS	113
 CHAPTER 7. ELECTROSPINNING PNIPAM FOR MAMMALIAN CELL CULTURE	
APPLICATIONS.....	115
7.1 INTRODUCTION	115
7.2 EXPERIMENTAL METHODS	117
7.2.1 FTIR.....	117
7.2.2 SEM.....	118
7.2.2 Thermoresponse.....	118
7.2.3 Transfer of harvested cells	118
7.3 RESULTS AND DISCUSSIONS	119
7.3.1 Preparation of mats	119
7.3.2 Elemental characterization of mats	122
7.3.3 Thermoresponse of mats.....	125
7.3.4 Cell response.....	126
7.4 CONCLUSIONS	131
 CHAPTER 8. THE RAPID FORMATION OF SPHEROIDS USING A “SMART” POLYMER	
8.1 INTRODUCTION	133
8.2 EXPERIMENTAL METHODS	134
8.2.1 FTIR.....	135
8.2.2 Thermoresponse.....	136
8.2.3 PDMS wells.....	136
8.2.4 Determination of spheroid size	137

8.3 RESULTS AND DISCUSSIONS	137
8.3.1 <i>Characterization of gels</i>	137
8.3.2 <i>Cell response</i>	140
8.3.3 <i>Spheroid formation</i>	143
8.4 CONCLUSIONS	145
CHAPTER 9. CONCLUSIONS AND FUTURE DIRECTIONS	146
9.1 CONCLUSIONS	146
9.1.1 <i>Optimizing parameters for rapid mammalian cell detachment</i>	146
9.1.2 <i>Development of novel deposition methods for reliable, controllable cell detachment</i>	147
9.1.3 <i>Processing pNIPAM for increased mass transfer and accelerated cell detachment</i>	148
9.2 FUTURE DIRECTIONS	149
9.2.1 <i>Rapid formation of uniform and co-cultured spheroids</i>	149
9.2.2 <i>Spheroid production and testing within microfluidic devices</i>	150
9.2.3 <i>Thermoresponsive microgels for harvesting individual cells</i>	151
9.2.4 <i>Hydrogels incorporated with fluorescent nanoparticles</i>	151
APPENDIX I	153
APPENDIX II	154
APPENDIX III	155
APPENDIX IV	156
REFERENCES	157

Chapter 1. Introduction

1.1 Impact of cancer

Cancer is a disease that affects populations around the globe (see Figure 1.1).¹ Currently, cancer claims over 570,000 lives every year in the United States alone, which accounts for approximately 1 in 4 deaths.² In 2010, the National Institute of Health (NIH) estimates that there were approximately 1.5 million new cancer cases. In addition, cancer led to an estimated \$263.8 billion in expenses for direct (treatment, cost of care, etc) and indirect (loss of economic output) costs in the United States. Due to these statistics, there is an obvious concern and need to understand, control, and treat cancer.

1.2 Traditional methods for studying cancer therapeutics

1.2.1 Characteristics of cancer

The study of cancer is a complex task. This is primarily due to the fact that “cancer” is not a single disease, but rather a group of diseases characterized by the uncontrollable growth and migration of abnormal cells.² Currently, several treatment studies are focused on the underlying mechanism of the growth and migration of these abnormal cells, with the aim of formulating treatments that target the source of the problem.³⁻⁵ One such study that is underway focuses on epidermal growth factor receptor, or EGFR, which is upregulated (i.e., over expressed) in cancers such as lung, pancreatic, and breast cancers.^{4, 6, 7}



Figure 1.1: Global occurrences of new cancer cases in 2007 by the American Cancer Society.¹

EGFRs are a family of transmembrane tyrosine kinases, including EGFR, HER2, HER3 and HER4. They are normally present as a cell-surface receptor to aid in the process of cell proliferation. In cancer cells, these receptors are over expressed, in particular EGFR, leading to uncontrollable proliferation, increased survival due to anti-apoptotic mechanisms, invasion, angiogenesis potential, and development of distant metastasis.⁶ Thus the ability to control the expression of EGFR has offered a method for slowing, or stopping, the proliferation and migration of these cells.

Two classes of molecules, monoclonal antibodies and tyrosine kinase

inhibitors, have been developed that target EGFR, as shown in Figure 1.2. One class consists of monoclonal antibodies that attach to the extracellular domain of the receptor, inhibiting binding for the natural ligands.^{5, 8} The other class targets the intracellular domain, acting as inhibitors of the tyrosine kinase region, competing with and preventing ATP from binding with the region.^{5, 8}

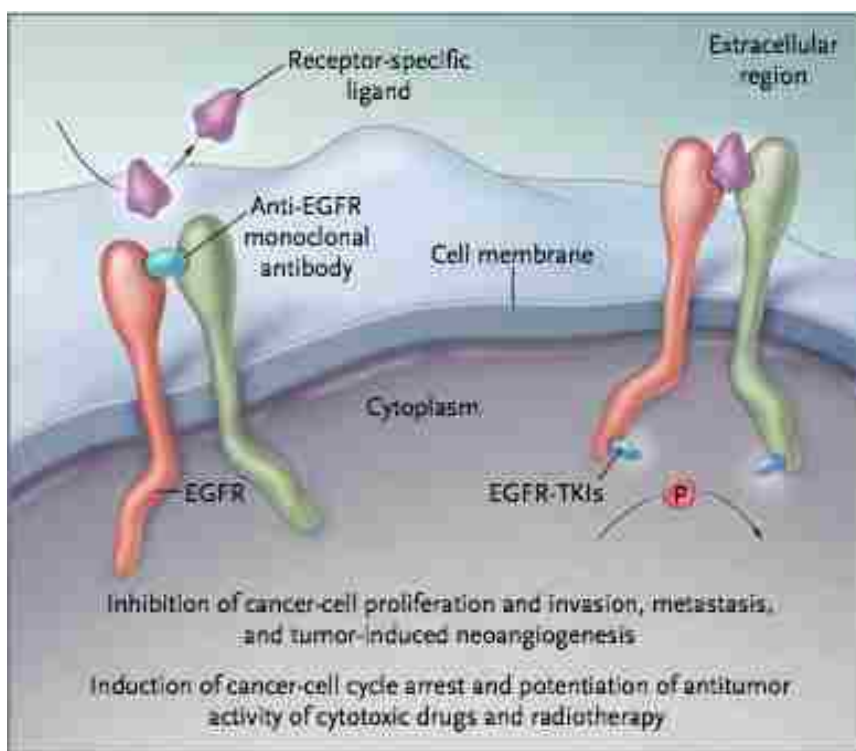


Figure 1.2: EGFR is a transmembrane protein, extending through the cell membrane. EGFR inhibitors target the pathway in one of two ways; either by blocking the extracellular receptor from the natural ligands (left), or blocking the intracellular tyrosine kinase region (right).⁵

1.2.2 2D *in vitro* models to study cancer therapeutics

Once a potential treatment for cancer is formulated, it will be tested for its effectiveness and safety. Most drug discovery studies rely on 2D systems for

initial testing, followed by animal testing. This two-tiered process has been implemented primarily because the 2D studies could not accurately predict *in vivo* responses.⁹⁻¹⁸ Although these studies have not been very successful in predicting *in vivo* responses, they have been incredibly useful in molecular targeting experiments, starting in the 1990's.^{19, 20} Since that time, an enormous amount of information about expression levels of proteins, mutational status of genes, and RNA levels has been discovered using these experiments.

Table 1.1: Percentage of significant genes upregulated when comparing cell line-to-tumor, cell line-to-normal, and tumor-to-normal from breast and ovary tissues. Table adapted from Ertel et al. demonstrates that cell lines have mutated and are no longer representative of the normal or cancerous tissues due to upregulation of specific genes.

Comparison	% Genes Upregulated	
	Breast	Ovary
Cell line-to-tumor	66	41
Cell line-to-normal	61	62
Tumor-to-normal	10	14

However, there are many reasons that 2D cultures have failed to predict clinically relevant results. Many of the cells used in these studies have been immortalized and passaged several times.²¹ With each passage, or sub-culturing, of the cells, tumor cells that rapidly proliferate and survive on tissue culture polystyrene (TCPS) are selected. The resulting selected cells will no longer be representative of the original tumor (see Table 1.1). In fact, cell lines developed from breast tissue have a 61% upregulation of genes when compared to normal

cells and 66% upregulation when compared to tumor cells. The upregulated genes are responsible for cell processes involved in proliferation. Therefore, cell lines will be extremely sensitive to treatments that target rapidly dividing cells, which may lead to an overestimate of the drug's efficacy.^{22, 23}

For 2D studies, cells that are of interest to tumor research are used. These cells typically are adherent, and will attach to a substrate in a monolayer (see Figure 1.3). Traditional methods to harvest cells for analysis from a substrate include enzymatic digestion and physical scraping.²⁴ A morphological change in the cells is seen when utilizing either of these harvesting techniques, possibly due to a disruption in the cellular membrane or the glycocalyx.²⁴⁻²⁷ In addition, both of these methods damage the extracellular matrix (ECM), shown in Figure 1.3.

The ECM is an intermediate layer between cells and the surface. The ECM relays signals to the cells, including whether to grow and proliferate or to begin programmed cell death (apoptosis). Furthermore, many transmembrane proteins (including EGFR) extend into the ECM, so when the ECM is damaged, the information that could be gained from studying the ECM is also lost. Traditional methods for cellular analysis such as a flow cytometry require that individual cells be suspended in solution. Therefore, usually cells are released using trypsin prior to analysis. It is likely that harsh treatment of the cells leads to a great deal of information, that would be found by studying the ECM, is not translated in the study.

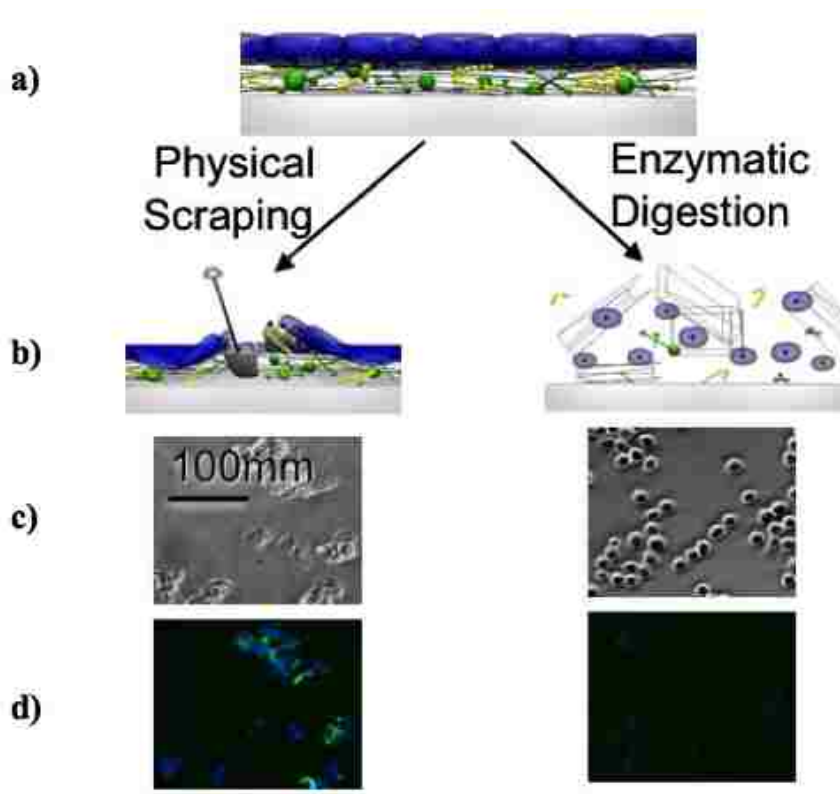


Figure 1.3: Schematic illustrating traditional cell harvest methods. Initially, the cells are attached to a substrate via the ECM (a) and are harvested using one of the two traditional harvesting methods, including physical scraping (b, left) and enzymatic digestion (b, right). These techniques result in cell aggregates or the disassociation of cell-cell interactions, as seen by the bright field images post-harvest (c). In addition, these methods also damage the underlying extracellular matrix (d), as shown in the fluorescent images of extracellular proteins. Image adapted from Canavan et al.²⁴

Beyond the issues related to cell culture techniques, when the cells are exposed to potential therapeutics, there are major differences in the exposure time and concentration.²⁸ Furthermore, there are differences in the rate of change of the concentration, metabolism, tissue penetration, and excretion, since there is no 3D microenvironment available in a monolayer of cells.^{9-18, 21, 28-35} In a

3D microenvironment, cells obtain information from soluble signals and surrounding cells in all directions through a concentration gradient that is dependent on the structure of the extracellular space and the 3D architecture, as shown in Figure 1.4.^{34, 36} These signals dictate whether the cells proliferate or enter apoptosis, thus drug screening that focus on cell proliferation and death will not accurately predict the drug activity *in vivo*.³⁷⁻³⁹ To mimic these 3D microenvironments, animal models are used as the second tier in this process.

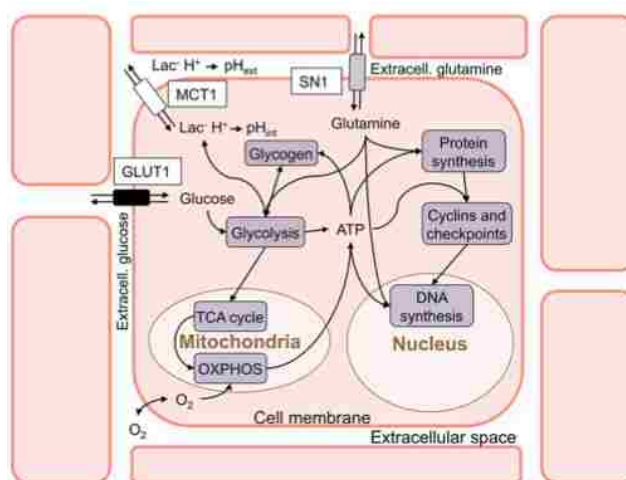


Figure 1.4: Schematic of a cell (pink) in a 3D microenvironment, to illustrate the complexity of the environment. Cells have cell-cell interactions, cell-matrix interactions, and concentration gradients that dictate cell signaling. Image adapted from Milotti et al.³⁴

1.2.3 *In vivo* models to study cancer therapeutics

Animal models remain the most relevant tool for understanding how a tumor will respond. However, there are numerous drawbacks to *in vivo* tests, including various ethical dilemmas. Jeremy Bentham applied ethical utilitarianism to animal rights, arguing that the advancements made using animal testing are irrelevant if

these sentient beings were suffering.⁴⁰ To address these types of concerns, the US has passed several laws (including the Animal Welfare Act of 1966) to enforce humane treatment of animals used for testing.⁴¹

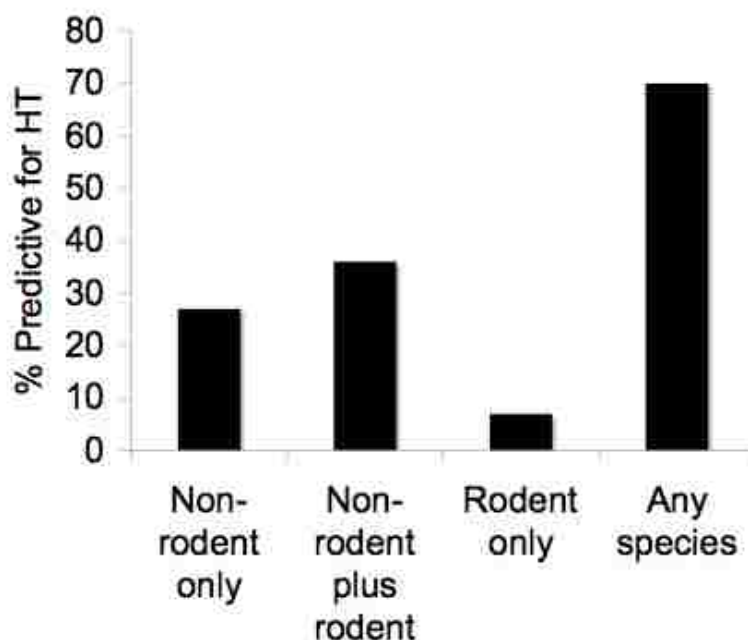


Figure 1.5: Image adapted from a study by Olson et al. on the ability of animal models to predict human toxicity (HT). Models included dogs, primates, rats, mice, guinea pigs, and rabbits. Combining all of the species resulted in ~70% predicative value for corresponding HT.⁴²

Furthermore, animal testing is expensive. It is estimated that in the US, animal testing is costing taxpayers ~\$9 billion dollars per year.⁴³ Part of this cost includes animal upkeep, which can last for several months, while waiting for a tumor to develop in the model. From an industrial standpoint, the main price is time lost when these models do not accurately predict the performance of drugs in humans.

Table 1.2: Comparison of patient and xenograft response (R) or lack of response (NR) to vinorelbine+cisplatin (regimen A). This table (adapted from Dong, et al.) shows that although the xenograft model was 75% predictive of tumor resistance, they were only 67% predictive of patient sensitivity to regimen A.⁴⁴

Case	Patients		Xenografts
	Clinical Outcome	Disease-free time (mo)	Response to regimen A
1	Recurrence	2	NR
2	Recurrence	16	NR
3	Recurrence	24	NR
4	Recurrence	11	NR
5	Metastasis	5	NR
6	Metastasis	11	NR
7	Recurrence	11	R
8	No recurrence	>24	NR
9	No recurrence	>24	NR
10	No recurrence	>40	R
11	No recurrence	>38	R

A study investigating the effectiveness of predicting human toxicity using a range of models demonstrated that only ~70% of the models were effective (see Figure 1.5).⁴² When studying the application of animal models for predicting human therapy, animal models tend to be more accurate at determining resistance to a drug than sensitivity. In one study, tumor resistance prediction in mice versus humans was found to be 75% accurate, but mouse models could only predict 50% sensitivity to the drug (see Table 1.2).⁴⁴ The variance between drug interactions in animals and humans is largely due to the differences in drug metabolism, pharmacokinetics, and pharmacodynamics.⁴⁵⁻⁴⁷ The limited predictive power of many animal models leads to a significant number of Phase II clinical trials that fail.^{37, 39, 46, 48} In fact, 89% of the studies that pass preclinical testing fail to gain FDA approval (see Figure 1.6), typically after ~\$400 million

dollars of investment.⁴⁹⁻⁵¹

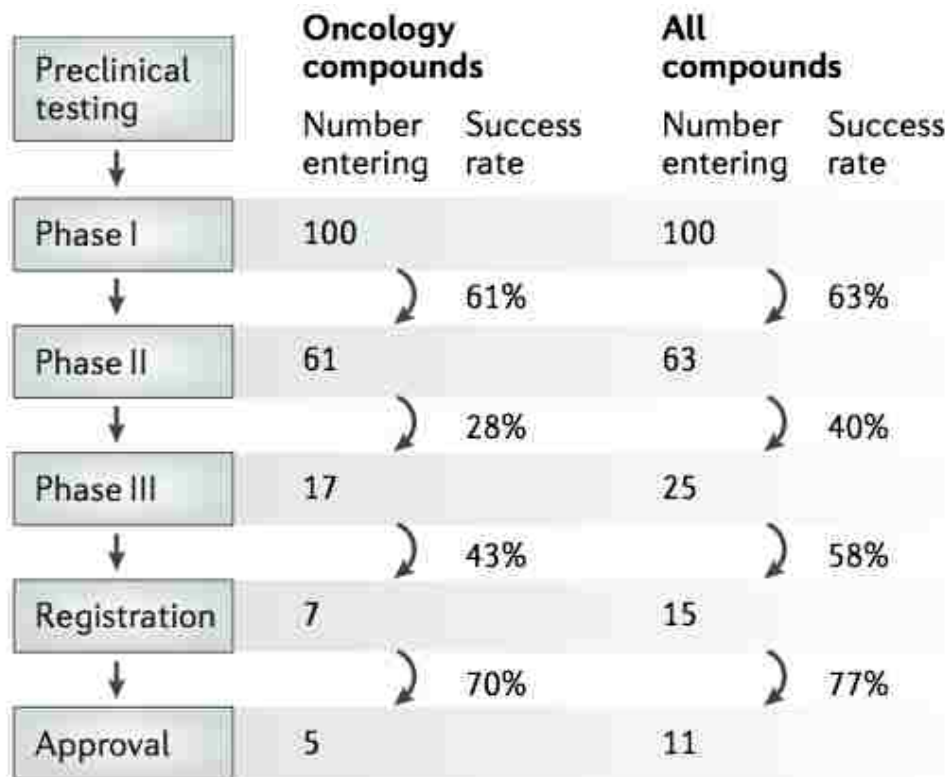


Figure 1.6: Attrition rate of cancer therapeutic compounds from 1991-2000 in the US and in Europe.⁵²

In an attempt to make these models more predictive, cancer studies have turned to genetically engineered mouse and xenograft models (see Figure 1.7).⁵¹ Xenograft models are obtained by surgically inserting cells or tumor fragments into mice.⁵³ Although a study comparing 2D cultures, animal testing, and patient data demonstrated that patient derived xenografts accurately predicted resistance in patients by 97% and sensitivity by 90%, these models are not easy to obtain.⁵⁴ Only 40-60% of tumors inserted into mice actually grow, and the microenvironment in immunodeficient mice lack the natural bacterial flora and immune system, which have been shown to affect carcinogenesis.^{55, 56 57-60} The

genetically engineered mouse models are more predictive of the tumor microenvironment found in humans, as the mice are not immunodeficient.^{46, 51, 54} However, there have been limited studies on the potential predictive power of these methods.⁶¹ One reason is tumor development can take several months before the model is available for testing. In addition, these models have spontaneous, multifocal tumor development, which can lead to inconsistent response to potential therapeutics.⁴⁶

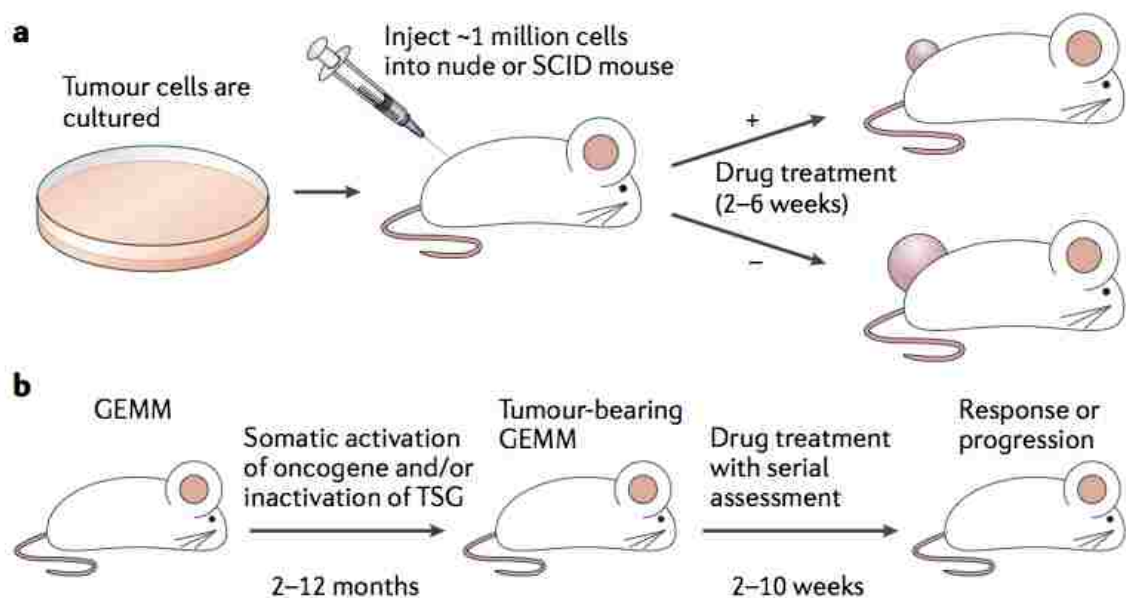


Figure 1.7: Mechanisms for obtaining mice as animal models for cancer studies. Xenografts, shown in route (a), are obtained when cells or tumors are transplanted into a mouse. Route (b) illustrates the manipulation of genes to initiate tumor development. Image adapted from Sharpless et al.⁵²

1.2.4 3D *in vitro* models to study cancer therapeutics

One potential approach to avoid the limitations associated with animal testing is to use an alternate method for drug testing, to eliminate many candidates

before animal testing is required. The best way to do this is to establish an *in vitro* system that mimics the 3D microenvironment *in vivo*, thereby increasing the efficacy of pre-screening, thus decreasing the number of animal studies required.

Examples of 3D systems that have been used for this very purpose included multiple layers of cells cultured on top of porous membranes, matrix embedded cells, hollow fiber bioreactors, and microfluidic devices.^{9, 62-76} These have been designed to study cell invasion, drug transport, migration, and therapy resistance. All of these models mimic aspects of the tumor environment, and have been used for understanding these different aspects.

1.3 Spheroids for studying cancer therapeutics

1.3.1 Relevance of spheroids

Spheroids, or small sphere-shaped cell aggregates, have been widely accepted as a reliable, physiologically relevant model for 3D tumor studies.⁷⁷ Spheroids display a number of growth characteristics and pathophysiological features of avascular tumor nodules, as shown in Figure 1.8. These features include an oxygen, nutrient (glucose), and waste (lactate) gradient. In addition, similar to an avascular tumor, spheroids over 500 μm have a necrotic core with a gradient in the cell cycle.

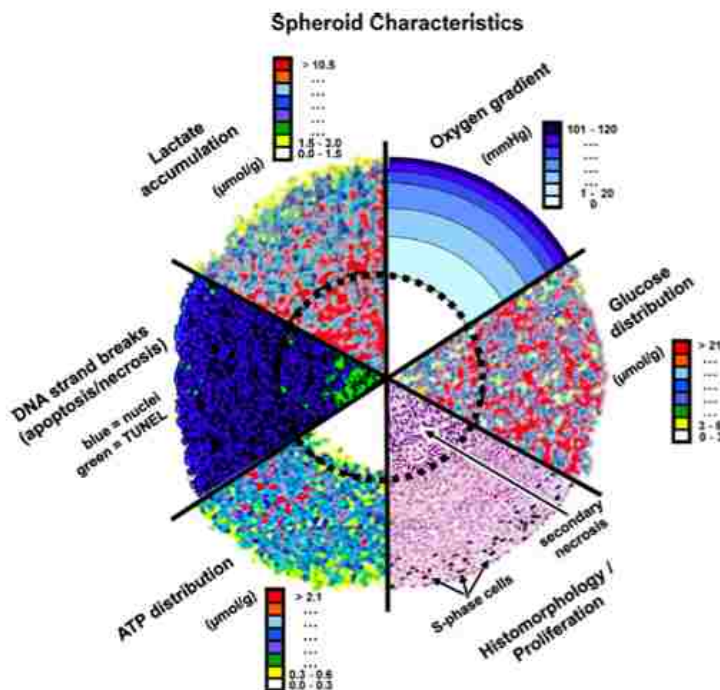


Figure 1.8: Schematic illustrating gradients in spheroids that are pathophysiologically relevant, and similar to *in vivo*, avascular tumors.⁷⁸

Spheroids in the literature have been referred to as tumoroids, spheres, aggregates, and organoids.^{9, 78-85} A spheroid is well-packed with a spherical geometry, which can be easily transferred, and maintains cell-cell and cell-matrix interactions.⁷⁸ The problem is that not all of the aforementioned terms necessarily refer to a spheroid in that they do not maintain all of the characteristics of a spheroid. In some cases, the spheres or aggregates are loosely packed which causes the loss of cell-cell and cell-matrix interactions.

Spheroids were first introduced into cancer research in the 1970's. Sutherland, et al., used spheroids to study radiobiology.⁸⁶⁻⁸⁹ The original model developed by Sutherland is still used today, but in the 1990's was expanded to include additional therapeutic research areas.⁹⁰ These models have evolved to better

predict human response by including such benefits as the use of human cells.⁹ Today these systems are used for negative selection in drug screening, since many drugs are known to be less efficient in a 3D environment. Spheroids are useful for determining whether a treatment will be efficient in penetrating a tumor, and if it is not, then there is no reason to do further testing.^{78, 91-95} Recently, spheroids have gained recognition as positive selection tools as well, as they do demonstrate pathophysiological traits similar to *in vivo* tumors.

Although spheroids cannot replace animal testing, they are useful models for pre-animal testing once an acceptable drug is found. This system accurately reflects tumor tissue conditions, and is suitable for entry into routine drug testing. In addition, these spheroids would be beneficial for studies that are currently underway to adapt flow cytometers to analyze 3D tissues.⁹⁶

1.3.2 Current methods to obtain spheroids

Current methods to obtain spheroids rely on forcing cells that are normally adherent into suspension, causing the cells to aggregate. This is typically achieved either by culturing cells in a stirred suspension or on a substrate that does not promote cell adhesion (e.g., soft agar).⁹ For instance, the rotating wall vessel, or NASA bioreactor shown in Figure 1.9, mimics a microgravity environment. Although useful, the complex set-up and expense of the NASA bioreactor seem to outweigh the only demonstrated advantage: reduced sheer stress.⁹⁷ Thus, the spinner flask method has remained as one of the most appealing methods of spheroid formation, where it is possible to maintain nutrient

delivery (see Figure 1.9). Recently, developments in spheroid formation include using microarrays for spheroid initiation and microfluidic devices.⁹⁸⁻¹⁰⁶ Using a microarray of collagen islands for initial cell attachment in a sea of PDMS, up to 5,000 uniform spheroids can be formed in a 35 mm well plate.¹⁰⁷⁻¹⁰⁹ Microfluidic devices can be utilized to form spheroids as well as for testing potential therapeutics with the formed spheroids.^{99, 106, 110}

Although all of the methods mentioned above have been reliable in forming spheroids they all result in spheroids with a wide size distribution (>12% variation). Current methods for obtaining homogeneous spheroids include sieves, sedimentation, and flow cytometry sorting.⁹ Sieves and sedimentation, while relatively rapid and inexpensive, do not provide a narrow size distribution. Using flow cytometry does provide a uniform size distribution, but requires expensive, specialized equipment. In addition, it is a relatively slow process, as the introduction of spheroids suspended in solution must be halted approximately every 5 minutes to ensure the spheroids remain suspended for flow through the flow cytometer. One method to control size is directing cell growth on a 2D substrate, limiting the number of cells that will be incorporated in the resulting 3D spheroid. The limiting factor in turning a confluent sheet into a cell aggregate is removing the cells from the culture substrate. As previously discussed, traditional methods for harvest damage the ECM. In addition, both of these methods damage cell-cell junctions, thus they are not useful for recovering aggregates.²⁴

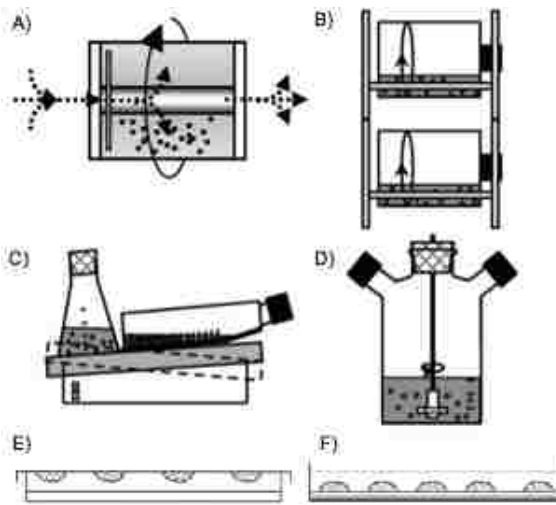


Figure 1.9: Current methods for fabricating spheroids, including (a) NASA bioreactor, (b) rotating flasks, (c) agitation of flasks with an orbital shaker, (d) spinner flask, (e) hanging drop, and (f) agar plate. Image adapted from Friedrich et al.⁹

1.3.3 Forming spheroids using pNIPAM

One method that has been employed for controlled cell growth and release is cell culture on poly(*N*-isopropyl acrylamide) (pNIPAM) treated substrates. PNIPAM is a thermoresponsive polymer that becomes relatively more hydrophilic at room temperature than it is at 37 °C (i.e., biologically relevant temperature).²⁶ Cells will adhere and proliferate on this polymer at 37 °C. When the temperature is shifted below 32 °C (the polymer's lower critical solution temperature), the cells spontaneously detach as an intact cell sheet (see Figure 1.10C).¹¹¹ Although a significant number of publications utilize pNIPAM substrates for mammalian cell culture applications, there are many inconsistencies in the literature. (See Appendix I for a representative list of pNIPAM deposition methods used for cell culture and inconsistencies between the studies.)

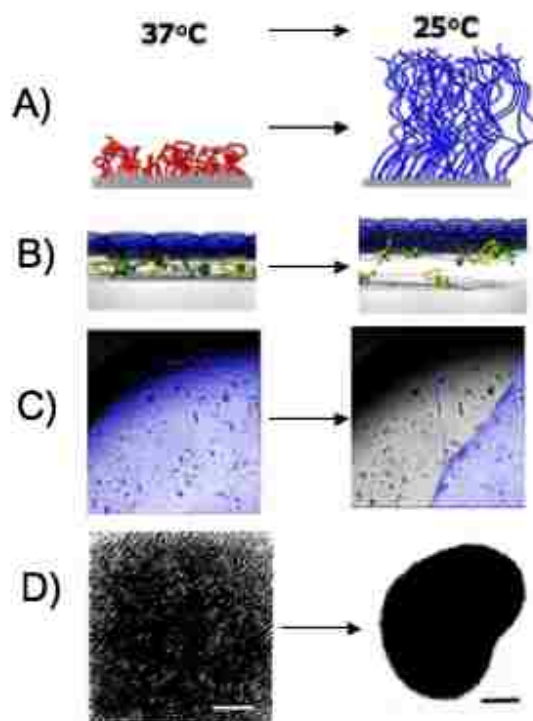


Figure 1.10: PNIPAM is relatively hydrophobic at 37 °C, or body temperature, and mammalian cells will attach to these substrates in a monolayer. At 25 °C the polymer is hydrophilic, and the previously attached cells will detach in a confluent sheet. This is shown in panel (c) with cells that have been false colored blue (adapted from Canavan et al.)²⁷ PNIPAM has been used previously to obtain spheroids, but the resulting spheroids were not uniform and asymmetric (image adapted from Takezawa et al.)¹¹²

The ability to harvest intact cell sheets from pNIPAM has led to a great deal of research for tissue engineering applications (e.g., corneal reconstruction implants¹¹³ and cardiac tissue grafts¹¹⁴). There have been fewer studies published on the use of pNIPAM to create spheroids (see Figure 1.10D).^{112,115} Very little work has been done to control the size of the spheroids below 400 μm using pNIPAM substrates.^{116,117} In addition, much of this research has resulted in asymmetric aggregates, which took as long as 3 weeks to form.¹¹² (See

Appendix II for a list of spheroids formed using pNIPAM substrates)

1.4 Summary

In this work, the use of pNIPAM to rapidly generate spheroids within a narrow size distribution will be investigated (described in Chapter 8). Prior to its use to generate spheroids, pertinent characteristics of low temperature detachment (e.g. temperature of experiment and type of media used for detachment) are investigated for their effect on the kinetics of cell detachment (described in Chapter 3). In addition, a novel, inexpensive method for obtaining pNIPAM films for mammalian cell detachment, combining pNIPAM with a sol-gel, was optimized (described in Chapter 4). This method of deposition was compared to plasma polymerization deposition for use with mammalian cells (described in Chapter 5). Furthermore, proper storage conditions (e.g. temperature and relative humidity) for these films were investigated to increase stability of the films use in tissue culture conditions (described in Chapter 6). As this work progressed, it was hypothesized that mass transfer was the primary limitation in cell detachment when using pNIPAM films, thus electrospun mats with a high surface area to volume ratio were utilized to improve cell detachment (described in Chapter 7). The work presented herein demonstrates and overcomes challenges that were previously unaddressed when utilizing pNIPAM films. The result is a platform appropriate for the rapid formation of spheroids. Table 1.3 presents each of these contributions as well as a reference to the journal in which the work first appeared.

Table 1.3: Summary of significant results discussed in this dissertation, the corresponding chapter, and the original publication location. *Submitted; ** In preparation for submission

Chapter	Title	Significant Results	Published In
3	The Effects of Cell Culture Parameters on Cell Release Kinetics from Thermoresponsive Surfaces	The most reliable, rapid cell detachment occurs in 4 °C serum free media	Journal of Applied Biomaterials and Biomechanics ¹¹¹
4	A Low-Cost, Rapid Deposition Method for “Smart” Films: Applications in Mammalian Cell Release	A novel, inexpensive method for mammalian cell detachment, combining pNIPAM with a sol-gel, was optimized, showing 0.35wt% pNIPAM was ideal	ACS Applied Materials & Interfaces ¹¹⁸
5	Effect of Polymer Deposition Method on Thermoresponsive Polymer Films and Resulting Cellular Behavior	Deposition of pNIPAM using plasma polymerization yields films that have the best thermoresponsive and mechanical properties, as well as minimal impact on cellular viability and function	<i>Langmuir</i> ¹¹⁹
6	Effect of Substrate Storage Conditions on the Stability of “Smart” Films Used for Mammalian Cell Applications	Deposition of pNIPAM with a sol-gel and plasma polymerization result in biocompatible substrates, that are stable when stored at 25 °C, low relative humidity conditions	Biomacromolecules ¹²⁰ *
7	Electrospinning Biodegradable “Smart” Substrates for Harvest of Intact Mammalian Cell Sheets	Electrospun mats from high molecular weight pNIPAM support mammalian cell attachment, growth, and rapid detachment due to the 3D structure	Journal of Applied Polymer Science**
8	Thermoresponsive Films for Rapid Formation of Tumor Models	PNIPAM substrates with 3D masks produce uniform, size tunable spheroids	Journal of Biomedical Research**

Chapter 2. Experimental Methods

2.1 PNIPAM

2.1.1 Characteristics and applications

Stimuli-responsive polymers (SRP) are employed by the biomedical community in tissue engineering,¹ drug delivery,² and biosensing.³ Specifically, poly(*N*-isopropyl acrylamide) (pNIPAM) is a SRP commonly used for biomedical applications and was the topic of the recent review by Cooperstein, et al.⁴ PNIPAM has the unique characteristic of being thermoresponsive near physiologically relevant temperatures (see Figure 2.1).

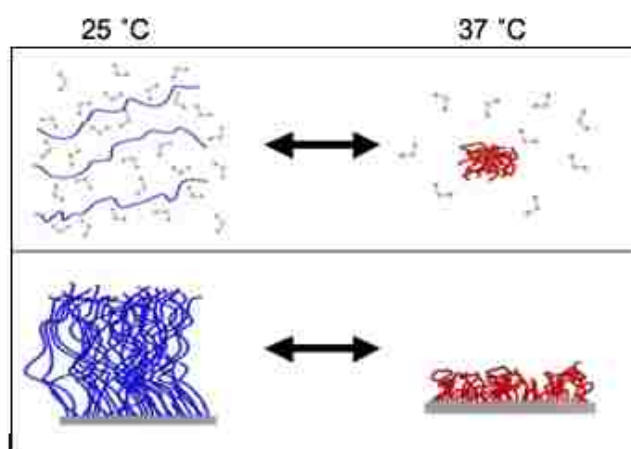


Figure 2.1: Below the lower critical solution temperature (LCST), around room temperature, pNIPAM is relatively hydrophilic (blue on left). Above the LCST, at physiologically relevant temperatures, the polymer is relatively hydrophobic, and will collapse on a surface when it is tethered to it (red on right, tethered on bottom).

At 37 °C, the polymer is relatively hydrophobic, and biological cells will readily

grow on a substrate coated with pNIPAM. By decreasing the temperature beyond the lower critical solution temperature (LCST) to room temperature, the polymer becomes relatively hydrophilic. The polymer swells below the LCST, and adhered cells detach spontaneously in a confluent cell sheet.⁵ This polymer response has previously been used for a wide range of bioengineering applications, including tissue engineering^{6,7} and protein separation.^{8,9}

2.1.2 Deposition methods

Depending on the application, the method used to deposit the pNIPAM film may be altered to achieve the desired properties, as reviewed by Da Silva.¹⁰ For instance, to study interactions of bacteria with pNIPAM, many groups have used self-assembled monolayers (SAMs) of NIPAM.¹¹ For microfiltration applications, pNIPAM has been deposited using atom transfer radical polymerization (ATRP).¹² Although these methods produce uniform films, they are most efficient and predictable on a flat surface, such as a glass slide, and are dependent on surface chemistry to initiate deposition. Other groups have used electron beam ionization to deposit pNIPAM for tissue engineering applications.¹³ This method also requires a flat substrate for deposition. In addition, the film thickness of electron beam ionization deposition of pNIPAM must be controlled very carefully. When a film deposited using this method is too thick (>20 nm), the cells do not attach to the coated substrate, but if the film is too thin (<10 nm), cells do not detach (see Figure 2.2).¹⁴ (See Appendix I for a list of commonly used deposition methods.)

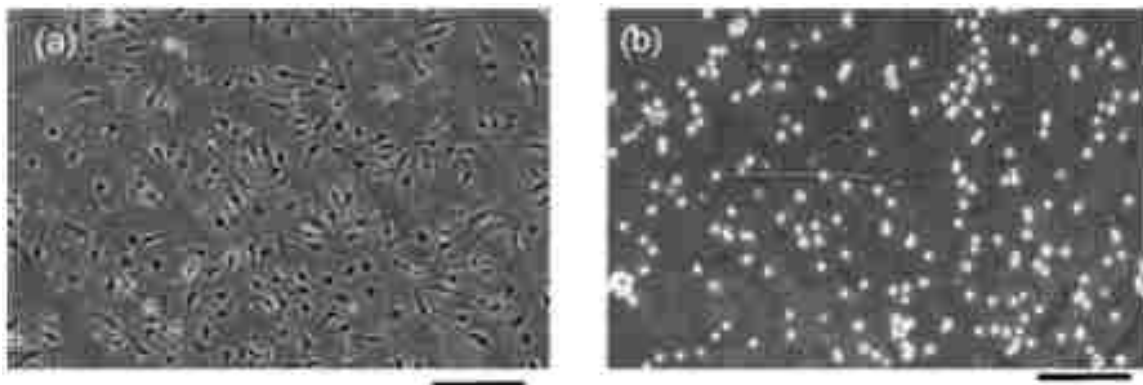


Figure 2.2: Bovine artery endothelial cells on pNIPAM substrates that are 15.5 nm (left) and 29.3 nm (right), illustrating that film thickness directly affects cell attachment. Scale bars are 200 μm . Image adapted from Aikyama et al.¹²¹

In this work, several methods for depositing and processing pNIPAM for use in mammalian cell culture, including pNIPAM deposition with a sol-gel (spNIPAM), plasma polymerization (ppNIPAM), electrospinning (espNIPAM), and hydrogels (hpNIPAM), were investigated. Each of these methods has its strengths and specific uses for different applications, and will be discussed in the following sections.

2.2 PNIPAM processing for mammalian cell applications

2.2.1 Surface preparation

Prior to coating any surface, all surfaces, besides commercially available pre-sterilized tissue culture polystyrene (TCPS) well plates, were cleaned as follows. Round glass cover slips (Ted Pella) and square cover slips (VWR) were cleaned by first submerging the surfaces into a 50% methanol (Honeywell Burdick and Jackson, Muskegon, MI), 50% hydrochloric acid (VWR International, West

Chester, PA) solution for 30 minutes, followed by rinsing each surface copiously with DI water and drying with nitrogen. Silicon wafers were prepared with a solvent wash, where the surfaces are ultrasonicated sequentially in dichloromethane (Honeywell Burdick and Jackson, Muskegon, MI), acetone (Honeywell Burdick and Jackson, Muskegon, MI), and methanol for 10 minutes and then dried with nitrogen. Once the surfaces are cleaned, they are stored until coated in Petri dishes under nitrogen sealed with Parafilm.

2.2.2 *spNIPAM*

Depositing pre-polymerized pNIPAM is of interest for many reasons, including the ease and speed of the process. As shown in Chapter 4, deposition of pre-polymerized pNIPAM is not stable for long-term cell studies without incorporating a sol-gel, made using tetraethyl orthosilicate (TEOS).¹¹⁸ In addition, as shown in chapter 6, TEOS is not cytotoxic, stabilizes the pNIPAM onto substrates during cell studies, and does not complicate the process, resulting in a rapid, inexpensive method to obtain pNIPAM-coated substrates.¹²⁰

Preparation of *spNIPAM* films follows a previously described method.¹¹⁸ A solution was prepared with 35 mg of pNIPAM (MW ~40,000 purchased from Polysciences, Inc, Warrington, PA), 5mL of distilled water, and 200 μ L of 1 Normal HCl were mixed, and a weight percentage of pNIPAM was determined. In a separate container 250 μ L TEOS sol (1 TEOS (Sigma-Aldrich, St. Louis, MO):3.8 ethanol:1.1 water:0.0005 HCl), 43 μ L distilled water, 600 μ L ethanol were mixed and weighed. To obtain 0.35wt% pNIPAM in sol, demonstrated to be

the ideal ratio for mammalian cell studies in chapter 4, the appropriate amount of the pNIPAM solution was added to the TEOS solution in order to achieve the desired weight percentage (ex. 3.5g pNIPAM solution added to 996.5g TEOS sol).



Figure 2.2: Spin coater used for co-depositing pNIPAM with a sol-gel, resulting in spNIPAM films.

100-200 μ L of the prepared solution was evenly distributed on clean surfaces placed on a spin coater (see Figure 2.3), model 100 spinner from Brewer Science, Inc. (Rolla, MO). The surfaces were then spun at 2000 rotations per minute for 60 seconds. The surfaces were stored under nitrogen in a Parafilm covered Petri dish until either used for surface analysis or cell culture tests.

2.2.3 *ppNIPAM*

Plasma polymerized pNIPAM substrates offer advantages not seen in the

spNIPAM surfaces, including films that are sterile.^{122, 123} Since solvents are not used for this process, sterility is maintained which is an important consideration when dealing with biological cells, and thus this method promises to be extremely beneficial for biomaterial applications. As demonstrated in Chapters 5 and 6, because ppNIPAM does not rely on solvent evaporation, it produces pinhole free films, which enhance cell sheet growth on them.^{119, 120}

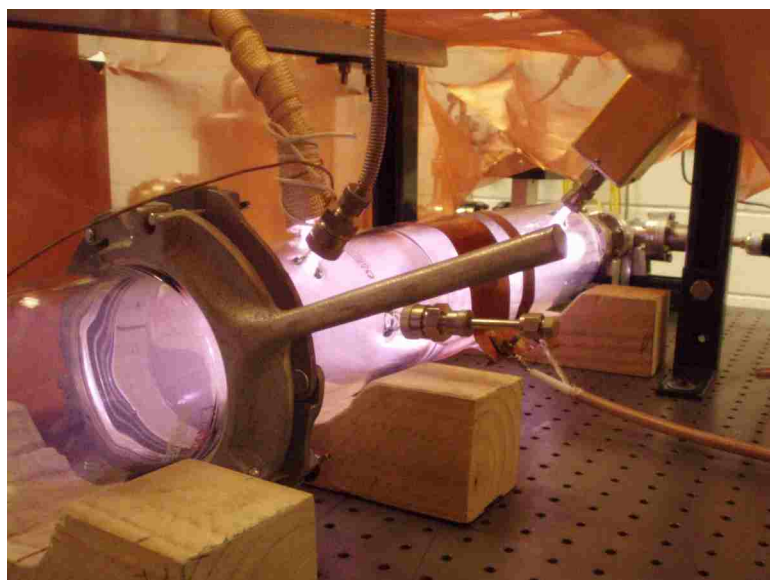


Figure 2.3: Plasma reactor chamber, with an oxygen plasma. Samples are placed inside the chamber in front of the first electrode.

Plasma polymerization was performed in a reactor chamber fabricated to our design specifications by Scientific Glass (Albuquerque, NM) shown in Figure 2.4 following a method previously described.^{124, 125} *N*-isopropyl acrylamide (99%) was purchased from Acros Organics (Geel, Belgium). To ignite a plasma in the chamber, two 2.5 cm copper electrodes are connected to a Dressler (Stolberg, Germany) matching network and a 13.56 MHz Cesar radio frequency (RF) power generator from Advanced Energy (Fort Collins, CO). Prior to depositing pNIPAM,

surfaces were treated with an Ar etch and coated with a CH₄ adhesion promoting layer. Ar flows into the reactor chamber at 15sccm at 390mT. The RF generator ignites the plasma at 40W for 2 minutes. This step etches the surface, preparing the surfaces for the following deposition of methane. Methane is deposited as an adhesion promoting layer for pNIPAM. The methane flows into the reactor at 2 sccm at 140 mT. The plasma is ignited at 80 W for 5 minutes. Finally, the monomer line is opened to allow the gaseous monomer to flood the reactor. The pressure is maintained at 140mT. During the pNIPAM deposition, the power setting of the RF generator is slowly decreased from 100W to 0W over 35 minutes. These settings were previously characterized by a former master's student for the optimal films for biological cell release from the final surfaces.¹²⁴

After the samples are removed from the reactor, they are rinsed with cold DI water in order to remove any uncrosslinked NIPAM from the surface, and dried with nitrogen. The surfaces are placed in a plastic Petri dish, evacuated with nitrogen, and sealed with Parafilm. The samples are then stored in a desiccator until surface analysis or cell culture is performed.

2.2.4 espNIPAM

Electrospinning is a popular method for creating cell scaffolds for tissue engineering applications. In part, this is due to the fact that this is an inexpensive method for creating surfaces with fibers on the size scale of the extracellular matrix (ECM). In addition, the mats produced using this method result in surfaces with a high surface area to volume ratio. This is a characteristic that is

very important when working with pNIPAM. Kwon et al. showed that pNIPAM deposited using electron beam ionization onto porous membranes overcame the mass transfer limitation normally seen with 2D films, and cell detachment was achieved in 30 minutes as opposed to 2 hours (see Figure 2.5).¹²⁶ Using this same reasoning, espNIPAM was utilized to create a porous substrate that would rapidly swell and result in quick cell detachment.

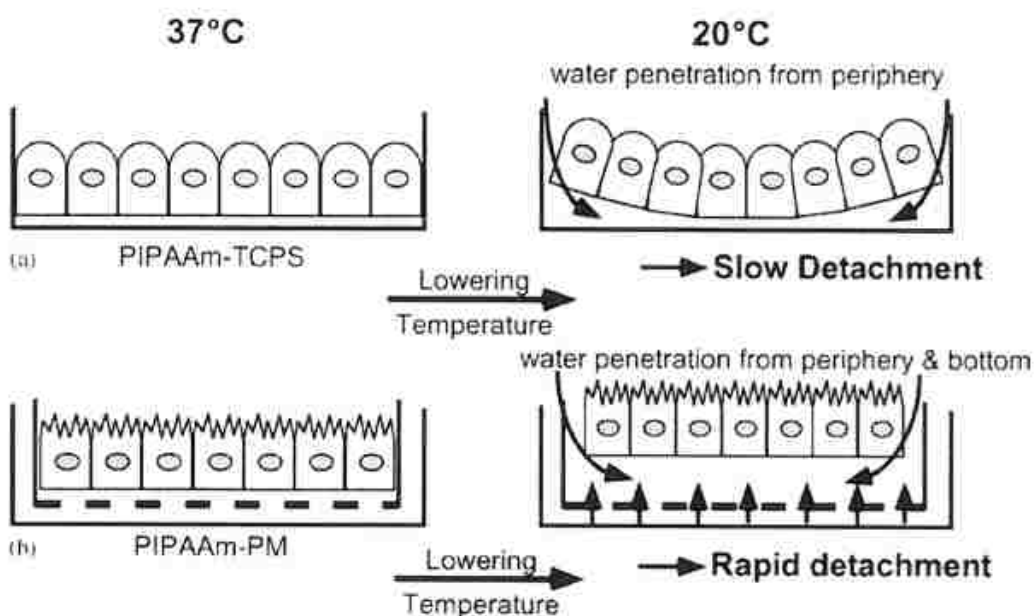


Figure 2.4: Schematic illustrating water penetration of pNIPAM films on TCPS (a) and pNIPAM-coated porous membranes (PM) (b), where there is rapid cell detachment from (b). Image adapted from Kwon et al.¹²⁶

Electrospinning occurs when a solution that is extremely volatile is pumped through a charged needle, and a voltage drop pushes the solution toward a collection plate. While in the needle, the solution becomes charged. When the static charge of the drop exiting the needle overcomes the surface tension, the solution is pulled toward the grounded collection plate. In the void between the

needle and the collection plate, the solution begins to evaporate and the remaining solid, which the final mat will be comprised of, is accelerated in a whipping action towards the collection plate (shown in Figure 2.6). The collected mat is comprised of micro to nanometer fibers of the polymer that was in the initial solution.

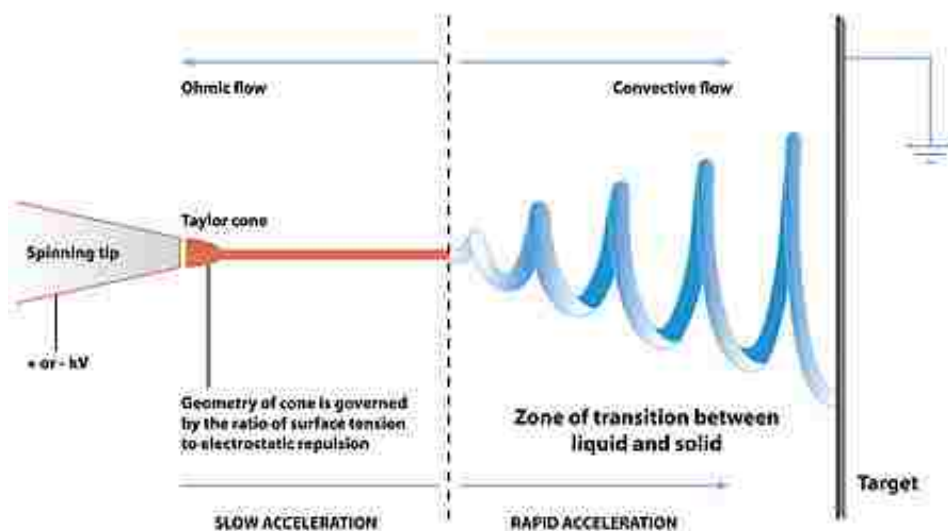


Figure 2.5: Schematic illustrating how the solution within the syringe is pulled to the target during electrospinning.¹²⁷ On the left, there is the needle attached to the syringe, and on the right, the target. Between the needle tip and the target, the solution begins to evaporate the volatile liquid, leaving only the pNIPAM solid, which is collected on the target.

The use of both low (MW ~40,000 Da purchased from Polysciences, Inc, Warrington, PA) and high (MW ~300,000 Da, Scientific Polymer, Ontario, NY) molecular weight pre-polymerized pNIPAM powders was investigated to determine which would best support cell sheet growth and detachment using an electrospinning device that was built in house (see Figure 2.7).¹²⁸



Figure 2.6: Electrospinning setup to produce espNIPAM mats.

Solutions of 10, 20, and 50 wt% of pNIPAM in methanol were loaded into 5 mL plastic syringes fitted with a 18, 21, or 30 gauge needle (Small Parts Inc, Seattle, WA). The syringes were then loaded into a NE-300 syringe pump (New Era, Farmingdale, NY) and the solution delivered at a constant rate of 3.5 mL/hr. The voltage source that is connected to the needle on the syringe was set at 15 kV, with the target 15 cm from the needle, and mats were collected on an aluminum foil covered copper plate over a period of 5 or 10 minutes to vary the mat density. The mats were then placed in a vacuum oven to remove any residual methanol and then either stored until characterization or attached to well plates with vacuum grease for cell studies.

2.2.5 *hpNIPAM*

Hydrogels offer advantages similar to espNIPAM, in that they have a larger surface area exposed to surrounding medium than tethered films. In addition,

they swell to approximately 3 times their original size rapidly upon temperature shifts below the LCST. Furthermore, hpNIPAM is easy to tailor to a specific size and shape, including monodispersed microgels. Finally, these gels can be rapidly fabricated with minimal equipment.

The procedure necessary to polymerize pNIPAM into a hydrogel was previously described.¹²⁹ Briefly, 9.4% (w/v) NIPAM, 0.7% (w/v) ammonium persulfate (Acros Organics, Geel, Belgium), and 0.64% (w/v) *N,N'*-methylenebisacrylamide (Sigma-Aldrich, St. Louis, MO), were mixed in 10 mL of Millipore ultra pure (18 mΩ/cm) water. This solution was then immersed in an ice bath to reduce the temperature. Once the solution had cooled, a 1:5 tetramethylethylenediamine (TEMED) (Sigma-Aldrich, St. Louis, MO) to water solution was added drop wise to accelerate cross-linking at this reduced temperature. Once the gel was formed, it was cleaned via temperature cycles through the LCST in fresh water.

2.3 Surface Analysis

2.3.1 XPS

X-ray photoelectron spectroscopy (XPS) is a quantitative technique that can be used to determine the elemental composition, bonding environments, and relative thickness of a surface. The surface is irradiated with mono-energetic X-rays (photons) causing photoelectrons to be emitted. (See Figure 2.8)

This process corresponds to the following equation:

$$KE = h\nu - BE - \phi \quad \text{Equation 2.1}$$

where KE is the kinetic energy of the emitted photoelectrons, $h\nu$ is the energy of the photon, BE is the binding energy of the emitted photoelectron, and ϕ is the work function of the device. The kinetic energy is measured using an electron energy analyzer, which allows for the calculation of the binding energy.

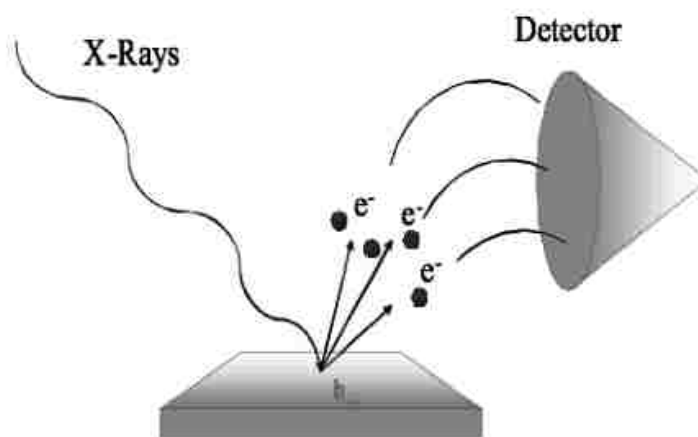


Figure 2. Schematic illustrating the function of an XPS instrument. X-rays are bombarded onto a surface, and electrons are ejected from the top 100Å, then collected at the detector. The kinetic energy of each electron is measured, and can then be related to the binding energy, which is specific to each element.

Electrons can escape from approximately the top 100 Å of the surface. From the binding energy and intensity of the photoelectron peak (based on the number of photoelectrons detected) the identity of the elements in the surface, the chemical state of each element, and the quantity of each element with an error of about 5-10% may be determined.¹³⁰⁻¹³² The survey spectrum will allow for the determination of elements that are present as well as the elemental composition (atomic %), while a high resolution spectrum will allow for the determination of

elemental binding environments.

All XPS spectra were obtained using a Kratos Axis-Ultra DLD spectrometer (see Figure 2.9). This instrument has a monochromatized Al K α X-ray and a low energy electron flood gun for charge neutralization. X-ray spot size for these acquisitions was on the order of 300x700 μm (Kratos 'Hybrid' mode). Pressure in the analytical chamber during spectral acquisition was $\sim 5 \times 10^{-9}$ Torr. Pass energy for survey spectra was 80 eV and 20 eV for high-resolution carbon 1s spectra.



Figure 2.7: A Kratos Axis-Ultra DLD spectrometer.

CasaXPS software (Manchester, UK) was used to analyze data. Core-level spectra peaks were fit using the minimum number of peaks possible to obtain random residuals. A 70% Gaussian/30% Lorentzian line shape was used to fit the peaks, and a linear function was used to model the background (see Figure 2.10).

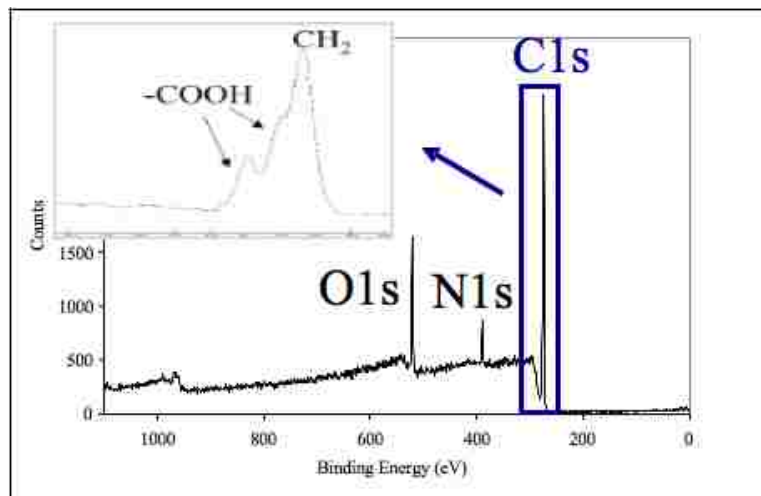


Figure 2.10: Data collected from XPS. The large spectrum is a survey with the elemental data and the inset is high resolution C1s with binding environments.

2.3.2 ToF-SIMS

Time-of-flight secondary ion mass spectrometry (ToF-SIMS) uses a pulsed primary ion beam (e.g., Ar^+ , O^- , Cs^+ , or Ga^+) to remove atoms and molecular fragments (secondary ions) from the top 10-20 Å of a surface (see Figure 2.11). The secondary ions are separated by their velocity, which is proportional to the mass to charge ratio (m/z) as determined by the amount of time the ions take to reach the analyzer (i.e., time of flight).

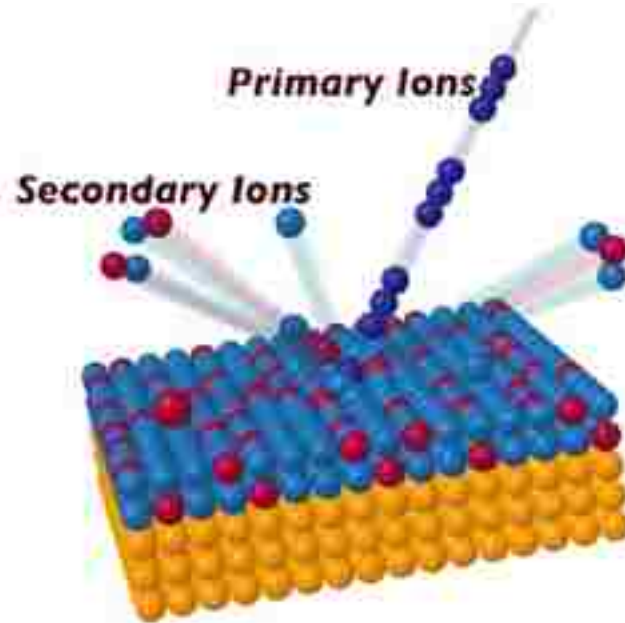


Figure 2.1: Schematic illustrating a primary ion beam bombarding a surface, as is done in ToF-SIMS, causing secondary ion fragments to be released from the surface. The secondary ions are separated by their velocity, which is dictated by the size of the fragment.

Both positive and negative spectra may be obtained using the mass to charge ratio versus the number of secondary ions at that ratio. See Figure 2.12 for a positive spectrum. Mass to charge (m/z) ratios of up to 10,000 Daltons can be detected using ToF-SIMS.¹³³ This technique has a detection limit of parts per billion and a mass resolution of over 10,000 $m/\Delta m$. Because of the high sensitivity, it is a valuable technique for surface sensitive applications, such as plasma processes.

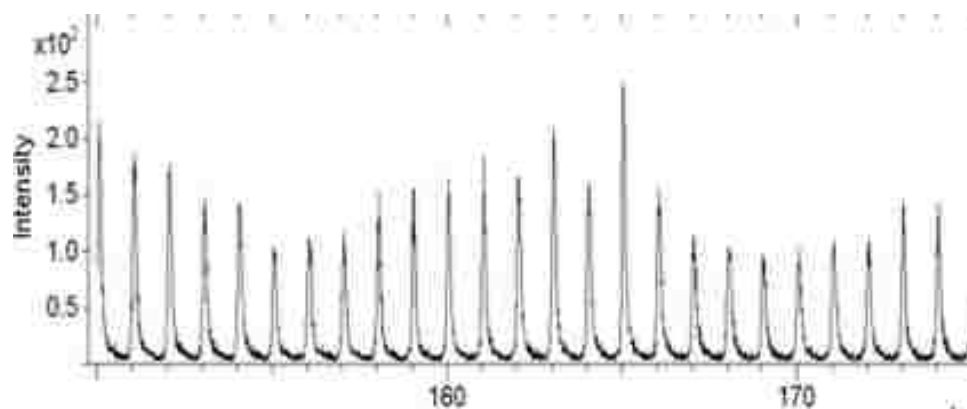


Figure 2.12: Positive ion spectrum obtained using ToF-SIMS.

ToF-SIMS spectra were acquired at the University of Washington using an IonToF ToF-SIMS 5 spectrometer (see Figure 2.13) with a 25 keV Bi^+ ion source in the pulsed mode and operated with at a current of 0.35 pA. Spectra were acquired for positive secondary ions over a m/z range of = 0 to 500. Secondary ions of a given polarity were extracted and detected using a reflectron time-of-flight mass analyzer. Spectra were acquired using an analysis area of 0.01 mm^2 . Positive ion spectra were calibrated using CH_3^+ , C_2H_3^+ , C_3H_5^+ , and C_7H_7^+ peaks. Calibration errors were kept below 10 ppm. Mass resolution ($m/\Delta m$) for a typical spectrum was between 8000 to 10,000 for $m/z = 27$ (pos). Statistically relevant data were obtained by repeating all procedures three times, with each replicate consisting of three surfaces and each surface analyzed in three different sites along the surface.



Figure 2.8: An IonToF ToF-SIMS 5 spectrometer.

2.3.3 PCA

Principle component analysis, or PCA, is a tool that can be used to determine differences in extremely complicated data sets. Since ToF-SIMS results in spectra with thousands of peaks, and each experiment was done in triplicate, the data set was large and did not readily reveal conclusions about the surfaces. Multivariate analysis techniques, such as PCA, are useful in these situations to determine what components are the most varied within the data, and how these data correlate between samples.^{134, 135}

PCA was performed using PLS Toolbox version 2.0 (Eigenvector Research, Manson, WA) for MATLAB (Math-Works, Inc., Natick, MA). All spectra were mean-centered before running PCA. A “complete” peak set was constructed containing all of the major peaks that were previously found to be indicative of

pNIPAM. Selected peaks, such as CH_3 , were then normalized to the total ion intensity to account for the fluctuations in secondary ion yield between different spectra. PCA was then used to capture the linear combination of peaks that described most of the variation within the data set. From this, both “scores” and “loadings” plots were obtained.

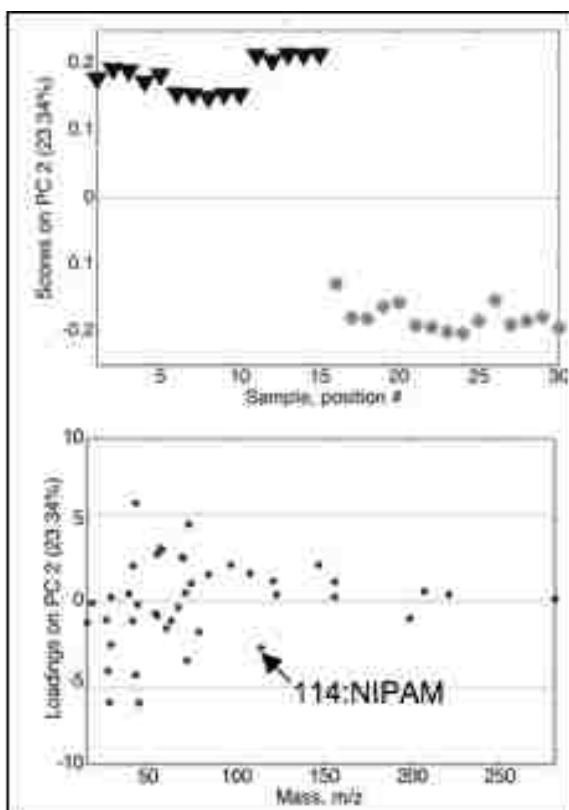


Figure 2.9: Scores (top) and loadings (bottom) plots from PCA.

The scores plot (see Figure 2.14, top) is a graphical representation of the primary differences in a sample set. The loadings plot (see Figure 2.14, bottom) allows for the user to decipher the scores plot by showing what fragments caused the separation.

2.3.4 Contact Angle

As previously stated, the relative wettability of pNIPAM is dependent on its temperature. At temperatures below the LCST, pNIPAM is hydrophilic. At temperatures above its LCST, pNIPAM becomes relatively more hydrophobic. Contact angles were taken to determine the surface wettability of ppNIPAM on Si as well as on a Si control chip. These experiments utilized a technique known as captive (or inverted) bubble. The surface is placed upside down in a quartz cell filled with ultra pure water (18 m Ω /cm) from a Millipore Academic unit. Using a syringe with an inverted needle, an air bubble is placed on the surface, and the angle between the drop and the surface is measured. (See Figure 2.15)

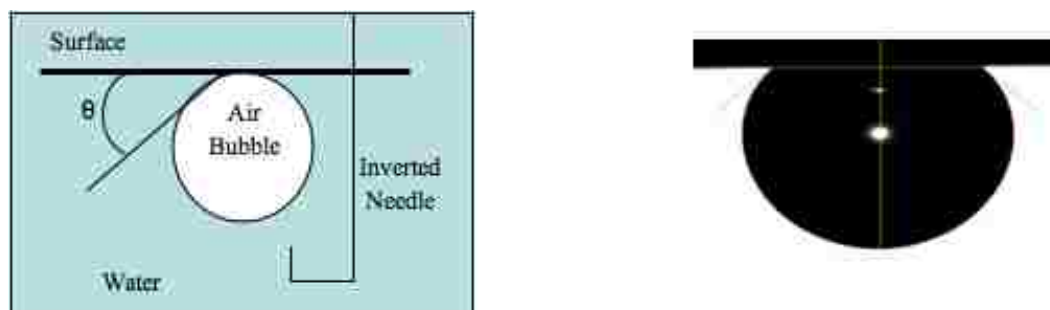


Figure 2.10: Schematic of inverted contact angle measurements on the left, showing an air bubble on a substrate, and the angle that is measured. On the right, a snapshot of an air bubble on a pNIPAM substrate.

An Advanced Goniometer model 300-UPG (ramé-hart instrument co., Mountain Lakes, NJ) with an environmental chamber and DROPimage Standard program was used to measure inverted bubble contact angles in ultra pure water (18 m Ω /cm). Contact angles were taken at room temperature (\sim 23 $^{\circ}$ C) and 37 $^{\circ}$ C using the Temp Controller model 100-500 connected to the environmental chamber. Statistically relevant data were obtained by repeating all procedures

three times, with each replicate comprised of three surfaces, with each surface analyzed in three different sites along the surface. The contact angles were compiled and compared above and below the LCST to determine changes in wettability (see Figure 2.16).

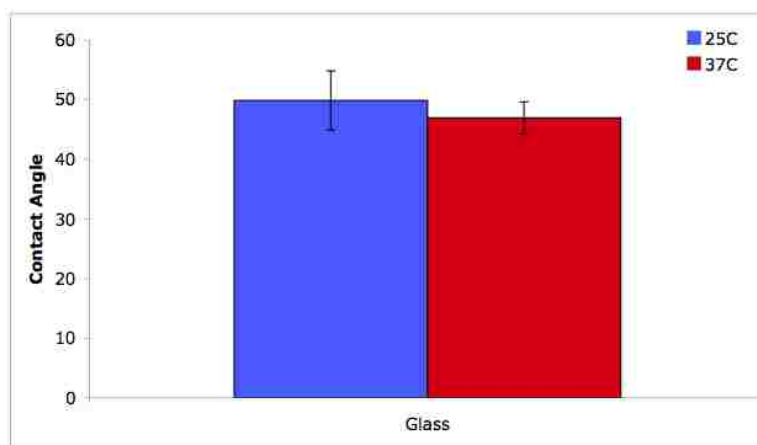


Figure 2.11: Compiled contact angle data on a blank glass slide, illustrating no change of wettability when the temperature is shifted from above (red) to below (blue) the LCST, as expected on a substrate that is not thermoresponsive.

2.3.5 AFM

Atomic force microscopy (AFM) is a scanning probe microscopy that has been shown to achieve resolution on the order of fractions of a nanometer. Using AFM, the user can determine thickness, surface roughness, topography, and Young's modulus with minimal initial sample preparations. In addition, these measurements can be taken in either liquid cells or in air at different temperatures, making it an ideal method of characterizing pNIPAM surfaces. As shown in Figure 2.17, a probe connected to a cantilever rasters the sample. Simultaneously, a laser reflects off of the cantilever onto a detector, which

records deflections in the cantilever.

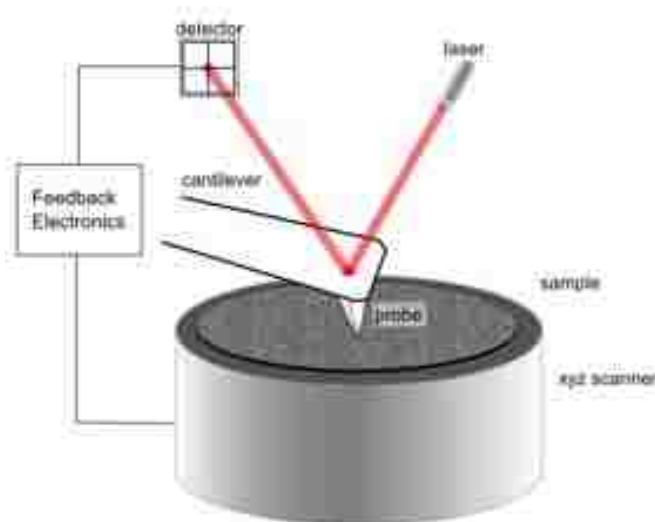


Figure 2.12: Schematic illustrating the function of an AFM instrument. A probe connected to a cantilever rasters the surface. In tandem, a laser reflects off of the cantilever onto a detector.

Force measurements and imaging were performed in the laboratory of Prof. David Keller at UNM using a Veeco Nanoscope IIIa controller (Plainview, NY) and J type scanner. (See Figure 2.18) An O-ring and fluid cell containing the AFM cantilever was then set on top of the sample. Degassed nanopure water was injected into the fluid cell and the film was allowed to equilibrate with the water for 30 minutes. The temperature was controlled with infrared heat lamps directed at the AFM. The entire apparatus was then placed in a Plexiglas enclosure on an isolation setup. There was a minimum of thirty minutes between temperature changes.



Figure 2.13: A Veeco Nanospec AFM.

Veeco software version 6.1 (Plainview, NY) was used to collect data. A silicon nitride cantilever, MSCT-UNM Veeco Probes, with a spring constant of 0.02 N/m was used for all force-distance and imaging results (see Figure 2.19). Statistically relevant data were obtained by repeating all procedures three times, with each replicate using three surfaces, analyzing in three different sites per surface.

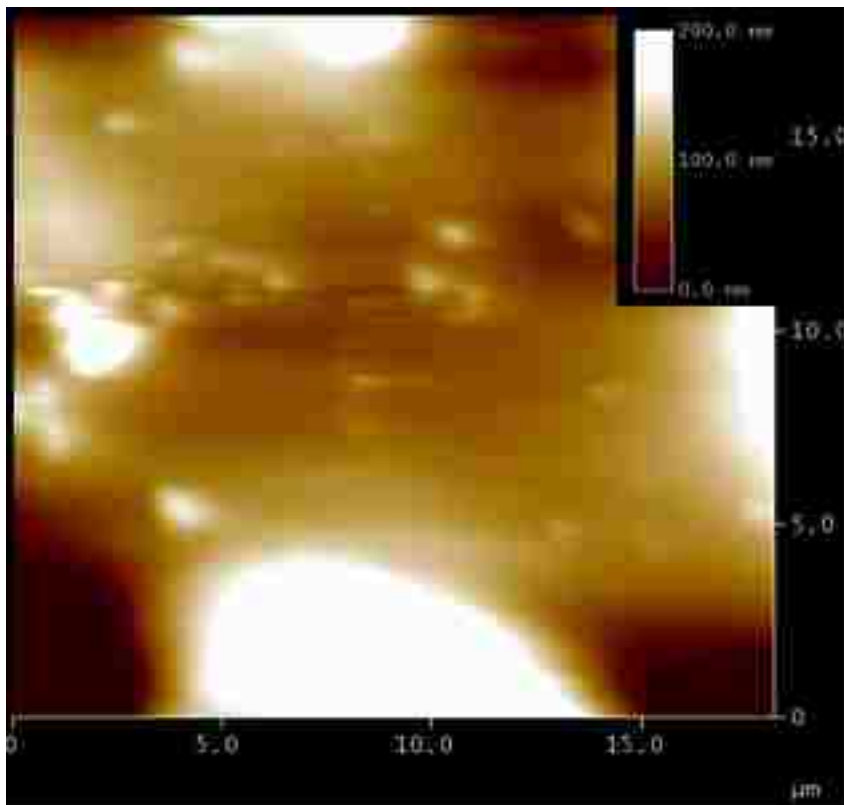


Figure 2.14: Topographical data of a spNIPAM substrate collected with AFM.

2.4 Cell Culture

2.4.1 General cell harvest

Various cell types were used in this work depending on the focus of the chapter. For instance, bovine aortic endothelial cells (BAEC) and MC3T3-E1 fibroblasts are cell lines that are commonly used in pNIPAM studies, and these cell lines were used as proof of concept in Chapters 3-7.^{111, 118-120, 136} Once it was determined that the surfaces supported normal cell growth, alternate cell lines commonly used for spheroid formation were substituted in Chapter 8. These cells include EMT6 (rat carcinoma), OVCA 429 (human ovary tumor cells), and SKOV (human ovary tumor cells). (See Appendix III for a complete list of cell types used

in this work.) Each of these cells were rinsed, and then harvested via enzymatic digestion, using 0.25% trypsin-EDTA from Gibco (Carlsbad, CA). All cells were grown in media purchased from Hyclone™ on TCPS. Once 70-90% confluent, the cells were harvested and seeded onto samples. Cells were incubated at 37 °C, 95% relative humidity, and 5% CO₂.

2.4.2 BAECs

Bovine aortic endothelial cells (BAEC) were cultured in Dulbecco's Modified Eagle Medium supplemented with 10% fetal bovine serum, 1% penicillin/streptomycin, 4.5 g/L glucose, 0.1 mM MEM nonessential amino acids, and 1 mM MEM sodium pyruvate. BAECs were obtained from Genlantis (San Diego, CA). Figure 2.20 shows healthy BAECs that have been cultured according to the above procedure.

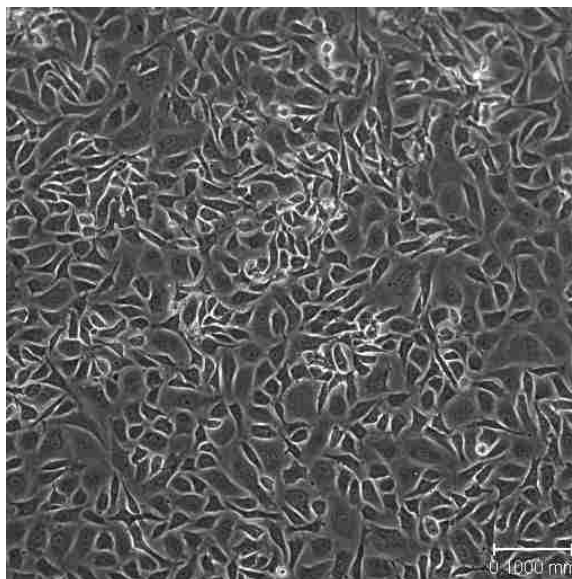


Figure 2.20: Bright field microscopy image of normal BAECs. Scale bar is 100 μm.

2.4.3 MC-3T3E1

These mouse fibroblast cells, a generous gift from Elizabeth Hedberg-Dirk, were cultured in Alpha Modified Eagle Medium supplemented with 10% fetal bovine serum and 1% penicillin/streptomycin. Figure 2.21 shows healthy 3T3s that have been cultured according to the above procedure.

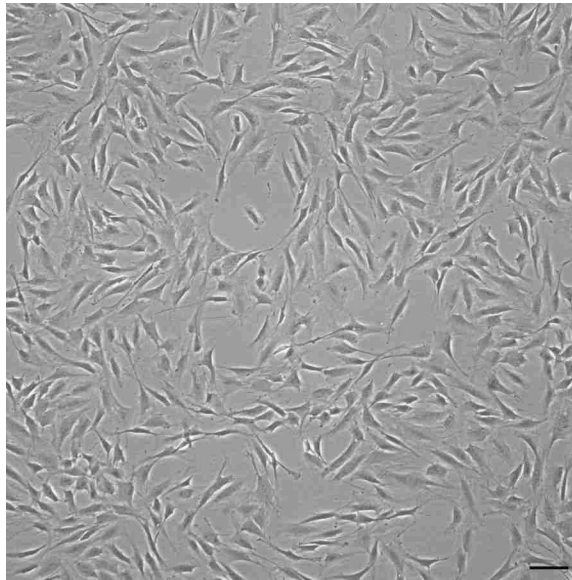


Figure 2.15: Bright field microscopy image of normal 3T3s.

2.4.4 EMT6

These rat carcinoma cells, a generous gift from James Freyer, were cultured in Alpha Modified Eagle Medium supplemented with 10% fetal bovine serum and 1% penicillin/streptomycin. Figure 2.22 shows healthy EMT6s that have been cultured according to the above procedure.

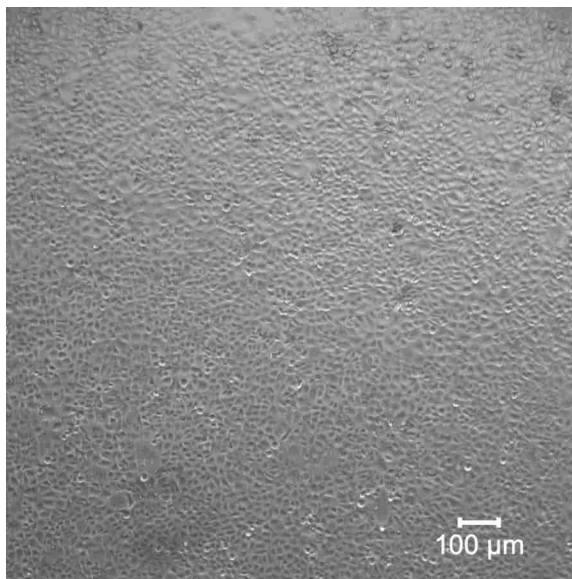


Figure 2.16: Bright field microscopy image of normal EMT6s.

2.5 Cell detachment

2.5.1 Cell detachment methods

Cells were detached a number of different ways, depending on the surface type and the objective of the experiment. For applications such as determining cell detachment from wells (Chapter 3), the cells were allowed to detach without assistance. Once the optimum conditions for cell detachment were achieved, cells were detached with assistance using a poly(vinylidene fluoride) or PVDF superstrate to maintain a cell sheet that could be relocated to a new well, as in Chapter 7.

2.5.2 Unassisted detachment

Cells were cultured until ~95% confluent (approximately 2-4 days). The media was removed, and 4°C serum-free media was added to each well, since a

previous investigation indicated this facilitated the fastest release from pNIPAM (see Figure 2.23).¹¹¹ The culture plate was then placed on a shaker platform for 2 hours (spNIPAM and ppNIPAM surfaces) or 5 minutes (espNIPAM), and observed via light microscopy (Nikon F100, Melville, NY) with a 20x objective. Images were captured at 3 locations, on 3 separate surfaces, and repeated 3 times before and after cell detachment using Spot Advanced software (Sterling Heights, MI). Images were analyzed with NIH ImageJ, using the Cell Counter plug-in, to determine the approximate percentage of cells that detached.

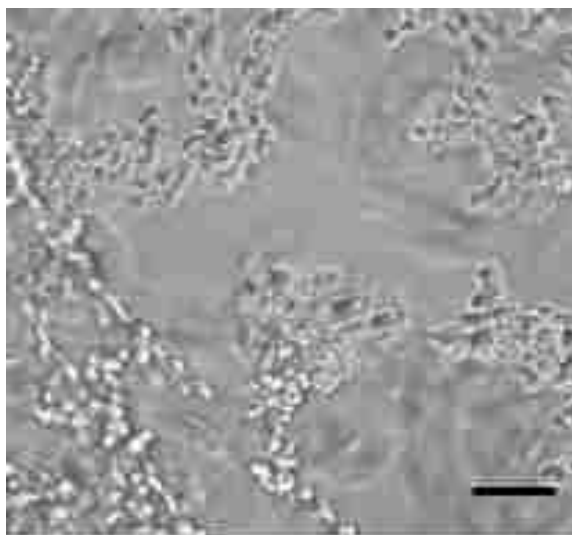


Figure 2.23: Bright field microscopy image of BAECs detaching without assistance from spNIPAM substrates, after the temperature has been reduced across the LCST.

2.5.3 Assisted detachment

Cells were cultured until confluence (approximately 2-4 days). Medium was removed until there was only a thin film on the cells. A sheet of PVDF was laid on top of the cell sheet and the plate was incubated at 37 °C for 30 minutes, to allow

the cells to attach to the PVDF. 4 °C serum-free media was added to each well, since a previous investigation indicated this facilitated the fastest release from pNIPAM.¹¹¹ The culture plate was then placed on a shaker platform for 30 minutes, at which point the PVDF was slowly peeled from the substrate with the cells (see Figure 2.24).

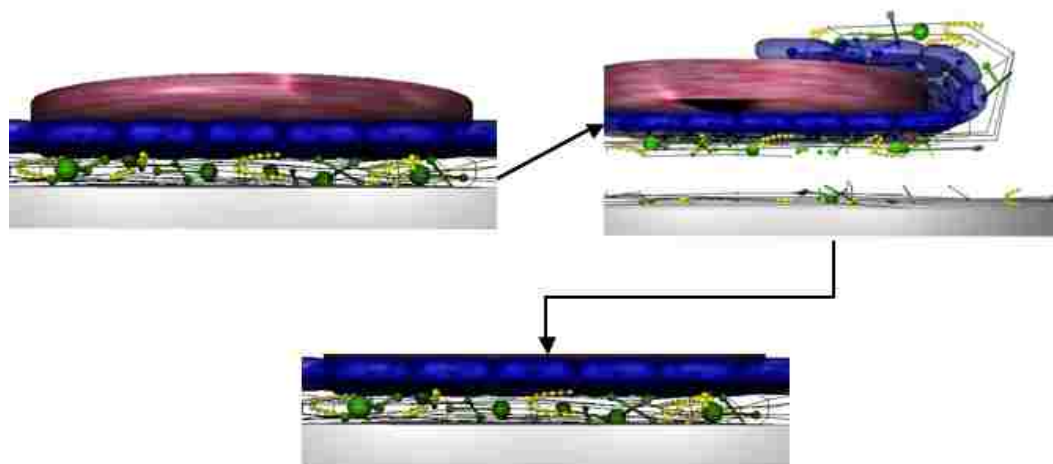


Figure 2.24: Schematic illustrating PVDF transferring cells. PVDF (pink) is used as a superstrate (top left). When cells detach from a pNIPAM substrate (top right), PVDF can be used to transfer the cells to a new substrate. As this bond between the PVDF and cells is not strong, when the cells are anchored to a new substrate (bottom), the PVDF can easily be peeled away from the cells.

The cells were then placed in another well plate and incubated for 30 minutes with minimal media. The remainder of the serum containing media was added to the well plate and the PVDF released from the cells. The cells were observed via light microscopy (Nikon F100, Melville, NY) with a 20x objective. Images were captured at 3 locations, on 3 separate surfaces, and repeated 3 times before and after cell detachment using Spot Advanced software (Sterling Heights, MI). Images were analyzed with NIH ImageJ, using the Cell Counter plug-in, to

determine the approximate percentage of cells that detached.

2.6 Cell analysis

2.6.1 Cytotoxicity

The pNIPAM-coated surfaces need to be able to maintain cell growth and, thus, cannot leach any cytotoxic chemicals into the medium. Cytotoxicity tests are used to determine if components from the pNIPAM surface are leaching into medium. Cells are initially grown on TCPS to ensure normal attachment and proliferation, followed by replacement media that has been exposed to the substrate of interest at normal cell culture conditions for 24 hours. The cells are exposed to this medium for 24 hours in various concentrations determining if there was anything in the substrate that would impart cytotoxicity to the cultured cells.

In this case, pNIPAM surfaces were submerged in normal growth medium for 24 hours and incubated at cell growth conditions. The treated medium was then collected. Simultaneously, cells were grown at normal conditions until ~60% confluent. The medium on these cells was replaced with 100%, 10%, 1%, and 0% treated medium. The cells were then cultured for another 24 hours in the treated medium. Cell viability was determined using a commercial LIVE/DEAD® for mammalian cells fluorescence assay from Invitrogen. Calcein AM is membrane permeant, and is cleaved by live cells, producing a cytoplasmic green fluorescence. Ethidium homodimer-1, on the other hand, is membrane impermeant, targeting nucleic acids in cells that have compromised membranes,

allowing dead cells to have a red fluorescence. To verify results, live controls (0% treated media) and dead controls (incubated in 0% treated media, followed by incubation in 70% methanol for one hour) were used for comparison. Figure 2.25 shows a fluorescent image of the live control that has been false colored using Spot Image.

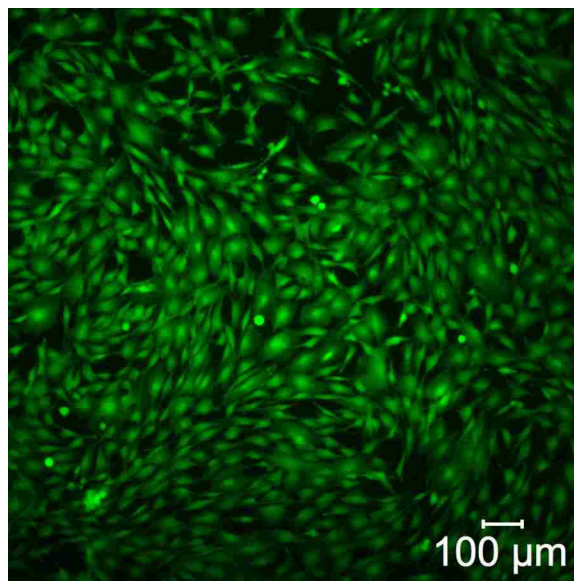


Figure 2.25: Fluorescent microscopy image of live 3T3s that have been false colored green.

2.6.2 Biocompatibility

Once it was verified that pNIPAM treatment surfaces did not leach any cytotoxic compounds, it was necessary to ensure that the cells would attach and proliferate onto surfaces, thus ensuring the surfaces were biocompatible. This test is pertinent to any study that requires cell attachment. In addition, since Akiyama et al. has determined that there is a crucial film thickness of pNIPAM films that results in surfaces that are not biocompatible, it was necessary to

investigate the biocompatibility of the surfaces used for this work.¹²¹

The cells were then grown on pNIPAM substrates to assess cell attachment and proliferation. The cells were seeded at a low density and their viability was checked using the LIVE/DEAD® assay explained in the previous section at 6 hours (attachment), 24 hours, and 72 hours (proliferation). (See Figure 2.26) Live controls (blank TCPS substrate) and dead controls (blank TCPS substrate, treated with 70% methanol for one hour) were used to verify results.

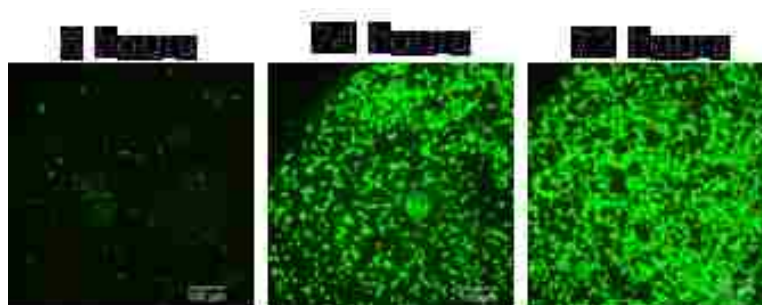


Figure 2.26: Fluorescent microscopy images taken at 6 (left), 24 (middle), and 72 (right) hours after seeded onto a ppNIPAM substrate. Cell attachment and proliferation indicate that the surfaces are biocompatible. Scale bar is 100 μm .

2.6.3 CellTracker™

Many of the pNIPAM substrates prepared for mammalian cell culture are opaque at physiologically relevant temperatures (37 °C). In order to image these cells, and ensure proper attachment and proliferation, the cells must be tagged with a fluorescent marker. This can be done prior to seeding the cells or once the cells have attached. The latter option is less desirable for several reasons, including there is no way to ensure cell attachment to the substrate. In addition, if the substrates are extremely sensitive to environmental cues, such as pNIPAM

substrates, it is difficult to do the procedure necessary to fluorescently label the cells without inducing thermoresponse in the substrate. Primarily due to this limitation of post-seeding labeling, CellTracker™ was used to tag cells prior to seeding surfaces.

CellTracker™ Green CMFDA (5-chloromethylfluorescein diacetate) was purchased from Invitrogen. CellTracker™ CMFDA has the unique property of being nonfluorescent until it interacts with intracellular esterases, as shown in Figure 2.28. CellTracker™ is initially membrane permeable, but transforms into an impermeable product, thus will not pass freely to neighboring cells. However, this probe is inherited in daughter cells for multiple generations, allowing for researchers to use this probe as a test of viability and proliferation.

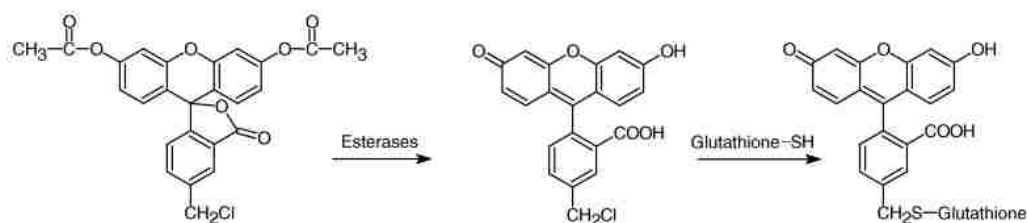


Figure 2.17: CellTracker™ requires a two-step intracellular reaction in order to be fluorescent. Although the dye may react initially with glutathione, intracellular esterases are necessary to complete the reaction. (Figure adapted from Invitrogen product information)

CellTracker™ is delivered as a powder, which is used to make a 10 mM stock solution in DMSO and frozen. Prior to use, the stock solution is thawed and a 25 μ m solution in serum free media is prepared, and replaces the media in the flask of confluent cells. The probe is incubated with the cells at cell culture conditions

for 60 minutes, and then replaced with normal growth media for 30 minutes. The cells are then rinsed with DPBS and harvested. Figure 2.29 shows cells that have been labeled with CellTracker™.

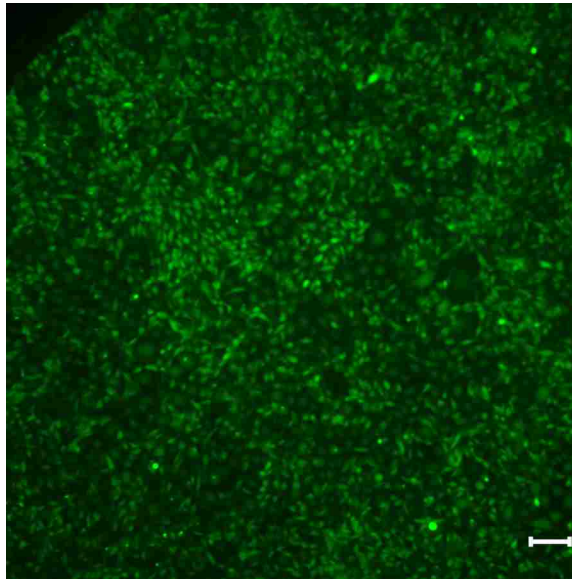


Figure 2.18: Fluorescent microscopy image of EMT6 cells with CellTracker™ probe. Scale bar is 100 μm .

Chapter 3. The Effects of Cell Culture Parameters on Cell Release Kinetics from Thermoresponsive Surfaces

Initially published by Reed, J.A.; Lucero, A.E.; Cooperstein, M.A.; and Canavan, H.E. in *Journal of Applied Biomaterials and Biomechanics*.¹¹¹

3.1 Introduction

As was discussed in Chapter 1, the thermoresponsive nature of pNIPAM has made it of great interest to the bioengineering community. One area in which pNIPAM has been used extensively is for the reversible adhesion of mammalian cells.¹³⁻²⁵ It has been demonstrated that many mammalian cell types attach to grafted pNIPAM in a similar fashion as when exposed to tissue culture polystyrene (TCPS): the cells proliferate into a confluent sheet. However, when the temperature of the cell culture is dropped below the LCST of the polymer, the cells will detach and can be harvested for tissue engineering applications. This is in contrast to cells grown on TCPS, which will not detach using a temperature drop, instead requiring enzymatic digestion (via trypsin) or mechanical scraping to remove them.²⁶

Since its initial demonstrations in 1968, many researchers have applied the technique of low-temperature liftoff to obtain their cell type of interest.¹³⁷ To date, bovine aortic endothelial, human dermal fibroblasts, Madin-Darby canine kidney, L929 mouse fibroblast, neonatal rat cardiomyocytes, primary parenchymal hepatocytes, human dental papilla fibroblasts, MC3T3-E1 mouse calvaria

osteoblasts, MEC human cholangioadenocarcinoma, and many other cells have all been demonstrated to release from pNIPAM-treated surfaces.¹³⁸

In addition to their use of different cell types, these researchers have used different conditions to initiate cell release from pNIPAM. For instance, in some cases, serum free media (SFM) is used to stimulate detachment,¹³⁹ while others have used media with serum (MWS).^{26, 139}

Another variable optimized was the temperature at which the “pop off” solution (e.g., MWS or SFM) is used, which ranges from slightly below the LCST of pNIPAM (i.e. 25 °C) to far below the LCST (4 °C).¹³⁹ In some of these published papers, rationale is given for why a particular parameter was chosen. For instance, Okano et al. used 20 °C MWS, reasoning that it was above the metabolically inactive temperature for cells (<4 °C).^{24-27, 140-142} However, in most cases, there is no mention of the reason that a particular solution or temperature was utilized for cell detachment.

Furthermore, the amount of time required to achieve 100% detachment of the cells is rarely reported.¹²⁶ The time required to detach adherent cells from pNIPAM is an important parameter to consider, as it affects not only experimental planning (i.e., how much time must be budgeted for cell release in a given set of experiments), but also in some cases experimental outcome (cells that are detached while still metabolically active may alter their expression of transmembrane proteins of interest).

In this work, the cell culture parameters were investigated to determine which

parameters initiate the most rapid release of cells from pNIPAM. A novel technique was used to obtain pNIPAM surfaces for this work based on a spin-coated solution containing pNIPAM and tetraethyl orthosilicate (spNIPAM). Following characterization of the spNIPAM substrates using traditional surface chemistry techniques (e.g., X-ray photoelectron spectroscopy, XPS; and contact angle measurements), identical populations of bovine aortic endothelial cells (BAECs) were grown to confluence on pNIPAM-treated glass slides. At confluence, the media used to culture cells was exchanged for one of four solutions [serum free media (SFM), media with serum (MWS), Dulbecco's phosphate-buffered saline (DPBS), and serum free media with a DPBS wash (DPBS/SFM)]. The temperature of each solution used was also varied from above the LCST of pNIPAM (37 °C), below the LCST (25 °C), and far below the LCST (4 °C). The cells were then observed using light microscopy and the time required to achieve 100% cell detachment was recorded. From these results, it was concluded that the fastest, most reliable release of BAECs occurred well below the LCST of the polymer at 4 °C in serum free media.

3.2 Experimental Methods

The majority of the experiments carried out herein follow the procedures outlined in Chapter 2, including spNIPAM deposition, XPS, contact angle goniometry, and cell culture. Three repetitions of all experiments, producing three surfaces, were performed. Each surface was analyzed in three spots, for a total of 27 analyses.

3.2.1 Cell detachment parameters

BAECs were cultured for 2 days to allow cells to become confluent. The media was removed and the respective solution (DPBS, serum-free media, culture media, or trypsin) at 4 °C, 25 °C, or 37 °C was added to each well. The culture plate was then placed on a shaker platform and timed for complete cell detachment as visualized via light microscopy. If complete cell detachment was not achieved within a hour, the time was extrapolated from the number of cells remaining on the surface. Extrapolations resulting in extremely long time periods were set to 2000 minutes for data plotting purposes.

3.3 Results

3.3.1 Surface analysis

PNIPAM-treated surfaces have been deposited using a variety of techniques, including co-grafting pNIPAM with other polymers,¹⁴³ immobilizing pNIPAM by photolithography,¹⁴⁴ by polymerizing pNIPAM with previously activated surfaces,¹²³ and by vapor-phase deposition of plasma polymerized NIPAM (ppNIPAM).^{118, 145, 146} Regardless of the preparation technique used, the detachment of cell sheets have been observed.

In this work, pNIPAM films were generated by spin-coating a solution containing high molecular weight pNIPAM with tetraethyl orthosilicate (TEOS), referred to as spNIPAM throughout the rest of this text. Rao et al. initially utilized this method for the purpose of creating thermoresponsive membranes, and

characterization for the purpose of mammalian cell culture will be further explored in Chapter 4.^{24-26, 122, 138} This technique was chosen for deposition as it is a relatively inexpensive method to produce many replicates and works with different substrate chemistries, including glass slides (for the transparent nature of which enabled visualization of cell cultures via light microscopy), as well as silicon chips (the smaller dimensions of which were used to increase replicates for surface analysis).

Table 3.1: Major elemental relative atomic percentages from XPS for spNIPAM surfaces. n=9 for spNIPAM surfaces with a standard deviation of less than 2%.

Description	Relative Atomic %			
	C	O	N	Si
Theoretical	75.0	12.5	12.5	0
spNIPAM	42.3	36.6	5.8	15.2

Prior to their use for *in vitro* cell culture, the chemical composition of the spNIPAM substrates was characterized. Previously, it was demonstrated that XPS is an excellent tool to verify the surface chemistry of thin pNIPAM films,^{121, 122} as the technique is sensitive to the upper ~20-100 Å of a film. As with the previous studies, survey spectra were obtained to provide elemental analysis of the pNIPAM films. Because the underlying substrates are silicon chips, the presence and amount of nitrogen detected are indicative of successful pNIPAM film deposition. Since the technique used in this work employs co-deposition of pNIPAM with tetraethyl orthosilicate [TEOS, Si(OC₂H₅)₄], the elemental

composition of the films (42.3% carbon, 36.6% oxygen, 5.8% nitrogen) differs from that predicted from the stoichiometry of the monomer (75% carbon, 12.5% oxygen, 12.5% nitrogen). (See Table 3.1) To a lesser extent, the same effect is observed in the high resolution carbon data, as the C-O bonds from TEOS component contribute to the peak at 286.8 eV, resulting in 20.6% (experimental) versus 16.7% (theoretical) composition of C-OH/C-N for these films. (See Table 3.2 and Figure 3.1).

Table 3.2: Relative atomic percentages from high resolution C1s for spNIPAM surfaces. n=9 for spNIPAM surfaces with a standard deviation of less than 3%.

Description	Relative Atomic %		
	C-H (285)	C-OH/C-N (+1.8)	N-C=O (+3.0)
Theoretical	66.7	16.7	16.7
spNIPAM	64.4	20.6	14.9

In addition to characterizing the surfaces' elemental composition, the thermoresponse of the films was measured via contact angle measurements. This technique is sensitive to the change in wettability of the films in response to temperature. As previously mentioned, when pNIPAM surfaces are cooled below the LCST of the polymer (~32 °C), they become relatively more hydrophilic. As indicated in Figure 3.2, there is a significant difference (~15°) in the contact angles taken from the pNIPAM surfaces bracketing the LCST of the polymer (25 and 37 °C). This result is consistent with comparable measurements using plasma polymerized NIPAM (an 11° increase) and silane-grafted NIPAM (a 12.7°

increase).^{147, 148} When the pNIPAM surfaces are further cooled below the LCST from 25 to 4 °C, there is little change in the contact angle, most likely due to the fact that both temperatures fall below the physical transition temperature of pNIPAM. In contrast to the pNIPAM substrates, no change is observed in the contact angles obtained at 4, 25 and 37 °C from the control silicon blank substrates.

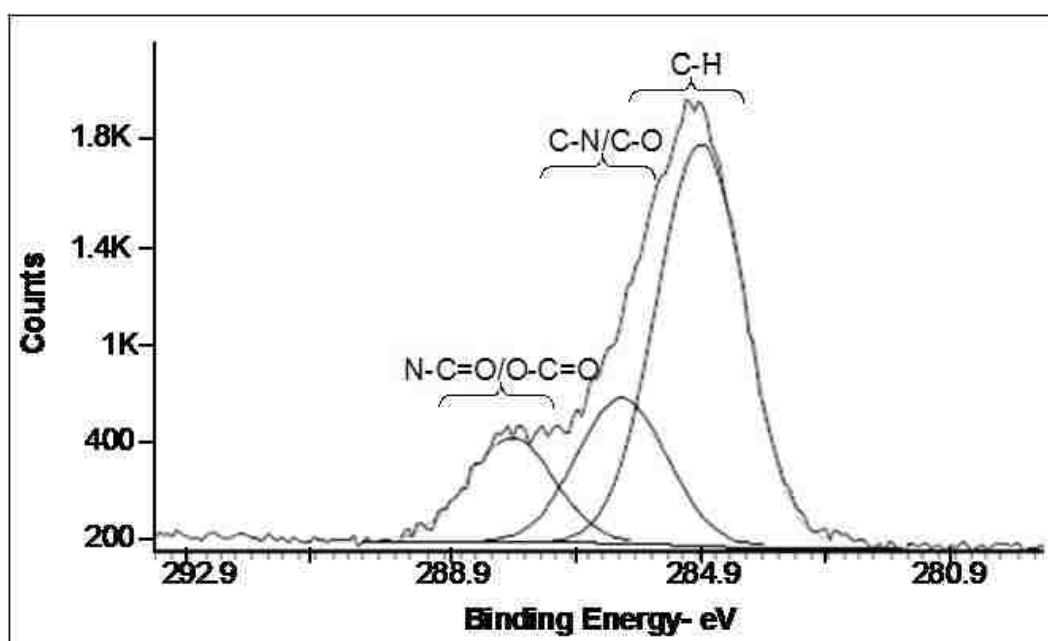


Figure 3.1: Representative high resolution XPS C1s spectrum of spNIPAM surfaces. The peak at 288.0 eV indicates N-C=O, verifying pNIPAM deposition on the surface.

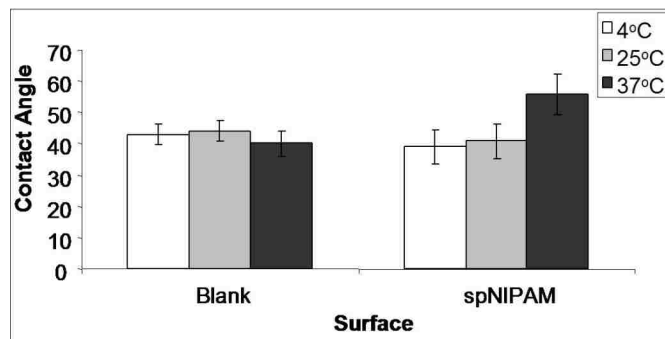


Figure 3.2: Contact angles show hydrophobicity change due to temperature shift in spNIPAM surfaces (right) as compared to control Si chips (left). Student t-test proves that above the LCST of pNIPAM (37 °C, black), spNIPAM surfaces are relatively more hydrophobic than spNIPAM surfaces below the LCST (4 °C, white; and 25 °C, grey) with 99% confidence.

3.3.2 Kinetics of BAEC release

At culture temperature (37 °C), the response of BAECs to spNIPAM surfaces is similar to glass controls; the BAECs have the cobblestone morphology indicative of a confluent sheet of BAECs. (See Figure 3.3, upper right and lower right corners). After the cells achieved confluence, the medium was replaced with a new solution to initiate detachment, such as serum-free media (SFM), media with serum (MWS), Dulbecco's phosphate-buffered saline (DPBS), or serum free media with a Dulbecco's phosphate-buffered saline wash (DPBS/SFM). The solution itself was either above (37 °C), below (25 °C), or well below (4 °C) the LCST of the polymer. Representative microscopy images from BAECs rinsed using SFM at all three temperatures are presented in Figure 3.3.

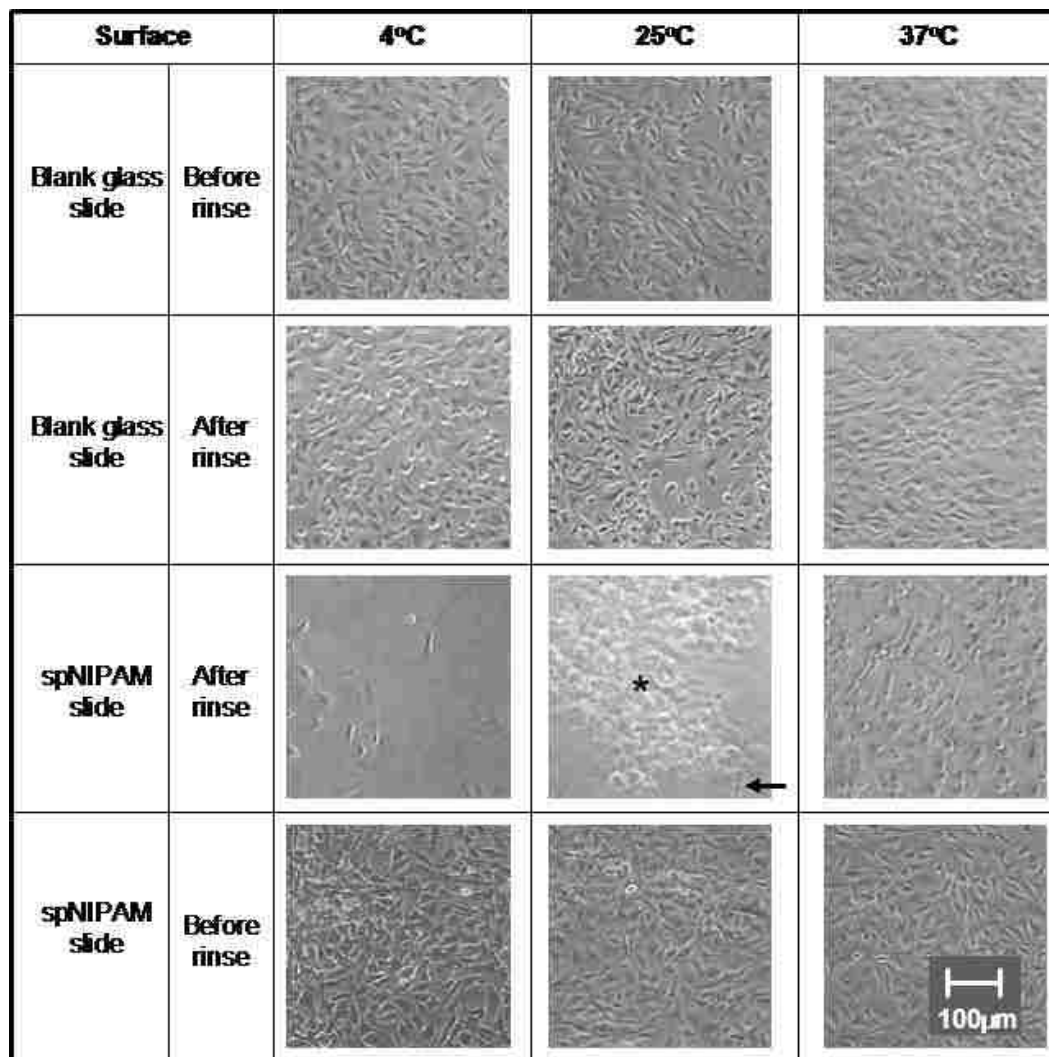


Figure 3.3: Representative cell adhesion and detachment images obtained from BAECs on blank glass (top and top middle rows) and spNIPAM surfaces (bottom and bottom middle rows). Cells grown to confluence (i.e., before rinse) have a cobblestone morphology. Following rinse with SFM at 4 (left column), 25 (middle column), or 37 °C (right column), aggregated clumps of cells detach from spNIPAM surfaces (indicated by asterisk). A cell that is still attached to the surface is indicated by an arrow. Best release was observed at 4 °C on spNIPAM surfaces.

Detachment times are compiled in Figures 3.4 and 3.5, as well as Table 3.3, in which they are compared to those obtained from cells detached using trypsin (a

conventional technique for cell detachment,^{24, 26, 27, 139} which is provided as a standard positive control for comparison).

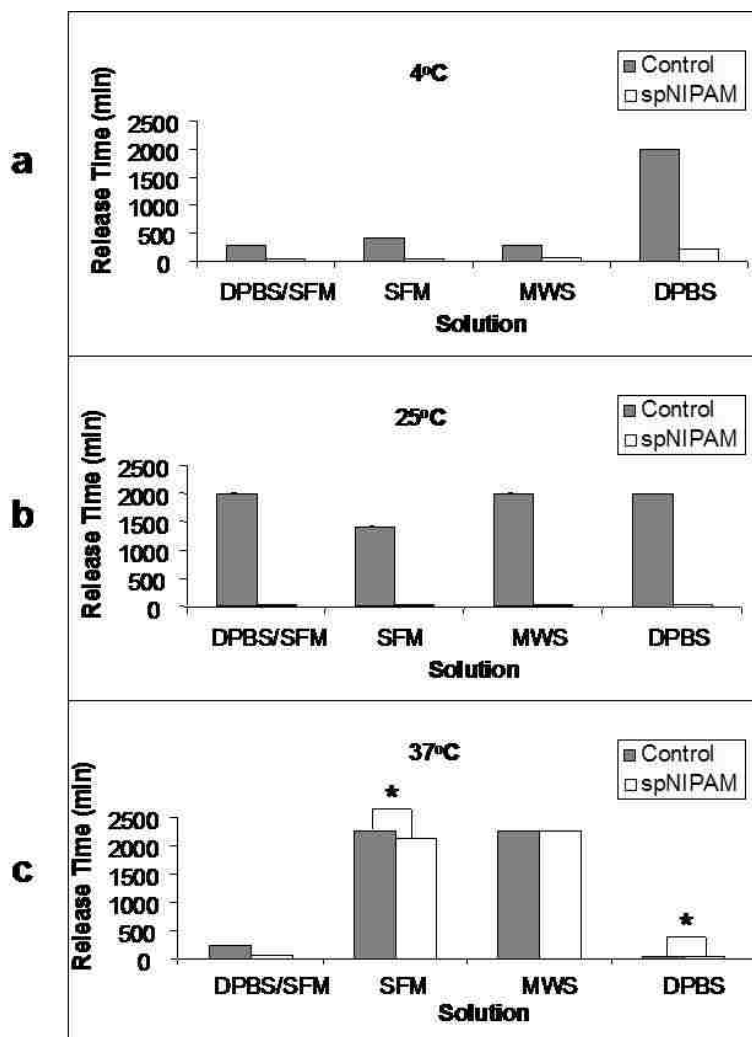


Figure 3.4: Time required for 100% BAEC detachment from control (grey) and spNIPAM (white) surfaces using media with serum (MWS), serum free media (SFM), DPBS, and SFM with a DPBS wash at 4 (a), 25 (b), or 37 °C (c). Asterisks are used, where it is not obvious, to indicate a difference between the control and spNIPAM surfaces that was 95% significant or more determined using a student t-test. The most significant difference occurred at 25 °C.

Above the LCST of the polymer (37 °C), it is evident that cells do not detach

from spNIPAM or the control glass blanks using the SFM solution within the experimental time frame (2000 minutes). (See Figure 3.3, right column; Figure 3.4c; and Table 3.3). The same is true for cells rinsed with MWS: no appreciable cell detachment is observed from either spNIPAM or the control glass blanks. These results are consistent with previous reports that the solution used must be below the LCST of the polymer to stimulate detachment.^{149, 150} However, it was surprising to note that both the spNIPAM *and* the control glass blank surfaces rinsed with DPBS or DPBS/SFM at 37 °C release cells (within 34 and 62 minutes, respectively). One possible explanation for this result is that DPBS does not contain calcium or magnesium, both of which are known to promote cell attachment.¹³⁹ As the BAECs had been cultured using serum containing both calcium and magnesium, use of DPBS in this step may therefore create an ionic imbalance. This may result in the release of calcium and magnesium from the cells, thereby promoting cell detachment, even though the solution is above the LCST of the polymer.

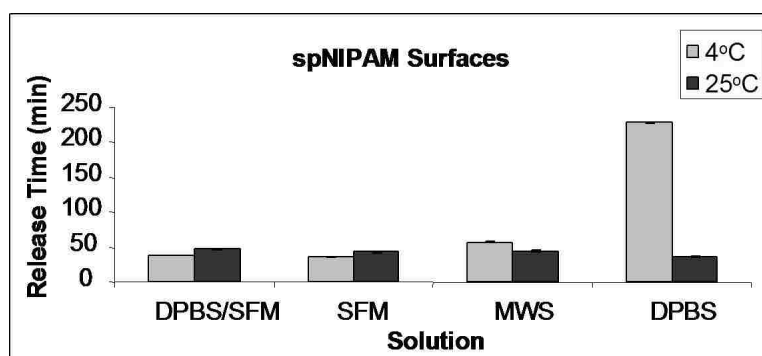


Figure 3.5: Comparison of BAEC release time from spNIPAM coated surfaces at 4 (light grey) and 25 °C (dark grey). Student t-test proves that all 4 and 25 °C release times are more than 99% significantly different. SFM at 4 °C proved to have the best release time.

Below the LCST of the polymer (25 °C), BAECs were released from the spNIPAM substrates using each of the solutions tested in under an hour. (See Figure 3.3, top middle row; Figure 3.4b; and Table 3.3) Of the solutions tested, release using SFM was the fastest at 37 minutes. The most likely explanation for why detachment initiated using SFM is more rapid than using MWS is that SFM does not contain additives normally found in serum (e.g., growth factors) that promote cell adhesion/resist cell detachment. In contrast with the results obtained at 37 °C, no cell detachment is from the control glass blanks using any of the solutions tested (including DPBS and DPBS/SFM) within the experimental time frame.

When well below the LCST of the polymer (4 °C), there is release from spNIPAM-coated surfaces. (See Figure 3.4a) When MWS is used to initiate detachment, the time for release is 13 minutes faster at 25 °C than at 4 °C. (See Figure 3.5) This result is consistent with observations by Okano that extremely cold MWS slows cell detachment.¹³⁹ When DPBS is used to initiate detachment, the difference in release time is even more striking, as it is 13 minutes faster at 4 °C than at 25 °C. However, the time frames for release using DPBS/SFM and SFM are actually faster at 4 °C than at 25 °C (8.8 minutes and 6.8 minutes, respectively). These results indicate that for SFM and DPBS/SFM, detachment is faster at 4 °C than at 25 °C, contradicting the hypothesis that cells must be near normal cell culture temperatures and remain metabolically active to achieve pop off.

Table 3.3: BAEC release times when 4 °C solutions were used during cellular release on blank glass slides (controls) and spNIPAM surfaces. Cell release using trypsin/EDTA is provided as a positive control for comparison. There is a large difference between the controls and the spNIPAM surfaces, indicating that the pNIPAM thermoresponse is causing cellular release. The most efficient cell release was achieved using SFM.

Solution	Surface	Release Time (min)
SFM	Control	407.1 ± 0.2
	spNIPAM	36.1 ± 0.3
DPBS rinse, SFM	Control	294.5 ± 0.2
	spNIPAM	37.6 ± 0.3
DPBS	Control	2000 ± 0.6
	spNIPAM	228.9 ± 1.0
MWS	Control	280.5 ± 0.6
	spNIPAM	57.4 ± 0.6
.25% Trypsin/EDTA	Control	5.5 ± 0.8
	spNIPAM	5.6 ± 1.0

3.4 Conclusions

This work presents a study of the effect of the solution and temperature used to initiate cell detachment from pNIPAM on the time required to achieve 100% detachment of cells. The pNIPAM films used in this work were generated using a novel technique using a spin-coated solution containing pNIPAM (“spNIPAM”).

The fastest, most reliable release of cells occurred below the LCST of the polymer at 4°C in serum free media (SFM). This result contradicts previous findings by Okano, et al., that cell release is significantly slower at 4 °C versus 25 °C.¹¹⁸ However, the authors of that work used media with serum (MWS) instead of SFM, which, as presented, results in slower detachment than SFM in general. In some cases, it may be desirable to stop cell metabolism at the time of detachment (e.g., to “freeze” protein expression prior to subsequent analysis). In such cases, the use of extremely cold SFM would be ideal.

Chapter 4: A Low-Cost, Rapid Deposition Method for “Smart” Films: Applications in Mammalian Cell Release

Initially published by Reed, J.A.; Lucero, A.E.; Ista, L.K.; Bore, M.; López, G.P.; and Canavan, H.E. in *ACS Applied Materials & Interfaces*.¹⁵¹

4.1 Introduction

PNIPAM has been utilized for the controlled attachment and release of bacteria,^{152,153} biosensors,¹⁵⁴ and tissue engineering.¹⁵⁵ All of these applications first require the deposition of pNIPAM onto a cell culture substratum. There are many methods used to polymerize NIPAM, such as free radical polymerization using a variety of initiators and solvents,^{156,157,158} or redox initiation using a variety of initiators and accelerators.^{159,160} Free radical polymerization, or ATRP, has the advantages of mild reaction conditions, the ability to use a wide range of monomers, and is insensitive to impurities, such as water, that are present during the reaction.^{161,162} Electron beam irradiation is a process that can be completed in mild conditions (e.g., room temperature, in water, at physiological pH), allows for high depth penetration, and does not need crosslinking or initiator agents.¹⁶³ The disadvantages to the techniques described above are that the surface that is coated usually has to be a flat surface (in the case of pouring and drying a solution¹⁶⁴), or is dependent upon a specific surface chemistry (in the case of activated substrates¹⁶⁵ and ATRP¹⁶⁶). A review of some common deposition methods used for to create pNIPAM films was recently published by Da Silva.¹⁴⁵

Most of the aforementioned methods require expensive equipment and long

deposition times. In addition, system calibration for these methods can be extensive and time intensive. Recently, Rao et al. patented a novel low-cost method for the rapid co-deposition of pNIPAM with a tetraethyl orthosilicate (TEOS) based sol-gel (spNIPAM).^{146,132} That work focused on the use of spNIPAM for the thermoresponsive membranes, with no investigation of their use for mammalian cell culture. In this work, spNIPAM is adapted for the reversible adhesion of mammalian cells, and explore its applications for bioengineering. Following characterization of these substrates using traditional surface chemistry techniques (e.g. X-ray photoelectron spectroscopy, XPS; and contact angle measurements), identical populations of bovine aortic endothelial cells (BAECs) were grown to confluence on treated glass slides. From these results, it was concluded that 0.35 wt% pNIPAM/TEOS (or 0.35 wt% spNIPAM) surfaces demonstrated the best thermoresponse and cellular response, thus generating affordable pNIPAM substrates. In addition, the current method only requires TEOS, pNIPAM and minor instrumentation (spin coater ~\$5K) compared to ~\$35K for an RF plasma reactor.

4.2 Experimental Methods

The majority of the experiments carried out herein follow the procedures outlined in Chapter 2, including pNIPAM deposition, XPS, contact angle goniometry, and cell culture. Three repetitions of all experiments, producing three surfaces, were performed. Each surface was analyzed in three spots, for a total of 27 analyses.

4.2.1 Sol-gel and pNIPAM preparation

35 mg of pNIPAM, 5 mL of distilled water, and 200 μ L of 1 Normal HCl were mixed, and a weight percentage of pNIPAM was determined. This solution is referred to as “pNIPAM only.” In a separate container 250 μ L TEOS sol (1 TEOS:3.8 ethanol:1.1 water:0.0005 HCl), 43 μ L distilled water, 600 μ L ethanol were mixed and weighed. This solution is referred to as “TEOS only.” To obtain different weight percentages of pNIPAM in sol, the appropriate amount of the pNIPAM solution was added to the pure TEOS in order to achieve the desired weight percentages for spNIPAM surfaces (ex. 3.5g pNIPAM solution added to 996.5g TEOS sol).

4.2.2 Sol and pNIPAM deposition

100-200 μ L of the prepared solution was evenly distributed on clean surfaces placed on a spin coater, model 100 spinner from Brewer Science, Inc. (Rolla, MO). These surfaces were then spun at 2000 rpm for 60s. The surfaces were stored under nitrogen in a Parafilm covered Petri dish until either used for a) surface analysis, or b) cell culture tests.

4.3 Results and Discussion

4.3.1 Characterization of surfaces

The spNIPAM surfaces are composed of a sol-gel (TEOS) and pNIPAM. To affect mammalian cell release, verification that the LCST occurred between room temperature (~ 25 °C) and cell culture temperature (~ 37 °C) was necessary.

Contact angle measurements, shown in Figure 4.1, indicate that there is a difference in the wettability of spNIPAM surfaces when the temperature is shifted from above the LCST (i.e. 37 °C) to below the LCST (i.e. 25 °C). However, the only statistically significant change, $13^\circ \pm 7^\circ$, was seen on 0.35 wt% spNIPAM surfaces. As expected, TEOS and control surfaces showed no statistically significant changes. The absence of a statistically significant contact angle change on the other surfaces suggests a lack of intact pNIPAM on the surface, possibly from delamination of the films.

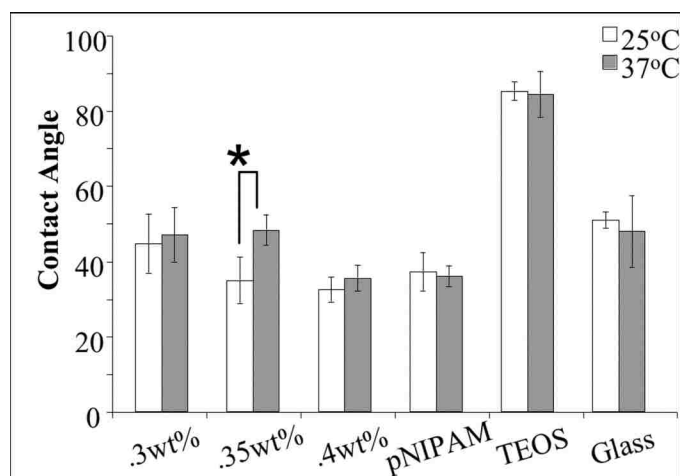


Figure 4.1: Contact angles show hydrophobicity change due to temperature shift from room temperature (25 °C in white) to culture temperature (37 °C in grey). A statistically significant change is demonstrated on 0.35 wt% spNIPAM surfaces, indicated with an asterisk.

The elemental composition determined via XPS indicated the presence of nitrogen on spNIPAM and pNIPAM only surfaces, thus verifying the presence of NIPAM (see Table 4.1). A similar trend is illustrated in the high resolution carbon spectrum (see Table 4.2 and Figure 4.2) with the C-OH/C-N peaks. Theoretical

values determined from the stoichiometry of the monomer (75% C, 12.5% O, 12.5% N) closely match those from the pNIPAM only surfaces (71.8% C, 11.9% O, 9.9% N, 6.4% Si), with the exception of the Si peak. Unlike the spNIPAM surfaces that have Si from TEOS, the Si peak on pNIPAM only surfaces most likely arises from the underlying Si chip. As there is a Si peak, the film thickness is less than 100 Å (the approximate sampling depth of the technique).¹²²

Table 4.1: Major elemental relative atomic percentages from XPS comparing spNIPAM and control surfaces. n=9 for all surfaces, with a standard deviation of less than 3%.

	Relative Atomic %			
	C	N	O	Si
Theoretical	75.0	12.5	12.5	0.0
0.3wt%	32.4	3.0	45.9	18.6
0.35wt%	34.9	4.2	41.8	19.0
0.4wt%	33.2	3.7	43.9	19.2
pNIPAM	71.8	11.9	9.9	6.4
TEOS	35.5	0.0	47.9	16.6
Blank Si	8.3	0.0	40.5	51.1

Table 4.2: Relative atomic percents from high resolution C1s comparing spNIPAM and control surfaces. N=9 for all surfaces, with a standard deviation of less than 3%.

	Relative Atomic %		
	CH (285eV)	CO/CN(+1.5)	O=C-N(+3.0)
Theoretical	66.7	16.7	16.7
0.3wt%	61.7	27.5	10.8
0.35wt%	60.0	27.0	13.0
0.4wt%	59.7	28.7	11.6
pNIPAM	65.0	22.3	12.7
TEOS	47.0	53.0	0.0
Blank Si	95.4	4.6	0.0

4.3.2 Cellular response

At 37 °C, cells adhered and proliferated equally well on all surfaces. After decreasing the temperature to 4 °C, cells were detached, with the most cell detachment occurring on 0.35 wt% spNIPAM surfaces (see Figure 4.3 and Table 4.3). This correlates with the observation that 0.35 wt% spNIPAM also had only significant contact angle change. In addition, while preparing the sol-gel/pNIPAM for deposition, it was observed that in the 0.4 wt% spNIPAM mixtures the pNIPAM would precipitate out.

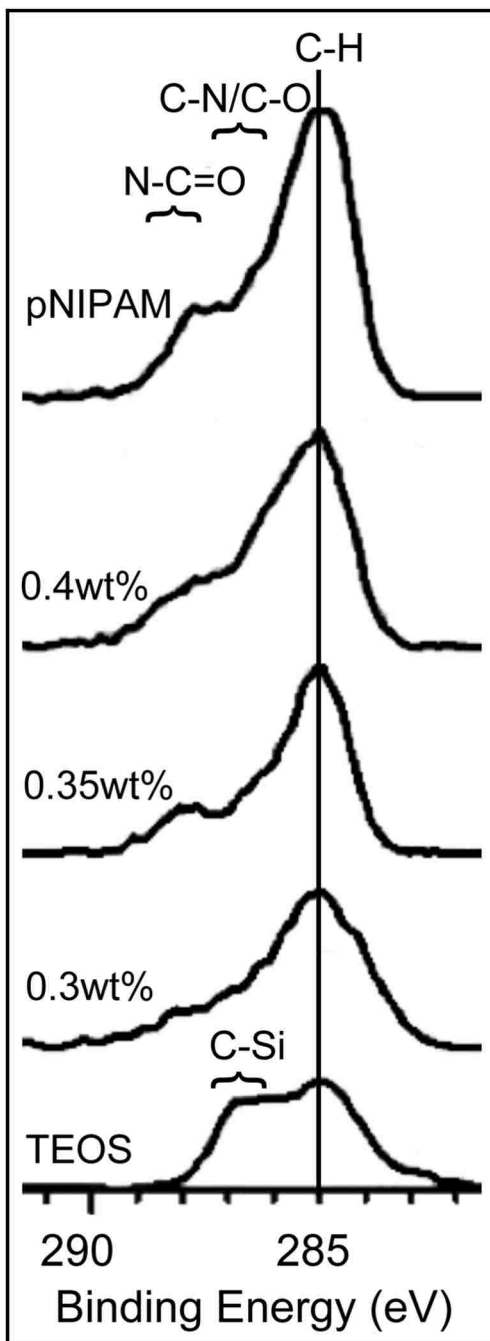


Figure 4.2: Panel of representative high resolution XPS C1s spectra for spNIPAM only, 0.4 wt% spNIPAM, 0.35 wt% spNIPAM, 0.3 wt% spNIPAM, and TEOS only. The top four spectra all look similar, with peaks at 286.5 and 288 eV indicating successful deposition of pNIPAM.

This observation would explain a lack of thermoresponsive pNIPAM on the

surfaces. In contrast, control surfaces composed of TEOS and blank glass cover slips did not release cells. All surfaces with pNIPAM demonstrated some cell detachment with the least detachment on pNIPAM only surfaces. This suggests co-deposition with TEOS enhances cell release, possibly by stabilizing the films and inhibiting delamination. It is also interesting to note that cells released from the center of surfaces in the form of aggregated clumps, as indicated in Figure 4.3 by asterisks. This phenomena is further investigated in Chapter 5. This is in contrast to other deposition methods, such as plasma deposited pNIPAM (ppNIPAM), where the cells release in confluent sheet starting at the edges of the surfaces.¹⁶⁷

Table 4.3: Bovine aortic endothelial cell release from spNIPAM (shaded grey) and control surfaces. n=9 for all surfaces with a standard deviation of less than 2%.

Surface	% Cell Release
0.3wt%	39.3
0.35wt%	75.3
0.4wt%	65.1
pNIPAM	30.4
TEOS	0.0
Blank Glass	0.0

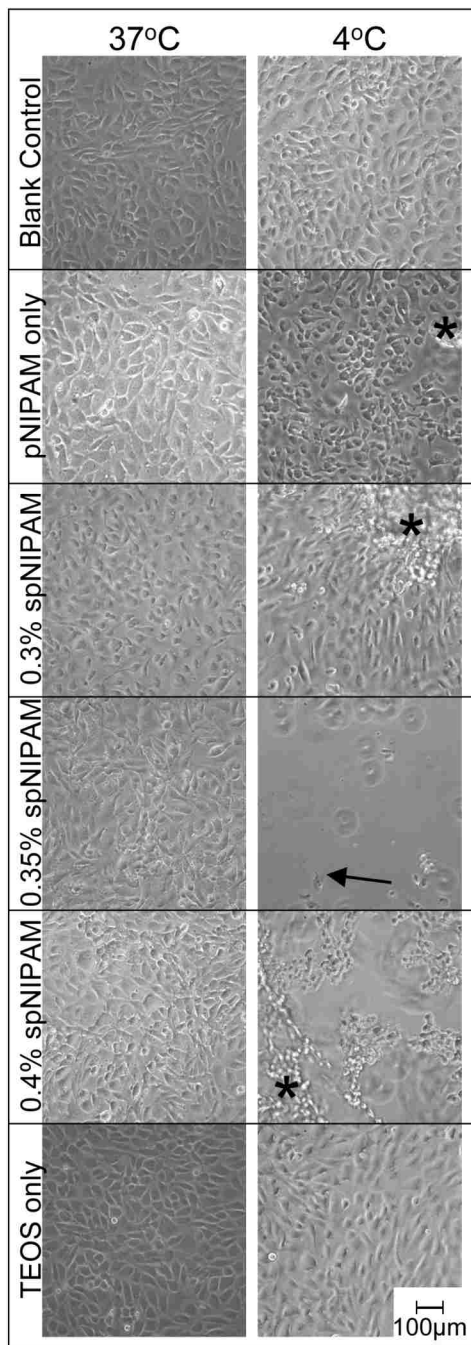


Figure 4.3: Representative cell images after cell detachment procedure showing the most cell detachment from 0.35wt% spNIPAM. The arrow indicates a cell is still attached to the surface. There was no cell detachment on the blank control slide and moderate detachment from 0.3wt% and 0.4wt% spNIPAM surfaces. The asterisks indicate aggregated clumps of cells that are releasing from the surface.

4.4 Conclusions

A method developed by Rao et al. was successfully adapted for the deposition of pNIPAM for bioengineering applications. Using this pNIPAM in conjunction with a sol-gel was found to be instrumental in maintaining film integrity during experimentation, where thermoresponse and cell detachment properties were tested. This method allowed for relatively inexpensive and quickly fabricated surfaces. Determination of the amount of pNIPAM to sol-gel demonstrated that 0.35wt% spNIPAM surfaces had both the best thermoresponse and cell release. Cells detach from the spNIPAM surface as isolated cells or aggregated clumps, which may limit the utility of this technique for cell sheet engineering, where intact sheets are desired. However, this technique is a simple and affordable alternative to previously described pNIPAM deposition methods for those applications that do not require intact cell sheets, such as protein preconcentration or biofouling release.

Chapter 5: Effect of Polymer Deposition Method on Thermoresponsive Polymer Films and Resulting Cellular Behavior

Published by Reed, JA; Love, S.; Lucero, A.E.; Haynes, C.; Canavan, H.E. in *Langmuir*.¹⁴⁰

5.1 Introduction

As was discussed in Chapter 2, pNIPAM has been used for a wide range of applications. Depending on the application, the method used to deposit the pNIPAM film may be altered to achieve the desired properties, as reviewed by Da Silva.¹⁰ Many techniques exist for the deposition of pNIPAM films (e.g., electron beam ionization,¹⁶⁸ grafting by UV,¹⁶⁹ and atom transfer radical polymerization^{161, 170}), but not all are compatible with cell culture, which is performed using sterile, optically transparent tissue culture polystyrene (TCPS) plates. In addition, few direct comparisons have been made between these methods to determine which method is most ideal for use with mammalian cells. In this work, two methods of deposition: plasma polymerization (ppNIPAM)¹⁵ and deposition of pNIPAM with a sol-gel (spNIPAM)¹⁶ are compared. These techniques were optimized separately^{15, 16} (see Chapter 4 and Lucero's thesis¹⁷¹) to ensure that the ideal conditions for both were used to perform the comparisons made in the current work. Additional surface characterization including time-of-flight secondary ion mass spectroscopy (ToF-SIMS) and atomic force microscopy

(AFM) were performed to determine the source of the differences in these two deposition methods. Furthermore, cell response to these surfaces was examined using carbon-fiber microelectrode amperometry (CFMA) to assess exocytosis function. From surface characterization of the resulting substrates, it was found that successful deposition of pNIPAM may be achieved using either deposition method, but AFM revealed a difference in topography that could explain why the cells responded differently depending on the deposition method. Amperometry studies indicate that mammalian cells grown on ppNIPAM behave more similarly to cells grown on uncoated glass, suggesting that ppNIPAM is more applicable for mammalian cell studies. From these results, it was concluded that deposition of pNIPAM using plasma polymerization yields films that have the best thermoresponsive and mechanical properties, as well as minimal impact on cellular viability and function.

5.2 Experimental Methods

The majority of the experiments carried out herein follow the procedures outlined in Chapter 2, including pNIPAM deposition, XPS, AFM, contact angle goniometry, and cell culture. Three repetitions of all experiments, producing three surfaces, were performed. Each surface was analyzed in three spots, for a total of 27 analyses.

5.2.1 MAMC cell culture

MAMC cells used as they have been fully characterized for amperometry experiments. This cell culture was performed in the laboratory of Prof. Christy

Haynes at the University of Minnesota (UMN). Primary culture murine adrenal medullary chromaffin cells (MAMC) were harvested from wild-type brown male mice (C57BL/6J, Jackson Laboratories, Bar Harbor, ME) less than 4 months of age, as previously described.¹⁹ Briefly, following euthanasia both adrenal glands were located and excised; then, cortical tissue was removed to reveal the medullary tissue. The medullary tissue was digested with neutral protease (Worthington Biochemical Corporation, Lakewood, NJ) for 30 minutes, rinsed with DMEM/F12 media (Hyclone, Logan, UT), triturated to create a cell suspension and then plated. All mice handling was done in accordance with the University of Minnesota Institutional Animal Care and Use Committee practices established under approved protocol #0509A75006.

5.2.2 Carbon-fiber Microelectrode Amperometry (CFMA)

This work was conducted at the University of Minnesota by our collaborators Sara Love and Christy Haynes. Exocytosis is used by the cell to excrete vesicles containing proteins and lipids, as shown in Figure 5.1. Using CFMA these exocytosis events are monitored using a microelectrode to collect a wealth of information. (See Figure 5.2 and 5.3) For instance, the spike frequency detected is an evaluation of the number of exocytosis events. When this value from cells on a surface are compared to a control surface that the cells would normally grow on, the spike frequency can be used to infer vesicle fusion events. If the spike frequency is higher on a coated substrate, this means that there has been a cytoskeletal reorganization that has led to more exocytosis events, or over

activation of the cell, which would be undesirable if these cells needed to model “normal” cells.

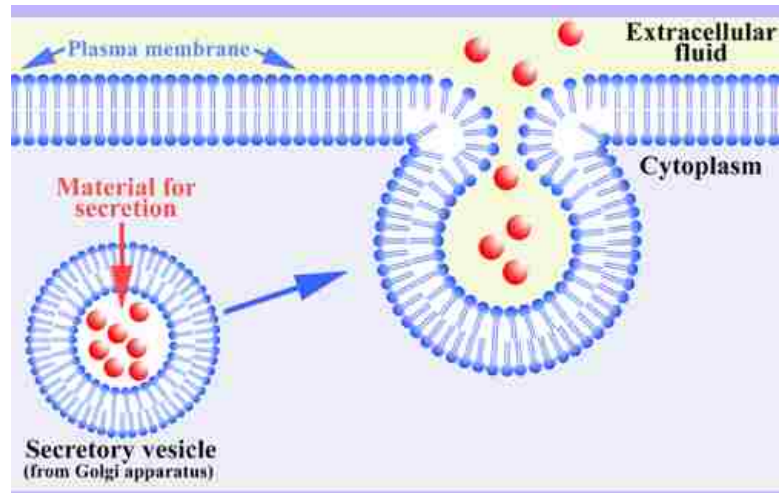


Figure 5.1: Exocytosis, as illustrated above, is the fusion of vesicles from inside of the cell with the membrane of the cell, to release proteins and lipids.¹³³

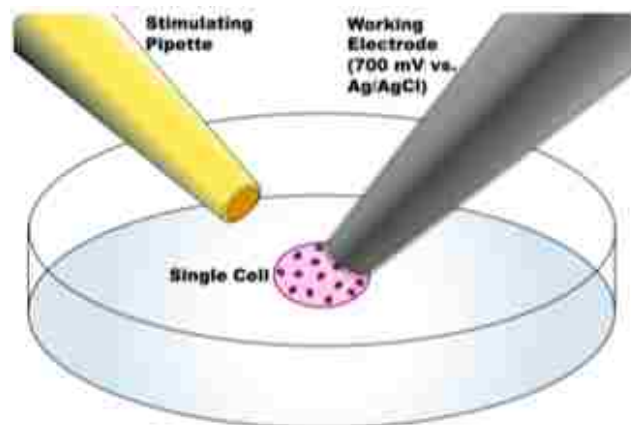


Figure 5.2: Schematic of CFMA, where a stimulating pipette encourages exocytosis, while an electrode collects information on each exocytosis event.

The number of molecules released, Q , describes the magnitude of signaling response while the average $t_{1/2}$, or full-width at half-maximum, describes the

kinetics of exchange between the vesicle and extracellular space. These two features provide insight into specific components of exocytosis. If the $t_{1/2}$ is perturbed that would mean that the surface is affecting the extracellular space in a manner that is reducing the kinetics of release by changing the osmolarity gradient.

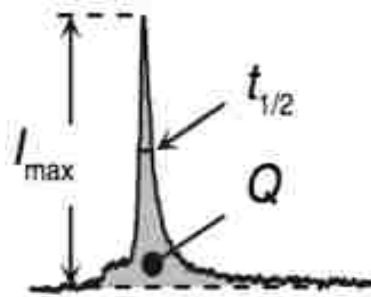


Figure 5.3: A single peak from CFMA data illustrating each element that is analyzed. The $t_{1/2}$ (peak half width) is related to the time for full fusion of vesicles with the cell membrane and Q (area) corresponds to the number of molecules released. Each peak (or spike) represents an exocytosis event.

Q is calculated by Faraday's law, shown in Equation 2,

$$Q = nNF, \quad \text{Equation 2.2}$$

where Q is the charge, n is the number of electrons in the oxidation (2 for epinephrine), N is the number of moles of epinephrine secreted and F is Faraday's constant). If Q is perturbed, the number of molecules released from each exocytosis event is changed. A similar problem is seen when there is a change in spike frequency, indicating that the exocytosis events are not consistent with normal cell growth. By examining these three specific characteristics, average Q , $t_{1/2}$, and frequency, one can determine if there are

alterations to normal cell signaling via exocytosis, after exposure to coated surfaces fabricated using various deposition methods.

To conduct these studies, carbon-fiber microelectrodes and stimulating pipettes were fabricated in-house at University of Minnesota, following previously published methods.¹⁶ A single carbon fiber (Amoco, Greenville, SC) was aspirated into a glass capillary (AM Systems, Carlsberg, WA). It was then pulled, trimmed, epoxied (Epoxy Technology, Billerica, MA) and cured. (See Figure 5.4) Electrodes were beveled at 45° using a diamond polishing wheel and soaked in isopropyl alcohol saturated with activated carbon for a minimum of 10 minutes prior to use.

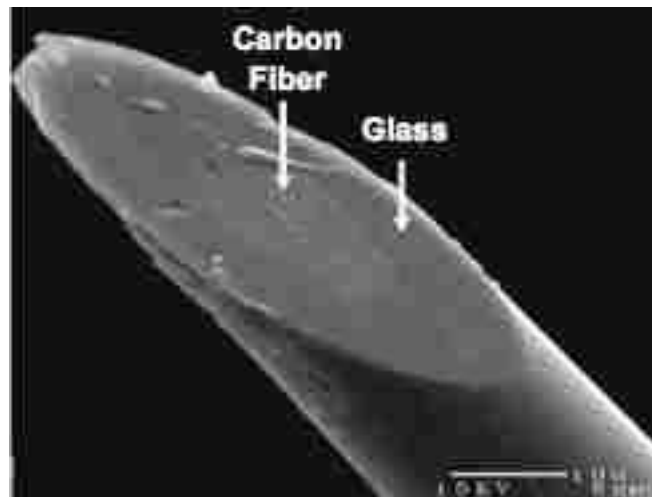


Figure 5.4: Carbon fiber in a glass capillary, to form a microelectrode for CFMA.

Microelectrode experiments were performed, as described previously,¹⁷⁻²⁰ on a Nikon® Eclipse TE2000U inverted microscope (Nikon USA, Melville, NY) equipped with Burleigh PCS500 piezoelectric micromanipulators (EXFO Photonics Solutions Inc, Mississauga, Ontario). Cell medium was removed from

the Petri dish and was replaced with warmed Tris buffer (300 mM sodium chloride, 12.5 mM trishydroxymethylaminomethane, 8.4 mM potassium chloride, 5.6 mM R-D-glucose, 4.5 mM calcium chloride, and 4.2 mM magnesium chloride). The temperature of the dish was maintained at 37°C with a TC-324B single channel temperature controller (Warner Inst, Hamden, CT) throughout experiments. The stimulating pipette was positioned approximately 30 to 50 μm from the cell being examined, and exocytosis was stimulated using a 3-second-bolus of 60 mM K^+ , delivered using a 1.5 psi nitrogen pulse. The microelectrode was held at +700mV vs. Ag/AgCl reference electrode to oxidize only secreted epinephrine/norepinephrine while current was monitored. Recording began three seconds prior to stimulation of exocytosis and data was collected for a total of 30 seconds. The current recording was obtained using an Axopatch™ 200B potentiostat (Molecular Devices, Inc., Sunnyvale, CA) where oxidation current was low-pass Bessel filtered (5 kHz) and amplified (20 mV/pA). This was collected using a home-built breakout box in combination with Tarheel Electrochemistry software run in LabVIEW™ (National Electrochemistry Suite software module in LabVIEW, National Instruments, Austin, TX). Exocytosis release was monitored from multiple cells in a dish within two hours of removal from incubation conditions, which typically resulted in traces from 5 to 15 cells per culture dish.

5.3 Results and Discussion

pNIPAM has many potential applications, thus there are many methods of

deposition used to tailor the coating to each use. For example, SAMs and ATRP deposition methods are used for bacterial studies, while electron beam ionization is used for tissue engineering. Each of the aforementioned techniques results in different surface characteristics. For instance, the change in wettability of these pNIPAM surfaces yield contact angles between 5°-65°. ³²⁻³⁴ Since differences in surface characteristics can influence cell attachment, proliferation, and release, ³⁵ a multiple surface analysis approach was used to compare the two deposition methods of interest, followed by cellular response studies, to verify that these surfaces are biocompatible and support the maintenance of normal cellular functions.

Previous work has investigated two promising pNIPAM deposition methods, including plasma polymerization (ppNIPAM)¹⁵ and deposition of pNIPAM with a sol-gel (spNIPAM).¹⁶ Using these two methods, it was observed that there are distinct differences in the cell response to the substrate coatings, and it was hypothesized that pNIPAM deposition must not only be altered to fit the substrates and surface chemistries necessary for the desired application, but also to obtain the least altered cell response. To test this hypothesis, this work compared the two methods currently used to deposit pNIPAM for applications using mammalian cells.

5.3.1 Surface characterization

XPS was used to ensure that pNIPAM was successfully deposited, regardless of deposition method. The presence of nitrogen in the elemental XPS data (see

Figure 5.5) demonstrates that both ppNIPAM and spNIPAM deposition methods resulted in pNIPAM substrates. The ppNIPAM substrates more closely mimicked the theoretical relative atomic percentages that were determined from the monomer structure. However, this is mainly due to the large presence of silicon in the spNIPAM surfaces, since this method requires the use of a silicon-based sol-gel (TEOS). The amide (288 eV) and amine (286 eV) peaks on the XPS high resolution C1s spectra also indicated pNIPAM deposition (see Figure 5.6). Unlike in the elemental XPS data, the high-resolution C1s spectra of spNIPAM and ppNIPAM were very similar, thus supporting the fact that the relative atomic percentages for spNIPAM in Figure 5.5 were different from ppNIPAM and theoretical values due to the Si peak from the sol-gel.

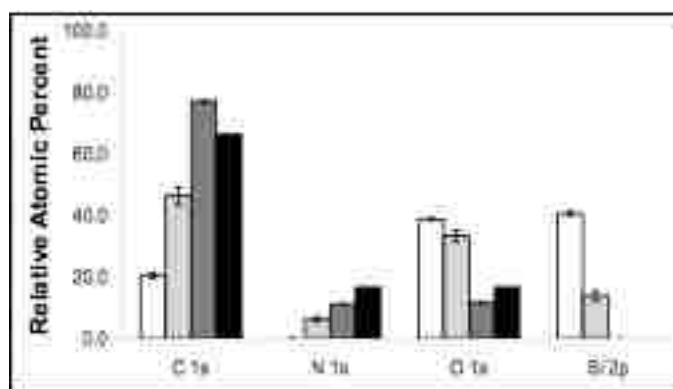


Figure 5.5: XPS elemental analysis of ppNIPAM (dark grey), spNIPAM (light grey), and blank Si controls (white). The presence of N1s on the ppNIPAM and spNIPAM surfaces indicates successful deposition of pNIPAM. When compared to the theoretical composition determined from the NIPAM monomer (black), ppNIPAM is most similar.

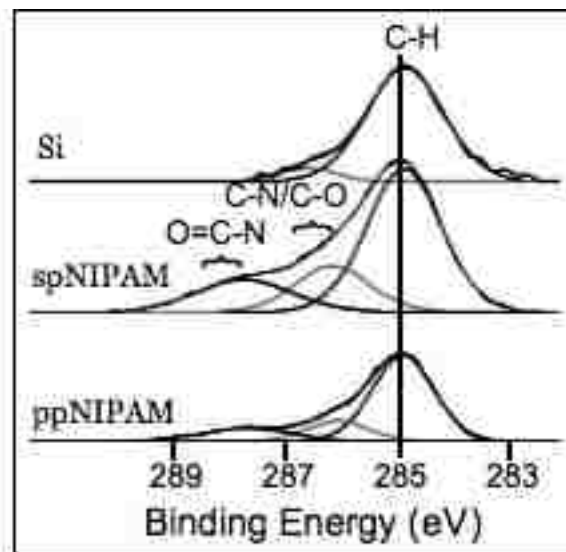


Figure 5.6: XPS high resolution C1s spectra of a blank Si control (top), spNIPAM (middle), and ppNIPAM (bottom) films. Presence of amide and amine peaks confirm pNIPAM deposition using both ppNIPAM and spNIPAM deposition methods.

ToF-SIMS was used to further characterize the surfaces. While XPS can determine the molecular bonding environments present and the elemental make up of a substrate, ToF-SIMS is useful for analyzing the molecular fragments present.^{134, 135} However, due to the complex data sets generated via ToF-SIMS, it is common to use PCA to analyze the data (see Figure 5.7).

The PC2 scores plot demonstrates that there is a distinct difference between the two deposition methods. However, as was shown with XPS, the difference is primarily due to the TEOS fragments. There are pNIPAM fragments in both the ppNIPAM and spNIPAM substrates (e.g. 43 and 57 m/z). However, the spNIPAM surfaces are characterized by more fragments from initial monomer (MW=114), while the ppNIPAM substrates tend to have more fragments with high molecular

weight (e.g. 156 m/z). The plasma used to deposit the ppNIPAM is high energy, thus resulting in larger fragments than those from the spNIPAM substrates where a pre-polymerized pNIPAM was used.

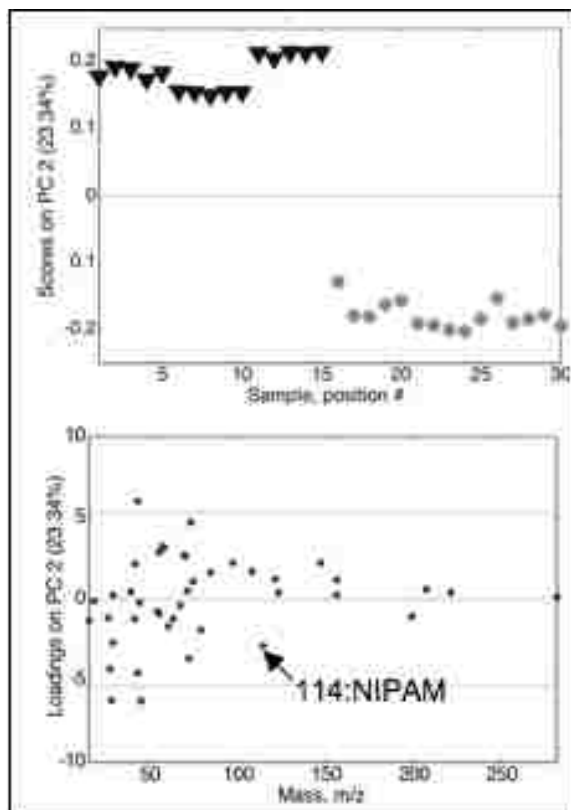


Figure 5.7: PCA scores (top) and loadings (bottom) of ToF-SIMS data collected from ppNIPAM (triangles) and spNIPAM (asterisks) films. There is a distinct separation between the data obtained from samples prepared by the two deposition methods, which is due to the silicon based sol-gel (TEOS) used for spNIPAM deposition.

5.3.2 Thermoresponse

Contact angles were used to determine if there was a change in wettability above and below the LCST (see Table 5.1). Both spNIPAM and ppNIPAM surfaces demonstrated a change in hydrophobicity when the temperature was

shifted from 37 °C to 25 °C.

Table 5.1: Contact angles for ppNIPAM, spNIPAM, and blank Si control surfaces, obtained above (right) and below (left) the LCST. Both ppNIPAM and spNIPAM demonstrated thermoresponse. There was no observable change on the Si controls.

	25 °C	37 °C
Blank Si Control	43 ± 2	44 ± 2
spNIPAM	49 ± 6	62 ± 5
ppNIPAM	24 ± 4	43 ± 9

There was a larger shift in the ppNIPAM substrates ($19 \pm 10^\circ$) than in the spNIPAM substrates ($13 \pm 8^\circ$), a property that may be beneficial when working with mammalian cells, although a shift in contact angles does not always reflect cell response (see Lucero thesis).^{24, 139}

Further investigation of thermoresponse showed a difference in the topography of the surfaces above and below the LCST as revealed by AFM analysis (see Figure 5.8). Above the LCST, at cell culture temperature, both types of surfaces are relatively smooth. Obviously, the spNIPAM surfaces that were spun cast onto substrates are rougher than the plasma deposited surfaces due to the manner of deposition. However, when the polymer swells below the LCST, there are significant differences in the topography depending on the deposition method.

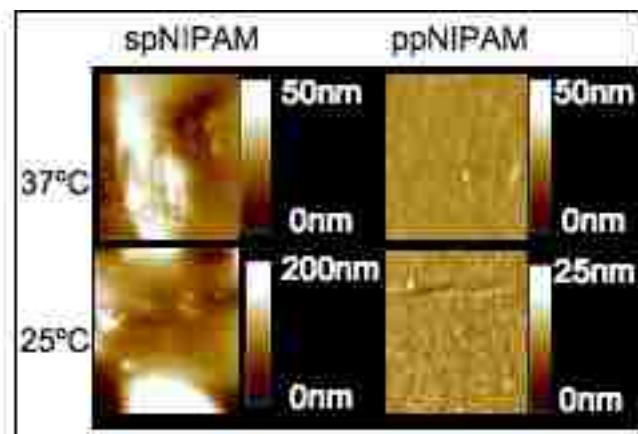


Figure 5.8: AFM images of ppNIPAM (left) and spNIPAM (right) substrates imaged in water above (top) and below (bottom) the LCST. At 37 °C, the surfaces are relatively smooth. However, when the temperature is shifted below the LCST, spNIPAM surfaces are extremely rough.

The spNIPAM surfaces appear to have large islands of aggregated and swollen pNIPAM that create ~200 nm features, with an RMS of 6.8 ± 1.8 . The ppNIPAM surfaces remain relatively flat, with only ~12 nm features, and an RMS of 1.1 ± 0.1 . This is due to the fact that the ppNIPAM surfaces are entirely pNIPAM that is tethered to the substrate, and the spNIPAM has a copolymer that the pNIPAM is separating from upon the change in temperature. This separation was imaged when ToF-SIMS data was collected, and is shown in Figure 5.9.

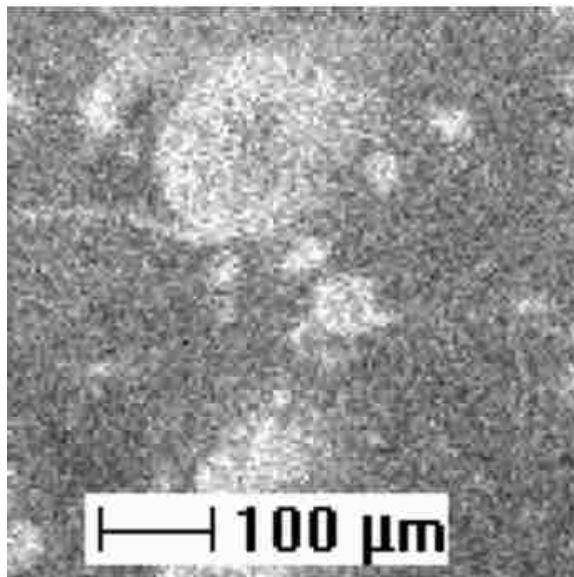


Figure 5.9: Positive ion figure from ToF-SIMS of spNIPAM surface clearly showing physical separation.

5.3.3 Mammalian Cell Culture

BAECs were cultured and proliferated on bare glass, spNIPAM and ppNIPAM substrates. MAMCs were unable to be used for cell detachment studies, as they are primary culture cells that do not proliferate in culture. Previous work suggests that cell-cell interactions have been shown to assist in cell release from pNIPAM.³⁶ Upon changing the temperature to below the LCST, the cells from the pNIPAM coated surfaces did begin to detach from the surfaces; however, the form of detachment varied depending on the deposition method (see Figure 5.10). The spNIPAM surfaces released in small aggregates of cells, consistent with the topographical changes seen using AFM where only large islands on the surface swelled. In contrast, the ppNIPAM surfaces release as full cell sheets, with only a few cells remaining on the surfaces. The uniformity in surface

topography along with the larger shift in contact angles likely determined the success in cell detachment seen using this deposition method.

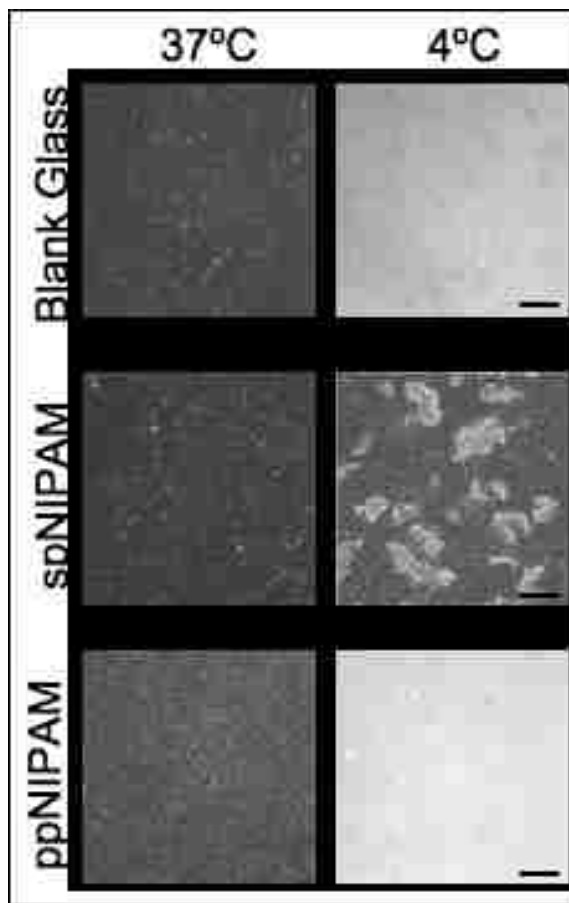


Figure 5.10: Bright field microscopy images of BAECs cultured on spNIPAM (middle), ppNIPAM (bottom), and blank glass control (top) surfaces. The cells attached and proliferated above the LCST (left) on all surfaces. After the temperature was shifted to 4 °C (right), as expected there was no cell release from the control surfaces. There was complete cell detachment from ppNIPAM surfaces as a sheet, but aggregated clumps of cells detached from spNIPAM films. (Black scale bars = 100 μ m)

5.3.4 CFMA Exocytosis Response

CFMA results indicate that these surface coatings do not have an impact in

exocytosis, as there were no perturbations in the average spike frequency for any of the coating conditions ($p > 0.05$, data not shown). Despite this result, cells were found to have altered exocytosis function after 24 hours of culture on both types of pNIPAM surfaces, as shown in Figure 5.11.

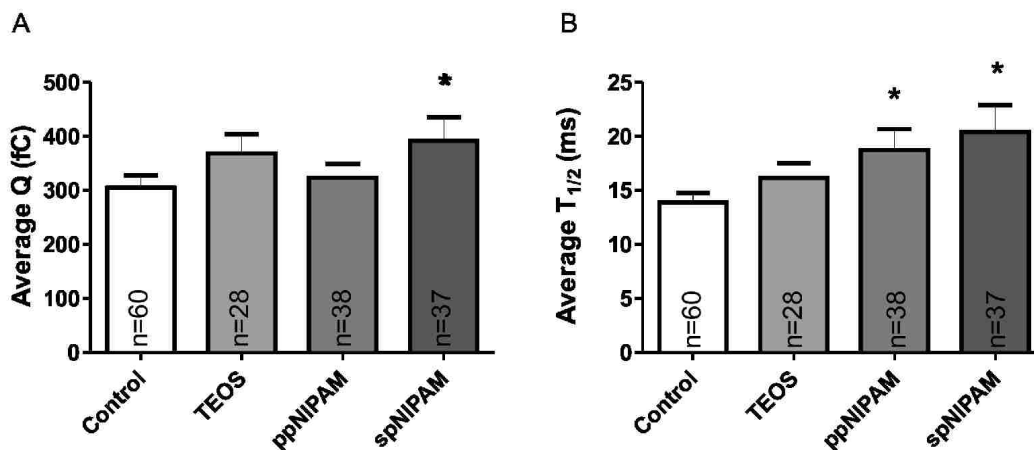


Figure 5.11: CFMA results from cells cultured on glass (white) and TEOS (black) control substrates, as well as spNIPAM (light grey) and ppNIPAM (dark grey) substrates. Perturbations in exocytosis for average charge (Q) and spike half-width ($t_{1/2}$) were revealed to change with surface deposition method, with more perturbations for the spNIPAM deposition. Statistical significance is denoted with * as calculated using a student's t-test, where p was < 0.05 .

In both conditions where pNIPAM surfaces were used, there was a corresponding increase in the spike $t_{1/2}$, 35 and 47% increase for plasma or spin coated surfaces, respectively, indicating that exchange between the vesicle and extracellular space was slowed ($p < 0.05$). As this process gives insight into the release kinetics of the matrix unfolding within the average vesicle, it appears that matrix expansion is inhibited by the presence of the pNIPAM coating, yielding slower release of vesicular content into the extracellular space. As the exchange

between vesicles and extracellular space is driven by a variety of forces, including an osmolarity gradient, the presence of a surface coating is likely to perturb this local environment and thus the driving forces of exchange. This was compared to a TEOS only-coated control, where an increase in $t_{1/2}$ was not seen, indicating that this alteration was specifically a result of the presence of a pNIPAM coating ($p > 0.05$).

Additionally, in the case of cells incubated on spNIPAM, there was also an impact on the average spike area, which is related to the total number of molecules released (see Average Q in Figure 5.11). The presence of the spNIPAM coating lead to an increase in the number of molecules secreted from the average vesicle, going from 960,000 to 1.3×10^6 molecules, a 35% increase ($p < 0.05$). Considering that there are approximately 22,000 vesicles within a single chromaffin cell, if they all released at this augmented level, a single cell would be releasing 4.5×10^9 more chemical messenger molecules. For tissue engineering applications, this type of hyper-activated state and exaggerated release could lead to dire consequences for the resultant tissues. For example, if instead of MAMCs, the engineered tissue contained cells secreting a neurotransmitter like histamine, hundreds to thousands of cells releasing 35% more molecules of histamine would certainly be detrimental to normal growth in this pro-inflammatory state.

These CFMA results suggest that pNIPAM coatings do have effects on the maintenance of normal cell functions during mammalian cell culture in a

deposition-dependent manner. During CFMA studies, it was also clear that there were qualitatively fewer cells in the TEOS only (control) and spNIPAM conditions. This suggests that while both deposition methods can support cell culture, ppNIPAM surfaces allow more normal cells to grow while having a smaller impact on each cell's function.

5.4 Conclusions

In this work, the differences in surface properties and cellular response of two pNIPAM deposition methods were compared. Using a multi-technique approach, including XPS and ToF-SIMS, the surface chemistry of films deposited using both deposition methods were analyzed, demonstrating successful deposition of pNIPAM. In addition, using AFM and contact angle measurements, it was demonstrated that thermoresponse was maintained. Topographical differences in the surfaces showed that, although both spNIPAM and ppNIPAM-coated substrates were relatively smooth above the LCST, there was significant roughness on spNIPAM substrates below the LCST. Finally, as these surfaces were primarily fabricated for mammalian cell studies, cell attachment, proliferation, detachment, and critical cell exocytosis function were analyzed. It was found that cells did proliferate on surfaces coated using both methods of deposition, with the most cell detachment from the ppNIPAM surfaces. Additionally, although cells grow on pNIPAM-coated surfaces obtained from both methods, there were significant changes in the cell densities and perturbations in cellular communications (as measured using CFMA) on spNIPAM surfaces.

Overall, cells cultured on ppNIPAM surfaces provided cellular responses, including both cell survival and function, most similar to cells cultured on uncoated glass.

From these results, it is clear that although pNIPAM can be successfully deposited using different techniques and maintain thermoresponse, the deposition method influences coating uniformity and behavior which, in turn, determine which deposition method is appropriate for the desired application. For instance, although both spNIPAM and ppNIPAM substrates both successfully release mammalian cells, for applications such as cell sheet engineering, cell culture using ppNIPAM substrates would be preferable, because maintenance of normal cellular function is more successful using ppNIPAM surfaces. In contrast, spNIPAM is a simple, inexpensive method of deposition that may be more appropriate for applications not requiring confluent (and unperturbed) cell sheets, such as protein separation. In summary, the work reported herein demonstrates that plasma deposition of pNIPAM is most useful for any application requiring an even topography, similar response across the substrate, and/or cells with minimal functional perturbations.

Chapter 6: Effect of Substrate Storage Conditions on the Stability of “Smart” Films Used for Mammalian Cell Applications

Submitted for publication by Reed, J.A.; Bluestein, B.M.; Canavan, H.E. in *Biomacromolecules*, February 21, 2011.

6.1 Introduction

To date, there has been limited development in the United States of engineered tissues from cell sheets harvested from pNIPAM due to an uncertainty of the mechanism behind the cell release.²⁷ Currently, it is unknown if pNIPAM detaches from the underlying substrate and is transferred with the cells upon cell detachment, which would raise concern as to whether pNIPAM is biocompatible (see Figure 6.1).^{169, 170, 172-187} Most of the research performed on the polymer focuses on the material characteristics, but do not assess the biocompatibility of the tethered polymer. In fact, there are very few studies on the cytotoxicity of pNIPAM.¹⁸⁸ Furthermore, the few studies that do exist report conflicting conclusions. One thing that is clear is that the monomer is toxic.^{157, 161, 166, 169, 170, 189} Thus, if there were any monomer remaining in a pNIPAM film for incubation of cells, the surface would engender questions about its biocompatibility as the monomer could potentially leach into the surrounding cellular environment. Furthermore, any instability of a pNIPAM film could lead to cytotoxicity, thus the method of deposition could affect the biocompatibility.

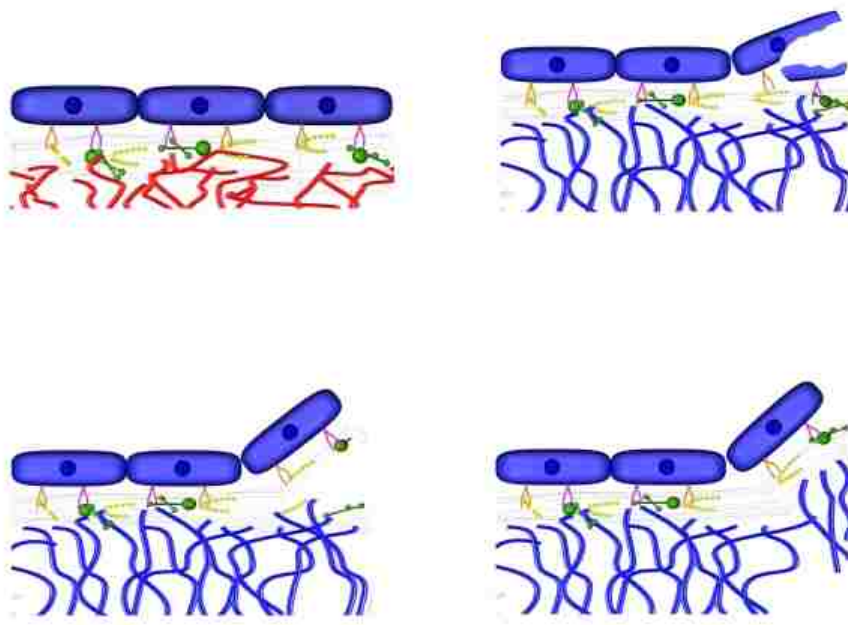


Figure 6.1: Schematic illustrating possible mechanisms of cell detachment from pNIPAM. Above the LCST, cells attach to pNIPAM-coated surfaces (top, left). When the temperature is shifted below the LCST, the polymer swells, and the cells detach either by disruption of the cells (top, right), the ECM (bottom, left), or the film (bottom, right).

There are many methods for depositing pNIPAM onto a substrate, including atom transfer radical polymerization (ATRP), electron beam ionization, and solution deposition.¹⁶⁷ In the previous chapter, two methods of deposition (plasma and co-deposition with a sol-gel) were compared, demonstrating that both were technically appropriate for obtaining thermoresponsive pNIPAM films. However, the surfaces that were co-deposited with a sol-gel seemed to cause some disruption in cell activity.¹¹² In that work, it was concluded that the cell behavior variation could be due to film instability, causing chemicals to leach out

from the surface. Takezawa et al. have previously stored their surfaces below the LCST before use, to ensure film stability.^{118, 125, 167}

The current study investigates the stability of both plasma polymerized and sol-gel co-deposited pNIPAM substrates for the amount of time required to obtain confluent cell sheets. As the ultimate goal is to use these substrates as cell culture platforms and thus film stability is required, claims that the conditions of surface storage affect the stability of pNIPAM films were also investigated. Thus in this work, a comparison of the two methods of deposition to determine if there is film instability was investigated, as well as if this instability can be avoided by altering the storage of the films pre-cell culture by assessing film chemistry, thermoresponse, cytotoxicity, and biocompatibility.

6.2 Experimental Methods

The majority of the experiments carried out herein follow the procedures outlined in Chapter 2, including pNIPAM deposition, XPS, contact angle goniometry, biocompatibility, cytotoxicity, and cell culture. Three repetitions of all experiments, producing three surfaces, were performed. Each surface was analyzed in three spots, for a total of 27 analyses. In addition, XPS and contact angle goniometry were performed on substrates after they were conditioned according to the parameters described below. XPS analysis was performed on 3 of the 4 conditions, described below, providing the information necessary to compare the 2 variables of interest (storage temperature and humidity).

6.2.1 Storage of surfaces

After modification the surfaces were stored at 25 °C with low humidity conditions (30% relative humidity), 25 °C with high humidity conditions (90% relative humidity), 37 °C with low humidity conditions, or 37 °C with high humidity conditions. Surfaces were stored in these conditions for at least 24 hours before use.

6.2.2 Delamination study

Coated silicon chips were used for surface analysis. These surfaces were submerged in DPBS for 2 hours and 48 hours to compare to cell response. Each silicon chip was rinsed thoroughly with Ultrapure water (18 M Ω) and dried with nitrogen after submersion in DPBS.

6.3 Results and Discussions

6.3.1 Initial conditions

Using XPS, it was confirmed that there was successful deposition of pNIPAM using both the spNIPAM and ppNIPAM deposition methods. As demonstrated by the relative atomic percentages (see Table 6.1), before submerging the surfaces in DPBS, all surfaces are relatively similar to the theoretical values (75% C, 12.5% O, and 12.5% N) calculated from the composition of the monomer. It should be noted that spNIPAM surfaces differed from theoretical values due to the presence of Si at 7-20%, which arises from the use of TEOS sol. In addition, pure pNIPAM would be composed of 66.7% CH/CC (285 eV), 16.7% amide (286 eV), and 16.7% amine (288 eV) bonds. The high resolution C1s spectra in Figure

6.2 and the data in Table 6.2 illustrates that spNIPAM (68.7% CH/CC, 17.1% amide, and 14.2% amine) and ppNIPAM (62.1% CH/CC, 20.8% amide, and 17.1% amine) surfaces have similar bonding environments to the theoretical values, as demonstrated previously, proving deposition of pNIPAM in each case.^{27, 167}

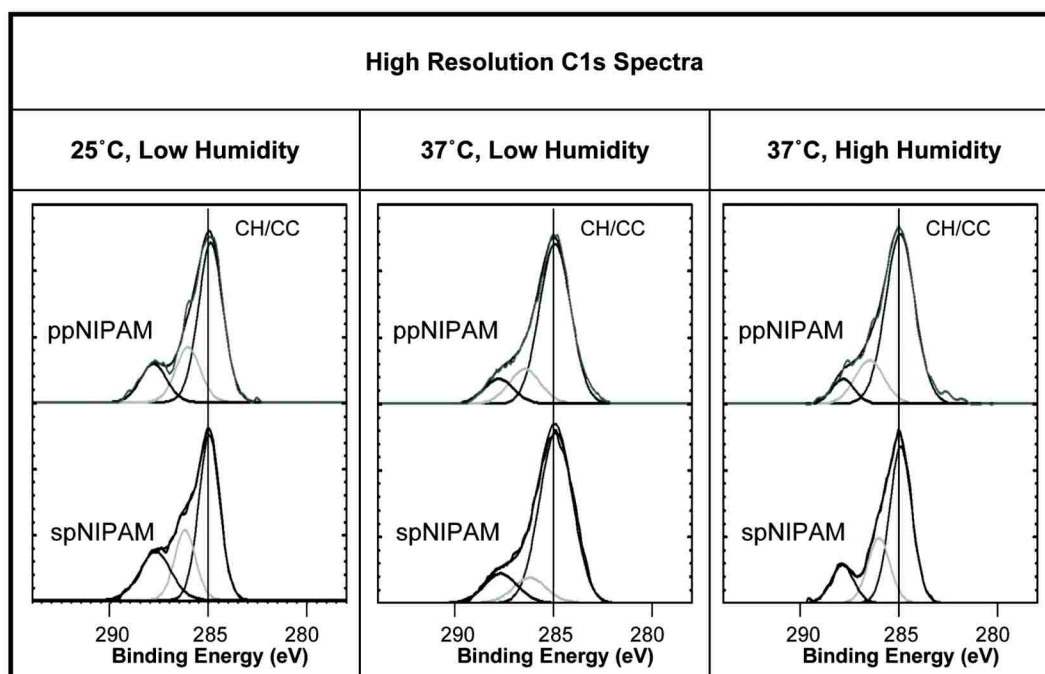


Figure 6.2: XPS high resolution C1s spectra of ppNIPAM (top) and spNIPAM (bottom) films after storage in 25°C, low humidity (left) and 37°C low (middle) and high (right) humidity conditions. All surfaces have the bonding environments indicative of pNIPAM deposition, including CH/CC (285eV), CN/CO (286eV), and O=CN (288eV).

Table 6.1: XPS survey data of ppNIPAM (top), spNIPAM (middle), and blank control Si chips (bottom) stored at 25°C low humidity (left), 37°C low (middle) and high humidity (right) conditions before submersion in DPBS for 0 (white), 2 (light grey), or 48 (dark grey) hours. PpNIPAM surfaces remained stable regardless of storage conditions. SpNIPAM surfaces were not stable over time, and the storage conditions affected the final surface composition. (n=9, standard deviation <5)

	XPS Survey: Relative Atomic Percent											
	25°C Low Humidity				37°C Low Humidity				37°C High Humidity			
	C	N	O	Si	C	N	O	Si	C	N	O	Si
Theoretical Composition	75	12.5	12.5	0	75	12.5	12.5	0	75	12.5	12.5	0
ppNIPAM 0hr	78.4	8.7	12.8	0	77.8	11.0	11.2	0	79.4	10.6	9.7	0.2
ppNIPAM 2hr	77.7	8.0	14.4	0	77.9	10.0	12.1	0	79.2	10.7	9.8	0.3
ppNIPAM 48hr	76.0	10.4	13.6	0	75.8	10.3	13.9	0	79.3	10.9	9.7	0.2
spNIPAM 0hr	33.5	5.0	43.3	18.2	37.4	5.6	40.1	16.9	34.7	5.0	41.9	18.3
spNIPAM 2hr	59.3	8.7	23.8	8.2	61.6	9.3	22.5	6.7	58.3	8.7	23.5	9.5
spNIPAM 48hr	28.3	4.1	47.6	20.0	22.8	2.9	52.4	21.9	22.8	2.1	52.1	22.9
Control 0hr	11.0	0	42.3	46.7	11.0	0	42.3	46.7	11.0	0	42.3	46.7
Control 2hr	11.2	0	40.5	48.3	13.8	0	41.6	44.7	13.9	0	43.1	43.1
Control 48hr	15.2	0	52.7	32.1	19.7	0	50.5	29.8	14.9	0	56.1	29.1

Table 6.2: XPS High Resolution Carbon data of ppNIPAM (top) and spNIPAM (bottom) stored at 25°C low humidity (left), 37°C low (middle) and high humidity (right) conditions before submersion in DPBS for 0 (white), 2 (light grey), or 48 (dark grey) hours. All surfaces maintain carbon binding environments indicative of pNIPAM deposition, regardless of storage conditions. (n=9, standard deviation <5)

	High Resolution Carbon: Relative Atomic Percent								
	25°C Low Humidity			37°C Low Humidity			37°C High Humidity		
	CH/CC 285eV	CO/CN 286eV	O=CN 288eV	CH/CC 285eV	CO/CN 286eV	O=CN 288eV	CH/CC 285eV	CO/CN 286eV	O=CN 288eV
Theoretical Composition	66.7	16.7	16.7	66.7	16.7	16.7	66.7	16.7	16.7
ppNIPAM 0hr	62.1	20.8	17.1	69.8	19.8	10.4	52.2	28.4	19.4
ppNIPAM 2hr	54.7	27.0	18.3	62.2	24.6	13.3	53.2	28.6	18.3
ppNIPAM 48hr	62.8	20.4	16.7	64.1	22.1	13.8	66.8	23.8	9.4
spNIPAM 0hr	68.7	17.1	14.2	62.1	20.2	17.7	65.1	20.2	14.7
spNIPAM 2hr	63.6	22.4	14.0	60.0	23.3	16.7	64.3	24.5	11.1
spNIPAM 48hr	72.4	13.2	14.4	60.6	23.4	15.9	62.2	22.3	15.5

Using contact angle goniometry, it was confirmed that the surfaces, prior to exposure to DPBS, were thermoresponsive (see Table 6.3). The thermoresponse at 0hr for both ppNIPAM and spNIPAM at all temperatures and relative humidity values follow the desired trend of higher contact angles above the LCST and lower contact angles below the LCST. PpNIPAM surfaces stored at 25 °C with low humidity change in contact angle across the LCST (~17°, with the standard deviation for all ppNIPAM contact angles at 0hr < 3.0°). While spNIPAM surfaces had a 6.4° change in contact angle (standard deviation for all spNIPAM contact

angles at 0hr are $< 2.5^\circ$). The control surfaces stored at 25°C with low humidity showed no statistical change across the LCST; as expected, the controls followed this trend throughout the experiment regardless of storage temperatures and relative humidity values. The controls did exhibit an increase in hydrophilicity after storage in DPBS for 48 hours, due to a film of trace salts. However, the surfaces were not thermoresponsive across the LCST.

With a shift to a higher relative humidity, ppNIPAM surfaces are still thermoresponsive, although the change in the contact angle across the LCST decreased compared to 0 hour (7.7° vs. 17° respectively). This could be due to increased incorporation of water in the film when stored at high humidity conditions. The spNIPAM surfaces remained relatively stable with a 6.3° change. When the temperature was shifted to 37°C at low humidity, ppNIPAM surfaces exhibited about a 5.9° change in contact angle, and spNIPAM exhibited a 9.3° change in contact angle. At 37°C ppNIPAM and spNIPAM surfaces remained stable with 8.7° and 9.1° changes in contact angle respectively when the humidity value was shifted to a higher relative humidity. This indicates that although the surfaces were all stored at different temperatures and relative humidity conditions, the surfaces had a 5° - 10° change in contact angle before submersion in DPBS, with thermoresponse that is similar to what has been previously reported.¹¹²

Table 6.3: Contact angles for ppNIPAM (top), spNIPAM (middle), and blank control Si surfaces (bottom) at all storage conditions taken above and below the LCST. Control surfaces show no thermoresponse, while ppNIPAM and spNIPAM surfaces before submersion in DPBS (0hr) were thermoresponsive. PpNIPAM surfaces maintained thermoresponse after 48 hours in DPBS, while spNIPAM surfaces showed either no thermoresponse or reverse thermoresponse. N=9 with a standard deviation less than 3, except for those marked with asterisk where the standard deviation is less than 5.

	Contact Angle							
	25°C Low Humidity		25°C High Humidity		37°C Low Humidity		37°C High Humidity	
	25°C	37°C	25°C	37°C	25°C	37°C	25°C	37°C
ppNIPAM 0hr	23.0	40.0	33.5	41.2	34.5	40.4	32.4	41.1
ppNIPAM 2hr	32.6	40.2	32.3	43.3	32.9	42.9	31.6	37.0
ppNIPAM 48hr	32.3*	44.8	34.5	39.7	30.3	41.1	34.0	39.2
spNIPAM 0hr	37.8	44.2	38.9	45.2	38.6	47.9	38.3	47.4
spNIPAM 2hr	39.5	45.3	39.6	43.6	38.1	40.8	41.0	44.8
spNIPAM 48hr	39.4	39.4	41.5	37.4	40.8	35.0	37.9	35.4
Control 0hr	45.8	47.6*	45.5	47.6	49.6	52.5	49.9*	53.5
Control 2hr	45.1	47.6*	43.0*	48.8*	45.1	47.1	41.1	48.3
Control 48hr	22.2	22.8*	26.8*	25.0	27.0*	31.0	26.6	27.7

6.3.2 Surface stability

Over the 2 day period necessary to obtain confluent cell sheets, ppNIPAM

surfaces appear chemically stable, showing no statistically relevant deviation in relative atomic percentage of species present initially (62.1% C, 20.8% N, and 17.1% O) regardless of the storage conditions. In addition, high resolution C1s spectra indicate that carbon species present also remained statistically unchanged, despite the storage condition or time exposed to DPBS (see Figure 6.2 and Table 6.2).

The relative humidity of the storage condition has very little influence on surface chemistry, as illustrated by the lack of change on spNIPAM films that were highly influenced by temperature. Above the LCST, regardless of humidity, the surface chemistry of spNIPAM films begin to deviate from the theoretical pNIPAM with a 5.0% and 12.3% increase in Si and O₂ and a 14.6% and 2.7% decrease in C and N respectively. This indicates that the pNIPAM maybe delaminating from the surface, and there is more Si (from either the underlying substrate or the sol-gel) than pNIPAM present on the surface. Below the LCST, a similar trend is seen with a decrease in 5.2% C and a 4.3% increase in Si, but there is not statistically relevant shifts in O or N.

PpNIPAM surfaces retained a 5°-12° change in contact angle across the LCST, with the most change seen on the ppNIPAM films stored at 25 °C with low relative humidity. As importantly, there was no statistical difference in thermoresponse seen by changing the storage conditions of the ppNIPAM surfaces.

The results also show that the thermoresponse for ppNIPAM films was most

affected by humidity, while spNIPAM films were affected by storage temperature. Furthermore, the best thermoresponse was seen on ppNIPAM surfaces that were stored at 25 °C and low humidity. Obviously, these results indicate that temperature is affecting the stability of the films. Takezawa et al. found that pNIPAM films air dried onto a substrate are also more stable when stored below the LCST (it should be noted that humidity was not a variable for their experiments).¹²⁵

In contrast, the spNIPAM surfaces appear to lose the thermoresponsive characteristic of pNIPAM regardless of storage conditions. In fact, at the time when these surfaces would need to be thermoresponsive to obtain cell sheet release (2 days), the surfaces have reversed thermoresponse (a -6° to 0° change). As early as 2 hours after submersion in DPBS, the surfaces have drastically reduced thermoresponse, dropping from a 6°-9° change to a 2°-6° change. These results indicate that there is a change in the spNIPAM films' characteristics almost immediately, possibly due to the delamination of the film.

From these results, it appears that ppNIPAM surfaces remain stable chemically and maintain thermoresponse during the experimental time frame that is consistent with cell culture. This would suggest that the ppNIPAM surfaces should have a better cell detachment than the spNIPAM surfaces. However, as determined by Lucero et al., thermoresponse is not always a reliable indicator of cell response.¹¹¹

6.3.3 Cell adhesion

BAECs were cultured using previously described technique. 190 Cells attached to ppNIPAM surfaces within 2 hours of seeding, comparable to blank control surfaces. However, images obtained 2 hours after seeding the cells indicate that the cells are less likely to attach to spNIPAM surfaces stored below the LCST initially (see Figure 6.3, middle row).

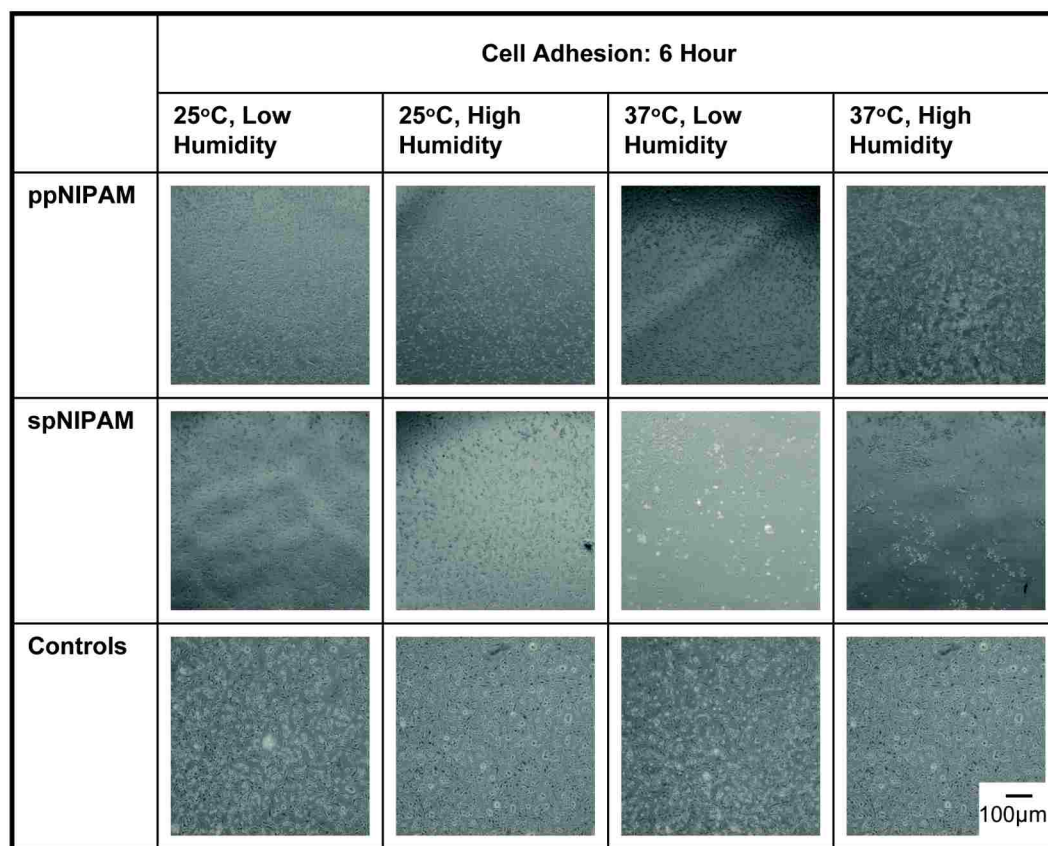


Figure 6.3: Bright field microscopy images of BAECs obtained 6 hours prior to cell seeding on ppNIPAM (top), spNIPAM (middle), or blank control glass surfaces (bottom). Within 6 hours, there was normal cell attachment onto ppNIPAM and control surfaces, but minimal adhesion to spNIPAM surfaces.

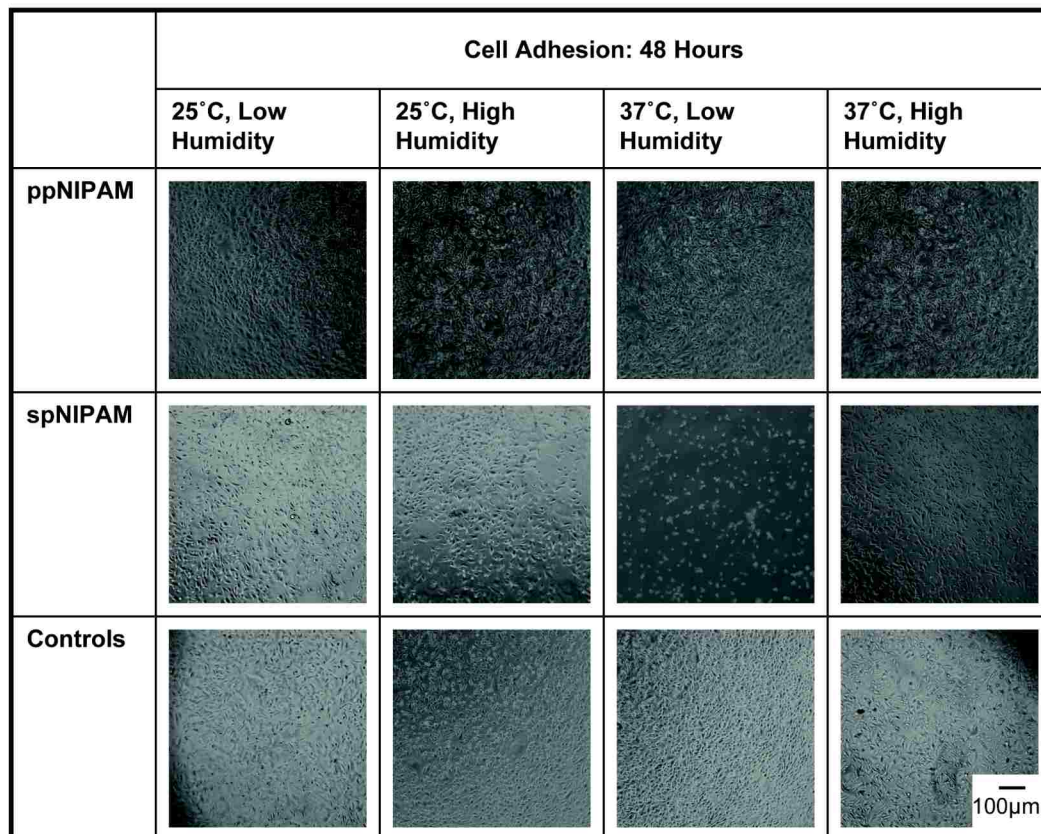


Figure 6.4: Bright field microscopy images of BAECs after 48 hours of incubation on ppNIPAM, spNIPAM, and control glass surfaces. Cells grown on ppNIPAM grew to confluence within 48 hours. However, on spNIPAM surfaces the cells did not spread or proliferate to confluence on any of the surfaces, where the 37°C low humidity storage condition for these surfaces demonstrated the least cell attachment.

Eventually, cells grew to confluence on all surfaces, suggesting that deposition and storage method do not affect the long term cell growth of the surfaces. Since the cells do ultimately attach to the surfaces (as shown in Figure 6.4), and surface analysis suggests that there is a change in the surface chemistry, the cells are most likely attaching after the surface changes for all surfaces except those stored above the LCST in low humidity conditions. In this case, there is still

limited cell attachment with many cell aggregates, indicating that these adherent cells would rather attach to each other than the substrate. Due to the aforementioned lack of cell attachment, the viability of the cells on the surfaces was analyzed.

6.3.4 Cytotoxicity

A cytotoxicity study was completed to investigate the effect of the pNIPAM leaching into the media. This was done by incubating the ppNIPAM and spNIPAM surfaces from each storage condition at cell culture conditions with media for 24 hours.¹⁹⁰ Since it was clear from surface analysis that there was disruption of the spNIPAM surfaces, anything that would leach out from the surfaces would be collected in this treated media. Therefore, if either the spNIPAM or ppNIPAM surfaces are leaching out something that is harmful to the cells, when the treated media is used during incubation with normal, healthy cells, the cells should no longer be viable. In this case, BAECs were incubated with 100%, 10%, 1%, and 0% treated media to determine if there was any cytotoxic chemicals leaching into the treated media, as well as to determine what amount of the cytotoxic chemicals would decrease cell viability. As shown in Figure 6.5, even when del cells were incubated with 100% treated media, there was no adverse effect on viability for either spNIPAM or ppNIPAM surfaces. The cells remained viable, staining green with a LIVE/DEAD® assay, with the highest possible amount of the leached chemicals.

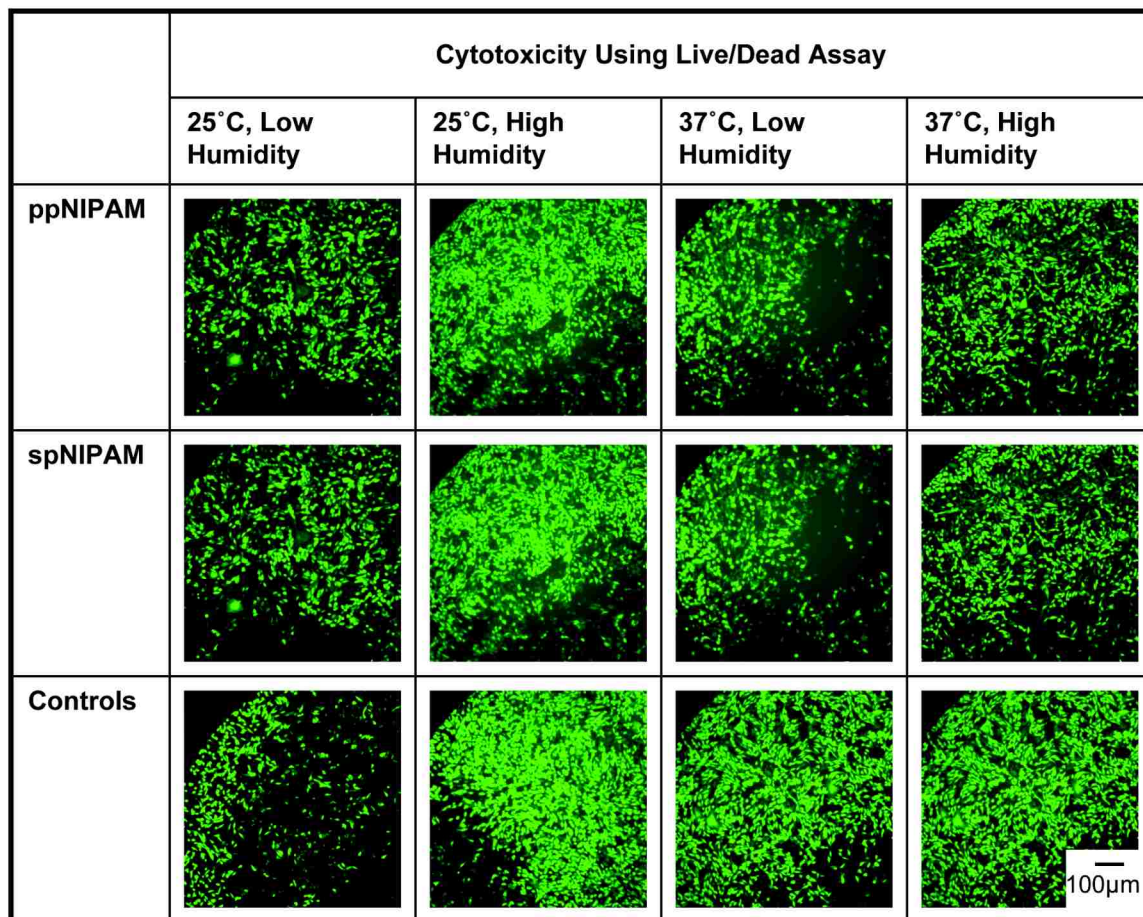


Figure 6.5: Fluorescent microscopy images showing live (green) and dead (red) BAEC after 24 hours of incubation with 100% treated media extracted from ppNIPAM (top), spNIPAM (middle), or blank control glass surfaces (bottom). All conditions maintained normal cell growth resulting in live cells after being exposed to treated media.

6.3.5 Biocompatibility

Finally, the cells were monitored at different time points when cultured directly on the substrates to see which storage conditions would be the most biocompatible, or which surfaces supported cell growth and proliferation. BAECs were seeded at a low density and incubated for 6 hours, 24 hours, and 72

hours.¹²⁶ Again, a LIVE/DEAD® assay to determine whether the cells that were present at each time point were viable. As previously mentioned, there was minimal cell attachment to the spNIPAM surfaces initially (see Figure 6.6). However, after 24 hours, all surfaces have some cell attachment and proliferation. At this time point, spNIPAM surfaces appeared to be less populated, with fewer cells attached, than the ppNIPAM surfaces, regardless of the fact that both surfaces were seeded with approximately the same number of cells. The most cell attachment for spNIPAM surfaces at 24 hours was on surfaces stored at 37 °C, low humidity. These were also the surfaces that had lost all thermoresponse at 2 hours, and thus have delaminated to the point that the cells can better anchor to the substrate. By the final time point at 72 hours, the cells were most confluent on ppNIPAM substrates previously stored at 25 °C, low humidity. As seen in Figure 6.6, all surfaces stored at 25 °C resulted in substrates that permitted for normal cell attachment and morphology as opposed to substrates stored at 37 °C, regardless of humidity. However, all surface conditions were technically biocompatible, resulting in eventual cell attachment, normal cell morphology, and limited apparent cell death.

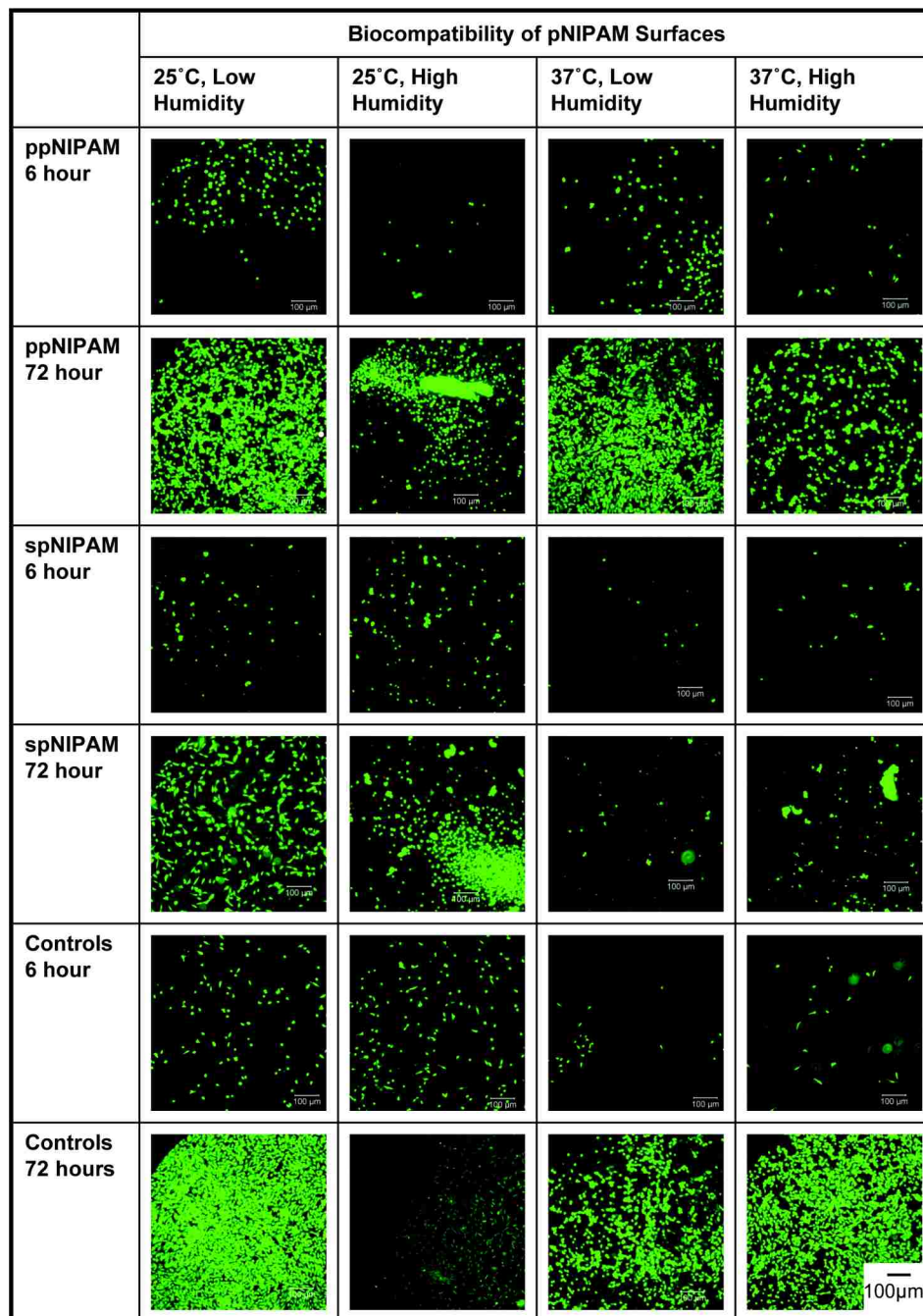


Figure 6.6: Fluorescent microscopy images of live (green) and dead (red) BAECs on ppNIPAM (top), spNIPAM (middle), and control (bottom) surfaces during the biocompatibility study at 6 and 72 hours of exposure to the surfaces. Cells attached and proliferated most on ppNIPAM surfaces.

These results illustrate that all of the surfaces, regardless of deposition

method and storage conditions, can be used for mammalian cell culture. Thus, even if the surfaces are delaminating, this is not affecting the growth or viability of the cells when compared to control substrates. However, since the primary use for these substrates is to generate cell sheets, which require intact pNIPAM films, ppNIPAM surfaces prove to be most useful. In the interest of thoroughness, five cell lines were tested for biocompatibility via culturing them on ppNIPAM films after storage at 25 °C with low relative humidity. All five cell lines showed normal adherence and viability and it was concluded that ppNIPAM films stored in this manner were biocompatible, and ideal for tissue engineering applications (Appendix IV).

6.4 Conclusions

Although it is possible to deposit pNIPAM using spin coating (spNIPAM) and plasma (ppNIPAM) deposition, the pNIPAM films clearly are affected by both deposition method and storage conditions. Over time, it was found that the spNIPAM surfaces are unstable, regardless of storage conditions. Interestingly, at temperatures below the LCST, the surfaces begin to resemble pure pNIPAM substrates, while surfaces stored above the LCST quickly lose thermoresponse and chemical environments indicative of a pNIPAM substrate. This surface change also affects cell attachment, resulting in limited attachment until the surfaces better resemble their final state. Since the ppNIPAM surfaces are more stable over time, regardless of the storage conditions, these surfaces have more cell attachment and normal cell morphology, making them more useful for cell

sheet engineering applications. In addition, storage below the LCST creates more stable surfaces for mammalian cell applications. Although humidity seems to only slightly affect surface chemistry, thermoresponse, and cell studies for ppNIPAM surfaces, there is a slight preference of cells to surfaces stored in low humidity conditions.

Chapter 7. Electrospinning pNIPAM for Mammalian Cell Culture Applications

Manuscript in preparation for publication by Cicotte, K.N.; Reed, J.A.; DeLora, J.A.; Canavan, H.E.; Hedberg-Dirk, E.L.

7.1 Introduction

Many deposition methods for pNIPAM have been explored for the purpose of mammalian cell culture and harvest, as described in Chapter 2. One limitation to many of these techniques is the relatively slow detachment of cell sheets from pNIPAM substrates. For instance, it has been reported to take up to 80 minutes for a cell sheet cultured on a 35 mm plate derivatized with pNIPAM using an electron beam ionization technique to detach from its culture substrate.¹²⁶ This slow release is most likely due to the limited access of hydrating water to flat (2-Dimensional) films, such as pNIPAM-treated Petri dishes, which results in slow swelling of the film at room temperature.

Previously, Kwon et al., demonstrated that one method to overcome this problem is to provide a surface that has a high surface area to volume ratio, such as a porous substrate.¹⁹¹ The method described in that work relied on pNIPAM copolymerized with polyethylene glycol (PEG) using electron beam ionization on PVDF membranes to accelerate the hydration of hydrophilic pNIPAM chains, and resulted in cells that were released in 20 minutes for tissue engineering applications. In this work, an alternative method for the formation of highly porous

pNIPAM materials for rapid cell release was explored. Namely, rather than treating a porous membrane with pNIPAM (which relies on the derivatization of a relatively non-reactive paper-based material with pNIPAM), instead porous mats that were composed entirely of pNIPAM via electrospinning (espNIPAM) were created for mammalian cell culture applications.

Electrospinning is an established technique for the fabrication of polymeric mats with nano to micron sized fibers. Electrospinning has been previously used to fabricate numerous biomaterial mats from natural (chitosan) and synthetic (PLLA) materials.¹⁹² Recently, Okuzaki et al. created thermoresponsive espNIPAM mats, although the mats were not used for cell culture applications.¹⁹³

Briefly, electrospinning uses a voltage drop to form fibers in the void between a needle and a collection plate. The solution begins to evaporate and the remaining solid, which comprises the resulting mat, is accelerated in a whipping action towards the target.¹²⁸ Importantly, the mats should be sufficiently porous to allow for rapid hydration to the whole surface (vs. only the apical surface of a pNIPAM-treated Petri dish, or the edges of a pNIPAM-treated membrane).

In this work, we investigated the use of an electrospinning device that was built in house.¹⁹⁴ The electrospinning technique pioneered by Rockwood et al., was optimized for cell culture applications, by varying characteristics such as the molecular weight (MW) of the pNIPAM powder used, the gauge of the needle used, and collection time.¹⁹² Prior to their use for cell culture, the mats' chemistry, thermoresponse, and topography/morphology were assessed using secondary

electron microscopy (SEM), Fourier-transform infrared spectroscopy (FTIR), XPS, and microscopy. Subsequent to the material characterization, the suitability of the espNIPAM mats was assessed by seeding them with EMT6 and MC3T3-E1 cells, and incubating them at cell culture conditions to allow cell sheet formation. Due to the hydrophilic nature of the polymer at low temperatures and the large surface area, we found that when the cells were confluent and the temperature was changed to ~ 25 °C, the mat swelled rapidly, resulting in a detached cell sheet that could be used for tissue engineering and cancer cell biology applications.

7.2 Experimental Methods

The majority of the experiments carried out herein follow the procedures outlined in Chapter 2, including espNIPAM processing, XPS, cytotoxicity, CellTracker™, and cell culture. Three repetitions of all experiments, producing three surfaces, were performed. Each surface was analyzed in three location, for a total of 27 analyses.

7.2.1 FTIR

FTIR was carried out at Sandia National Laboratory using a Nicolet™ 6700 FT-IR (Thermo Electron Corporation) equipped with a continuum microscope. OMNIC™ Software (ThermoScientific) parameters included selecting a transmission ESP accessory, detector (DTGS KBr) and beamsplitter (XT-KBr).

Sample preparation for pNIPAM included making a 1 mg/ml solution in

methanol (MeOH) and drop casting the solution on a KBr plate (Aldrich), and for electrospun mats (espNIPAM) the spectra was recorded as spun (neat). Data were collected for 64 scans at a resolution of 4, from 400-4000 cm^{-1} . Spectra were exported as an .asc file and analyzed in Excel (Microsoft Corp.). All Spectra were normalized to the C=O stretching at 1640 cm^{-1} .

7.2.2 SEM

SEM analysis was performed with a Zeiss Supra 55VP Field Emission Gun SEM at Sandia National Laboratory. The samples were sputter coated with AuPd in an Edwards S150B sputter coater for 12 seconds. Imaging was done with 2 to 5kV acceleration voltage, depending on how the sample was reacting (i.e. charging). Image acquisition was performed with SmartSem software provided by Zeiss. Image analysis utilized Image J to determine the diameter of fibers in the mats.

7.2.2 Thermoresponse

The thermoresponse of the mats were tested using a CO₂ microscope stage incubator from Okolab (Naples, Italy). Using the Okolab software, the temperature of the stage incubator was held constant at temperatures ranging from 26 °C to 40 °C. Within the incubator, mats were exposed to water and observed via light microscopy (Nikon F100, Melville, NY) and a 10x objective.

7.2.3 Transfer of harvested cells

The above assays made it clear that cells would attach normally on pNIPAM

substrates. It was still unclear, however, whether the harvested cell sheets were intact and would proliferate normally if transferred to a new substrate. To assess the condition of the cells, they were detached, aided by PVDF as described in Chapter 2, and relocated into a new well. Cells were monitored for 24 hours.

7.3 Results and discussions

7.3.1 Preparation of mats

EspNIPAM mats were fabricated by adapting a previously published method,^{191, 193} although that publication is focused on the fabrication of espNIPAM mats using only a singular set of parameters (polymer concentration vs. voltage). In this work, we adapted a number of conditions, including MW, needle gauge size, and mat collection time. These parameters were chosen as they would affect mat density and fiber size, which are important considerations when using the mats for cell culture.¹⁹⁴

Briefly, both high molecular weight (HMW, ~300 kDa) and low molecular weight (LMW, ~40 kDa) pNIPAM were prepared as a 10 wt% solution in methanol. Mats were produced using a generic electrospinning set up with collection on a target in the horizontal position (Figure 7.1). Various stainless steel, blunt tip needle gauges, including 15 (ID = 1.372 mm), 21 (0.495 mm), and 30 (0.140 mm), as well as various collection times (5 and 10 min) were compared.

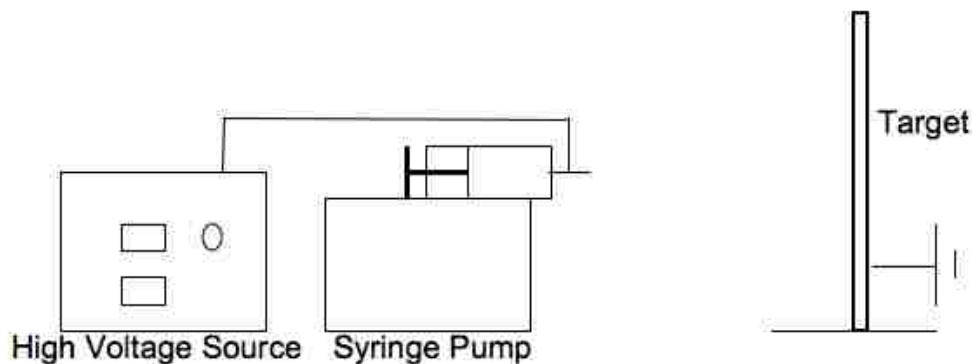


Figure 7.1: Schematic of the electrospinning design used for making espNIPAM mats, with a high voltage source attached to the tip of a needle. A 10wt% pNIPAM/methanol solution is pumped out of the syringe, and pulled toward the horizontal grounded target.

We found that uniform, “dog bone”-shaped fibers on the order of $<1 \mu\text{m}$ in diameter were generated from each of the variations on the technique, as shown in the SEM images (see Figure 7.2).¹⁹¹ In particular, there appeared to be no statistical difference in fiber diameter, regardless of needle gauge (Figure 7.3). However, mat thickness was found to depend linearly on collection time: by increasing collection time from 5 min to 10 min, mat thickness increased from 12 to 24 μm .

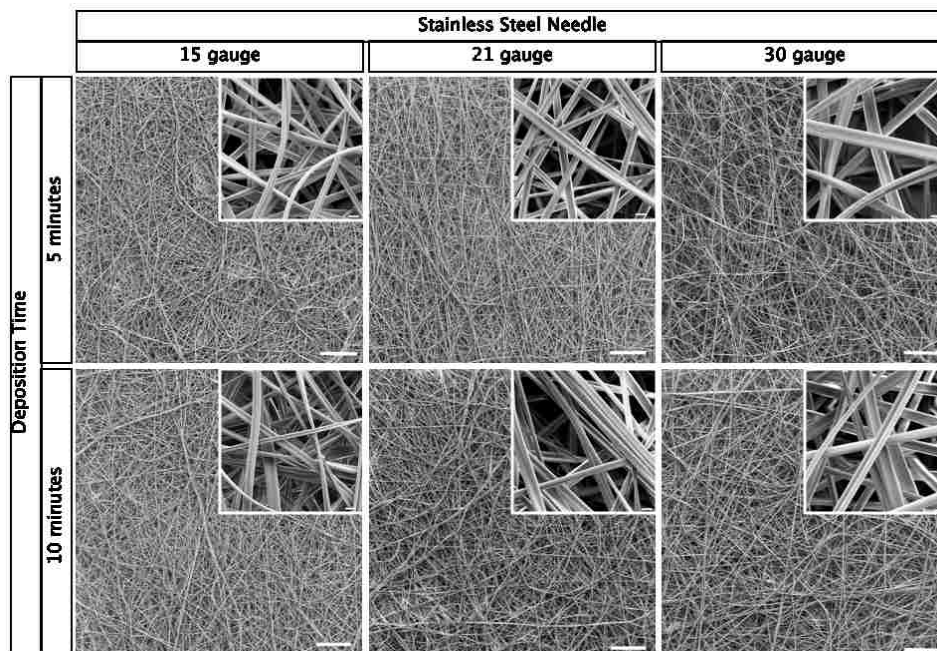


Figure 7.2: SEM images of espNIPAM mats spun for 5 (top) or 10 (bottom) minutes, using a 15 (left), 21 (middle), or 30 (right) gauge needle. Scale bars for larger view images are 100 μm and are 2 μm for the inset pictures.

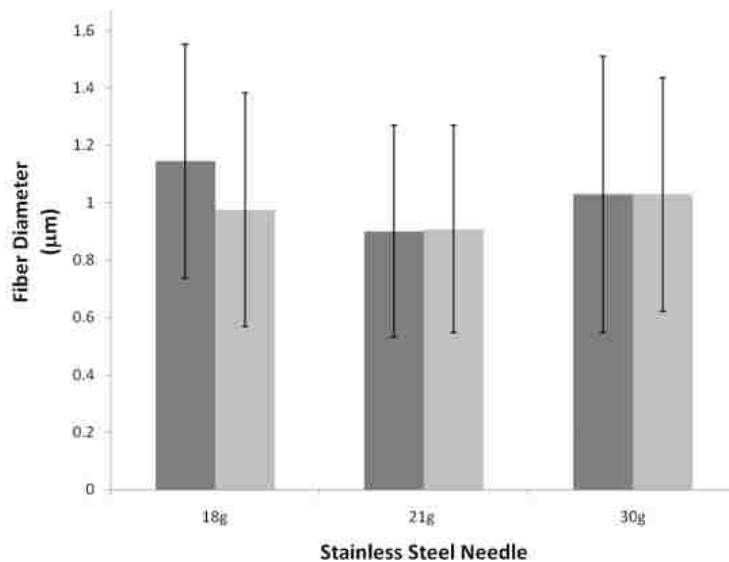


Figure 7.3: Fiber diameters measured using SEM and Image J, showing that regardless of gauge size (15, left; 21, middle; 30, right) the fiber diameters are statistically the same. In addition, the fiber collection time does not affect the fiber diameter (5 minutes in dark grey, 10 minutes in light grey).

7.3.2 Elemental characterization of mats

In order to ensure that the as spun pNIPAM fibers had the same chemistry as its powderized pNIPAM precursor, FT-IR and XPS were performed on each of the LMW and HMW powder, as well as the spun mat. (See Figure 7.4) Close observation of FT-IR spectra generated from the three samples show that the characteristic functional groups of pNIPAM are present in all three without major shifts. For instance, the presence of C=O stretching at $\sim 1645\text{ cm}^{-1}$, CH_3 asymmetric stretching at $\sim 2970\text{ cm}^{-1}$, and N-H stretching at $\sim 3301\text{ cm}^{-1}$ are present in all three spectra. One obvious difference of the three spectra is the relatively high background of the espNIPAM mat, which can be attributed to the thickness of the sample. These results indicate that the bulk of the espNIPAM mats' chemistry closely resembles that of its powderized pNIPAM precursor, thus the processing of the mats has not altered the resulting chemistry.

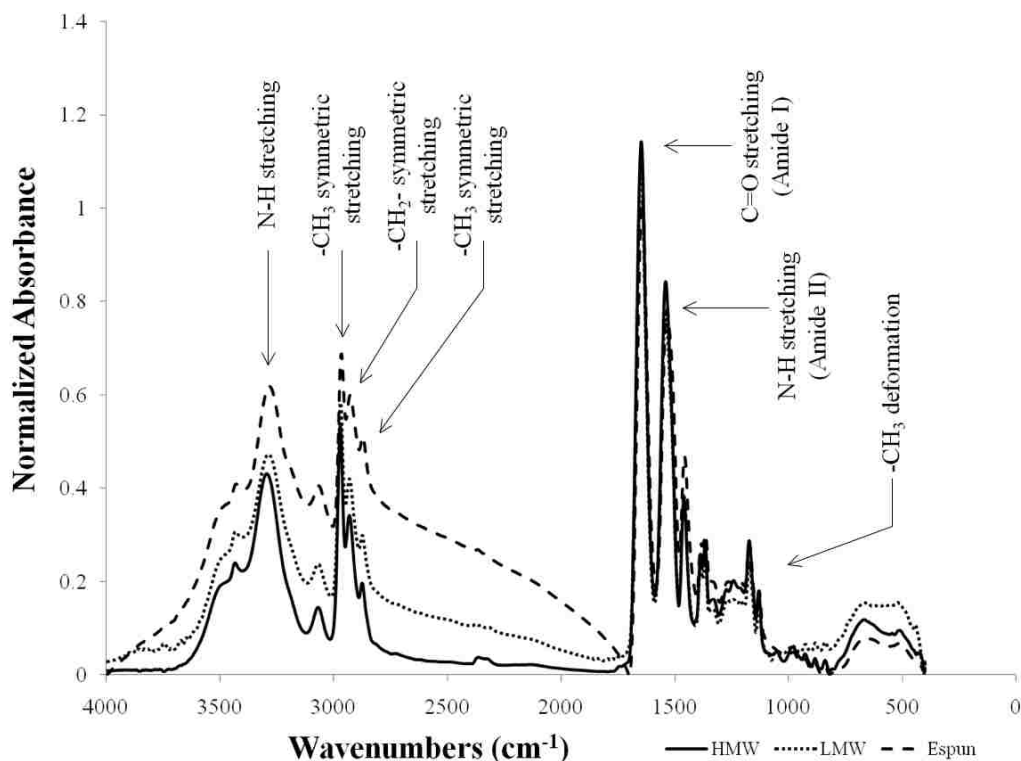


Figure 7.4: FTIR of high (HMW, solid) and low (LMW, short dashes) molecular weight pNIPAM powders, as well as a HMW espNIPAM mat (long dashes). All samples have similar stretches associated with pNIPAM.

To confirm the chemistry of the espNIPAM mats, they were analyzed using XPS. It should be noted that as the size of the fibers generated using each of the needles is on the order of a micron, it is well below the resolution of the XPS; therefore, the films generated using different needle size were not tested by XPS. As shown in Table 7.1 and Figure 7.5, the elemental composition of the espNIPAM mats generated from HMW and LMW polymers closely resemble the theoretical values expected from pNIPAM. The mats generated from HMW pNIPAM were 78.6% C, 11.3% N, and 10.1% O; whereas mats generated from LMW pNIPAM were 79.0% C, 10.2% N, and 10.8% O. These results are within

the experimental error of the instrument (~2-5% for elemental survey spectra), and are nearly identical to the structure predicted by the stoichiometry of the NIPAM monomer (75% C, 12.5% O, and 12.5% N), thus verifying the composition of the espNIPAM mats. Observation of the high resolution C1s spectra further confirms that the electrospun mats have the same chemical species as pNIPAM, including hydrocarbon (at 285 eV), as well as equal amounts of amine and amide characteristics (at +1.5 and 3.0 eV). (See Figure 7.5)

Table 7.1: Relative atomic percentages of high (HMW) and low (LMW) molecular weight espNIPAM mats from XPS, as compared to theoretical values for pNIPAM.

	Relative Atomic %		
	C	N	O
Theoretical	75.0	12.5	12.5
HMW	78.6	11.3	10.1
LMW	79.0	10.2	10.8

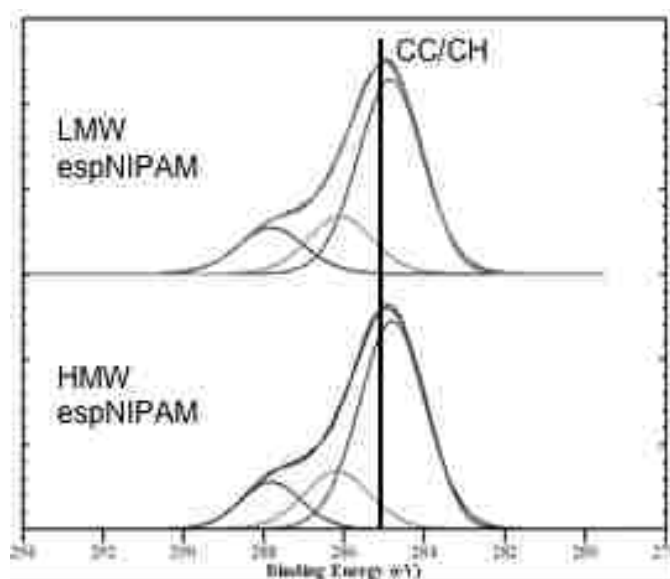


Figure 7.5: High resolution C1s spectra of low (LMW) and high (HMW) molecular weight espNIPAM mats. Both mats have amide and amine peaks, indicative of pNIPAM.

7.3.3 Thermoresponse of mats

Having established that espNIPAM mats generated from HMW and LMW pNIPAM retained the proper chemistry, they were tested to ensure thermoresponsive characteristics remained intact. As the topography of the mats varies widely due to the overlapping fibers that make up the mat, contact angle goniometry was not a sufficient technique for the observation of the mats' thermoresponse. Instead, the mats were held stable at temperatures ranging from 40 °C to 26 °C and imaged using an inverted microscope. (See Figure 7.6) It was found that the LMW mats were not stable, dissolving immediately in water. However, the mats formed from the HMW powder were stable in solution, and demonstrated reversible thermoresponse. Upon hydration above the LCST (~31 °C), the HMW espNIPAM mats originally collapsed, but rapidly (within 5 minutes)

swelled when the temperature shifted below the LCST. These results indicate that the HMW espNIPAM mats are more useful for reversible cell attachment, thus were the only espNIPAM mats further investigated.

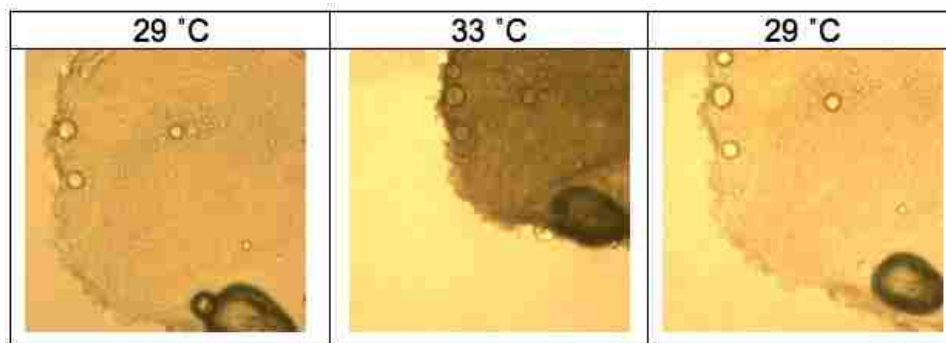


Figure 7.6: Bright field microscopy images of espNIPAM mats initially below the LCST (29 °C, left), collapsing when the temperature changes to above the LCST (33 °C, middle). When the temperature is lowered below the LCST again (right), the mat reversibly swells.

7.3.4 Cell response

As previously mentioned, there are conflicting results in the literature as to whether the method used to fabricate pNIPAM substrates may influence whether the resulting films are biocompatible or not. For this reason, HMW espNIPAM mats generated were assessed for cytotoxicity. As described in Chapter 2, this process includes incubating the mat in normal growth media at cell culture conditions for 24 hours in order to identify whether there are any substances that may leach into the media, interfering with cell viability and proliferation. This treated media will replace media on cells that are ~60% confluent. After 24 hours of exposure to the treated media, cells remained 99% viable and proliferated, thus the mats were not toxic to the cells and could potentially be used for rapid

cell detachment experiments. (See Figure 7.7)

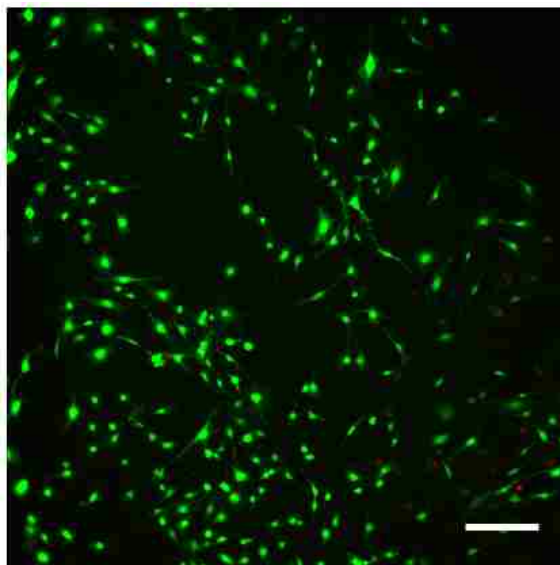


Figure 7.7: Fluorescent microscopy image of 3T3s stained with LIVE/DEAD® after exposure to espNIPAM treated media for 24 hours. Cells remain viable, verifying espNIPAM is not cytotoxic. Scale bar is 100 μm .

Initially, cells were seeded onto the mats at a high ratio (100,000 cells/well for 3T3s and 50,000 cells/well for EMT6) to ensure cell attachment and rapid cell proliferation. As it was extremely difficult to see the cells on the mats in their collapsed state (i.e., opaque), observation of cellular behavior was achieved using fluorescent microscopy (using CellTracker™) rather than bright field or phase contrast microscopy (as described in Chapter 2). Briefly, CellTracker™ was used to view the 3T3s on the mats 24 hours after seeding, as shown in Figure 7.8. The temperature was then shifted below the LCST using the traditional method (exchange with cold media, as described in Chapter 2), to determine if the cells would detach from the mats.

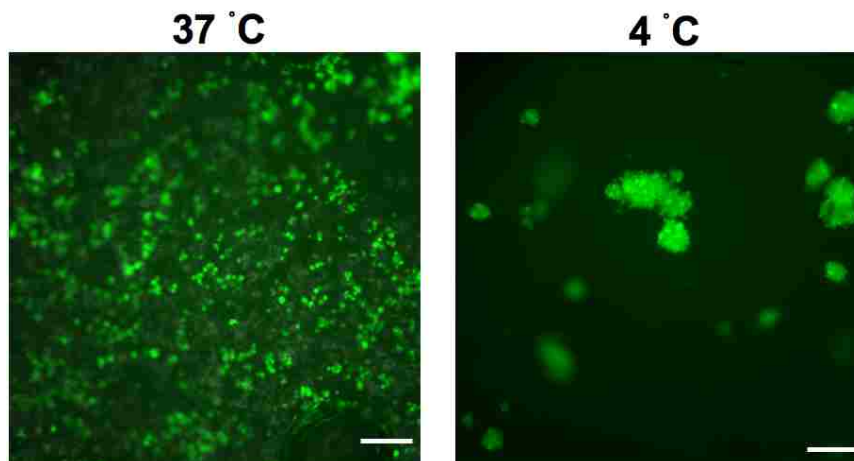


Figure 7.8: Fluorescent microscopy image of 3T3 cells tagged with CellTracker™, allowing images of the cells to be taken through the opaque espNIPAM mat above the LCST (left) and after the cells have detached below the LCST (right). Scale bar is 100 μm .

Figure 7.8 illustrates that, subsequent to the shift below the LCST of the polymer, the cells detach from their espNIPAM mat substrates. It is interesting to observe that although both 3T3 and EMT6 cells detached from mats, the 3T3 cells did not spread and proliferate to the same extent as EMT6 cells. It is also interesting to note that such a disparity in the adhesion and proliferation of these cell types has not been observed for plasma polymerization. There was a disparity in the adhesion of EMT6 and BAEC cells on spNIPAM substrates, resulting in EMT6 spheroid development on these substrates.

Due to their rapid growth, EMT6 cells were used in the remaining experiments to determine which characteristics of the mats would support cell sheet attachment/detachment. Although it was established using SEM that the gauge diameter did not change the size distribution of the resulting fibers within

espNIPAM mats (see Figure 7.3), the mats produced using a 30 gauge needle supported cell sheets better than the other mats (see Figure 7.9).

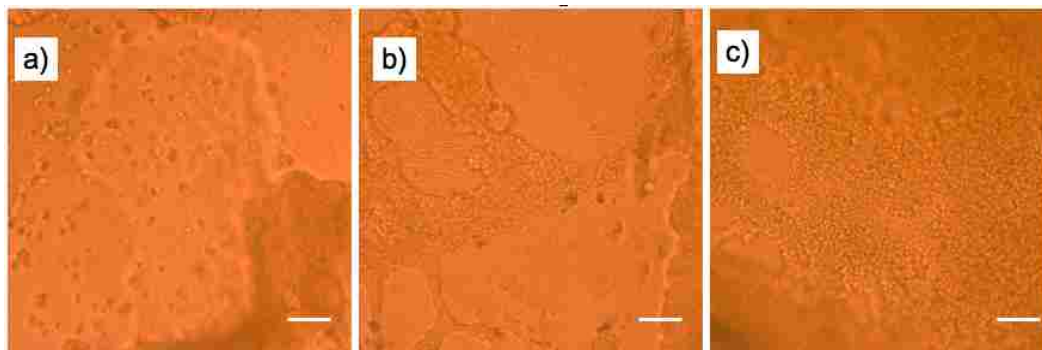


Figure 7.9: Bright field microscopy images of EMT6 cells that have released from espNIPAM mats after the temperature was shifted below the LCST. Cells released from mats collected for 5 minutes (a) and 10 minutes (b and c), produced with 21 gauge needles (a and b) as well as 30 gauge needles (c). Mats with smaller, denser fibers (c) supported cell sheets, and resulted in intact cell sheet detachment. Scale bars are 100 μm .

These results are consistent with previous work, indicating that dense, small fibers create a mat that has lower interfiber distance, thus minimizing cell penetration into the mat, forming a mat that is perceived by the cells as a 2D substrate, thus supporting cell sheet formation.⁴⁶

Having demonstrated that the cell sheets may be released in an unassisted manner from espNIPAM mats generated from HMW pNIPAM, the ability to relocate the cell sheet into a new well using a PVDF superstrate was tested. To achieve assisted cell transfer, a PVDF superstrate was attached to the apical surface of EMT6 cells cultured atop espNIPAM mats. As a negative control, the same procedure was attempted using a PVDF membrane to transfer replicate

cells cultured atop blank TCPS (no pNIPAM). The temperature was changed below the LCST, and the mats were removed from the well, with cells still attached. These cells were relocated into a new TCPS well, after which the PVDF membrane was removed. The cells were imaged 24 hours after their transfer to assess their proliferation.

As shown in Figure 7.10, the cells that were detached from the espNIPAM mats using PVDF readily attached to the new TCPS well. These results indicate that when cells are detached from the espNIPAM films assisted by PVDF membranes, their ECM remains intact, and promotes the adhesion of the cells to their new culture substrate. In contrast, the cells that were removed from blank TCPS wells using PVDF, and were thus peeled from the substrate as opposed to being detached with pNIPAM, did not attach to a new culture substrate after 24 hours of relocation.

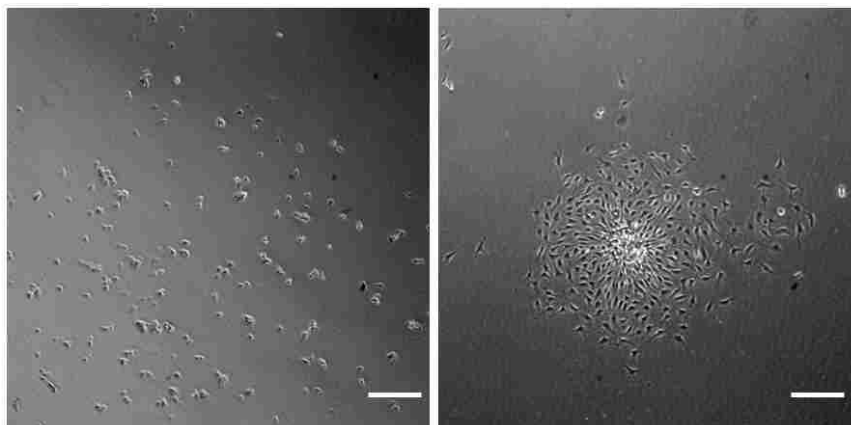


Figure 7.10: Bright field microscopy image of cells that have been transferred to a new well with PVDF superstrates from thermoresponsive espNIPAM mats (right) and control TCPS (left). Cells from the espNIPAM mats have retained their ECM and rapidly attach when transferred, as opposed to the control. Scale bars are 100 μm .

7.4 Conclusions

In this work, electrospinning was utilized for the fabrication of highly porous, thermoresponsive pNIPAM substrates. These substrates were then optimized for the fabrication of biocompatible mats for reversible cell adhesion. After varying the parameters used during electrospinning, the resulting espNIPAM mats were characterized. It was demonstrated that espNIPAM mats generated using the technique retain the same chemistry as the pNIPAM powder, as well as its reversibly thermoresponsive behavior near physiologically relevant temperatures. Although both LMW and HMW pNIPAM powders were capable of producing espNIPAM mats, due to concerns over cytotoxicity and complete collapse of LMW espNIPAM mats, only the HMW espNIPAM mats were appropriate for mammalian cell culture.

Interestingly, although both cancerous and non-cancerous cells readily formed cell sheets on the mats, the non-cancerous cell lines attached, but did not form cell sheets. As importantly, this method yielded faster cell release than many other methods reported in the literature: 80% of the cells detached within 5 minutes from the mats when the temperature was shifted below the LCST (as opposed to 80 minutes for electron beam ionization). Using EMT6 cells, it was shown that small, dense fibers better supported cell sheet formation. Interestingly, we found that, regardless of the gauge of the needle used when spinning the mat, similar fiber distribution was produced. However, the espNIPAM mats generated from the 30 gauge needles were more dense, and more suited to cell sheet detachment. This indicates that mats generated using these parameters will be ideal for cell sheet engineering and cancer cell biology studies.

Chapter 8. The Rapid Formation of Spheroids Using a “Smart” Polymer

Manuscript in preparation for publication by Reed, J.A.; DeLora, J.A.; Bluestein, B.M.; Freyer, J.P.; Canavan, H.E.

8.1 Introduction

At present, drug discovery studies rely heavily on tumor models for testing. As described in Chapter 1, traditionally animal models are employed, which can take up to several months for a tumor to grow.^{78, 91-95} To avoid the ethical dilemmas associated with animal models, and to expedite the research process, spheroids have become an increasingly popular tumor model alternative.^{9, 96}

One of the most commonly used methods for forming spheroids is seeding cells on an agar plate.¹⁹⁵ In this method, normally adherent cells will instead attach to each other (as opposed to the agar plate), forming the desired spheroids. Another method includes forcing the cells into suspension with a spinner flask, where the cells will, again, attach to each other.^{24, 27} (See Figure 8.1) Several other techniques use similar approaches to form spheroids by creating an environment where the only surface available for cell attachment is another cell. These techniques are discussed further in Chapter 1.

However, these methods present the drawback that they begin with cells that have recently been trypsinized. This enzyme treatment results in cells that lack cell/cell junctions, as well as the associated ECM layer. As previously mentioned,

pNIPAM has been used extensively for the non-destructive removal of cells from surfaces, and has been demonstrated to preserve cell/cell interactions, as well as many proteins (e.g., laminin, fibronectin, and collagen) of the ECM.¹¹² Recently, pNIPAM has been used to generate and release cell sheets that can ultimately fold to form spheroids.^{116, 117} To date, the cell sheets detached from pNIPAM substrates that have been used have been very large, resulting in a significant period of time between the detachment of cells from the pNIPAM substrate and the full spheroid formation (up to 3 weeks).¹²⁹

In this work, pNIPAM hydrogels (hpNIPAM) were used to create platforms appropriate for rapid, healthy cell sheet release for the purpose of spheroid formation. These gels have significantly more surface area exposed to the surrounding media than either spNIPAM or ppNIPAM substrates. As discussed in Chapter 7, this is a significant benefit allowing for rapid cell detachment. Due to this result in apparent pNIPAM surface area, the hpNIPAM substrates quickly swell when the temperature is shifted below the LCST. Using these substrates, spheroids have been formed in 28 hours, making this method ideal for rapid generation of spheroids. (See Figure 8.1)

8.2 Experimental Methods

The majority of the experiments carried out herein follow the procedures outlined in Chapter 2, including hpNIPAM processing, cytotoxicity, CellTracker™, and cell culture. Three repetitions of all experiments, producing three surfaces, were performed. Each surface was analyzed in three spots, for a total of 27

analyses.

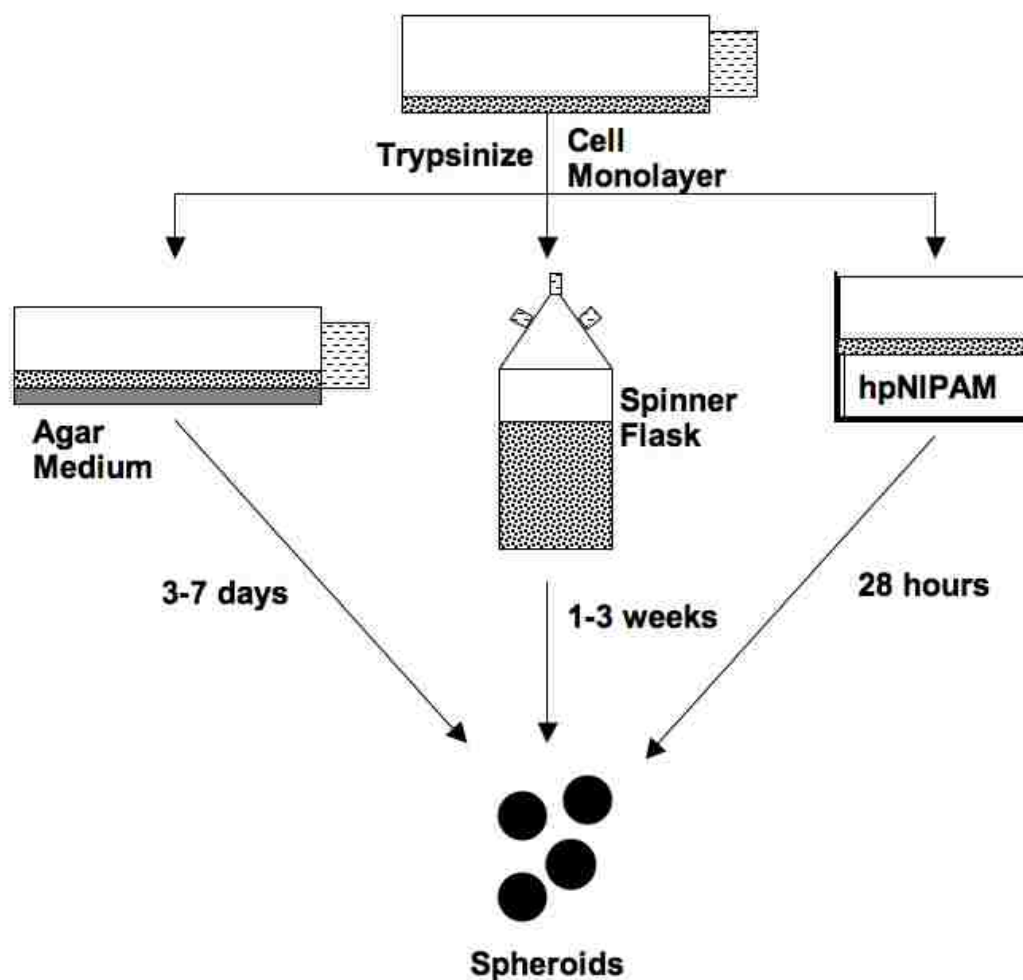


Figure 8.1: Methods for obtaining spheroids. On the top, a monolayer of cells is trypsinized and split either onto agar medium (left), into a spinner flask (middle), or onto a hpNIPAM gel (right). Although spheroids begin to form within 12 hours using traditional methods, it can require up to 3-7 days (left) or 1-3 weeks (middle) to form spheroids on the order of $\sim 500 \mu\text{m}$ or larger. Spheroids of any size can be formed using hpNIPAM within ~ 28 hours after splitting the cells (right).

8.2.1 FTIR

FTIR was carried out at Sandia National Laboratory using a Nicolet™ 6700 FT-IR (Thermo Electron Corporation) equipped with a continuum microscope. OMNIC™ Software (ThermoScientific) the bench setup included selecting a transmission ESP accessory, detector (DTGS KBr) and beamsplitter (XT-KBr).

Sample preparation was limited and hpNIPAM gels were imaged as prepared (neat) using the microscope attachment in reflective mode. Data were collected for 64 scans at a resolution of 4, from 400-4000 cm^{-1} . Spectra were exported to an .asc file and analyzed in Excel (Microsoft Corp.). All Spectra were normalized to the C=O stretching at 1640 cm^{-1} .

8.2.2 Thermoresponse

The thermoresponse of the gel was tested using a CO₂ microscope stage incubator from Okolab (Naples, Italy). Using the Okolab software, the temperature of the stage incubator was held constant at temperatures ranging from 26 °C to 40 °C. Within the incubator, gels were exposed to water and observed via light microscopy (Nikon F100, Melville, NY) using a 10x objective.

8.2.3 PDMS wells

Polydimethylsiloxane (PDMS) wells were fabricated in a two step process. First, two thin PDMS films were made. Sylgard® 184 base and curing agent (Dow Corning, Midland, MI) were mixed at a 10:1 ratio, and poured into a 24 well plate as a thin film. The films were cured at 70 °C for 45 minutes. One of the PDMS films was removed from the 24 well plate and a 6 mm hole was punched

out using a biopsy punch (Sklar Instruments, West Chester, PA). The two films were attached using an oxygen plasma treatment at 60W for 20 seconds. The result was a 6 mm well made entirely of PDMS, which is highly mobile, and will discourage cell attachment.

8.2.4 Determination of spheroid size

Spheroids were measured using light microscopy (Nikon F100, Melville, NY) with a 10x objective. Images were captured and measured using Spot Advanced software (Sterling Heights, MI).

8.3 Results and Discussions

8.3.1 Characterization of gels

Characterization of the hpNIPAM substrates was necessary to ensure the appropriate chemistry and characteristics were maintained through the processing of hpNIPAM. FT-IR, as shown in Figure 8.2, of the hpNIPAM gels found stretches that are indicative of pNIPAM, including C=O and N-H stretching at 1645 cm^{-1} and 3301 cm^{-1} (indicative of Amide I and Amide II stretching, respectively). These functional groups, in addition to the CH₂ and CH₃ asymmetric stretching (found at 2970 cm^{-1}), indicate that the functional groups expected to be present in pNIPAM are present in the hpNIPAM gels.

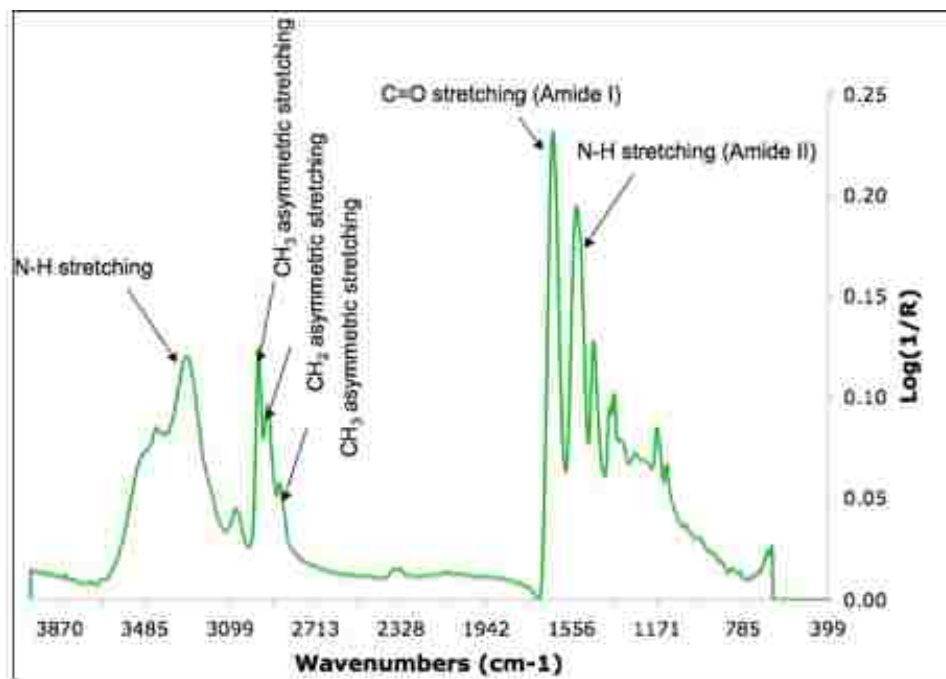


Figure 8.2: FTIR of hpNIPAM gels, with stretches indicative of pNIPAM.

Further characterization included testing the gels for thermoresponse. This process was completed using monodisperse microgels fabricated with a previously established procedure.^{172, 185, 187, 196, 197} Briefly, the water/monomer solution was injected into a microfluidic device. Using oil to create an emulsion, the water/monomer solution was focused, as shown in Figure 8.3.

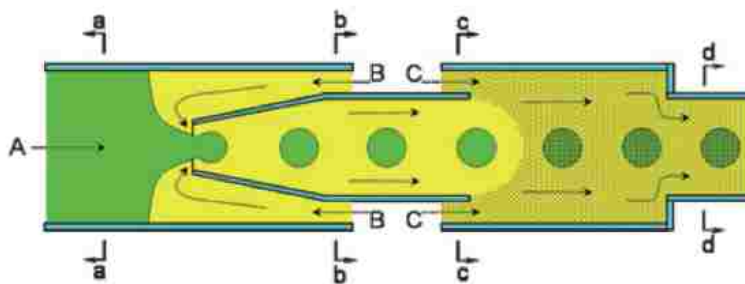


Figure 8.3: Schematic of microfluidic device utilized to form monodisperse pNIPAM microgels. A monomer/water solution is introduced to the device at point A. Oil was introduced at point B, creating an emulsion at the tip of the capillary within the device, forming monodisperse droplets of monomer/water within the bulk oil phase. At point C, oil with the initiator (which was soluble in both water and oil) was introduced, resulting in monodisperse pNIPAM microgels at point D.¹²⁹

Once monodisperse microgels were produced, an initiator was introduced to the system to initiate cross-linking, resulting in monodisperse pNIPAM microgels appropriate for testing the gel's thermoresponse. The sizes of the gels were measured using microscopy, and the results are presented in Figures 8.4 and 8.5. Above the LCST, the gels were relatively uniform, with an average diameter of 100-150 μm . (See Figure 8.4) When monitored in water while the temperature of the system was reduced below the LCST, the gels swelled up to 3 times their original size, or $\sim 375 \mu\text{m}$ in diameter. (See Figure 8.5) It is also interesting to note that the size dispersity of the gels increases greatly at lower temperature ($\pm 100 \mu\text{m}$ at the lowest temperature), as evidenced by the error bars in Figure 8.5.

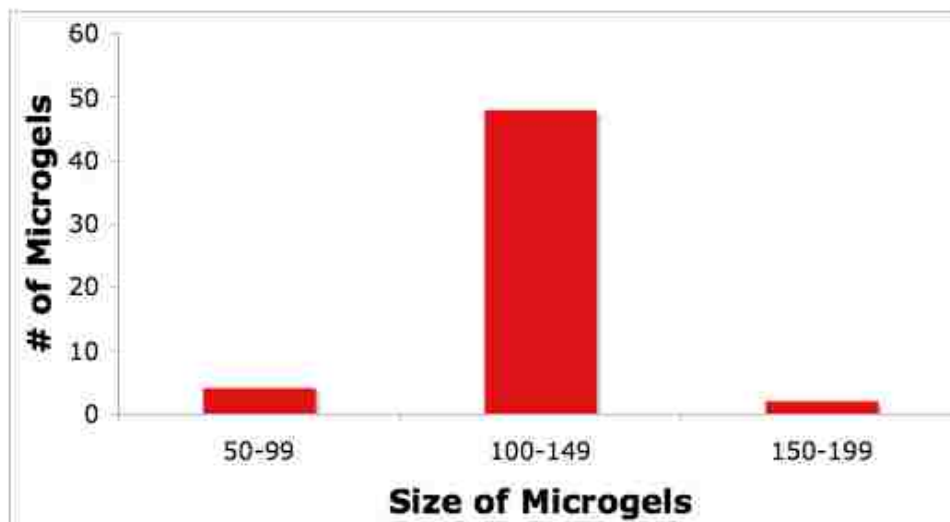


Figure 8.4: Microgels were imaged above the LCST and measured using Spot Image® software. The gels were monodisperse (~100-150 μm) above the LCST.

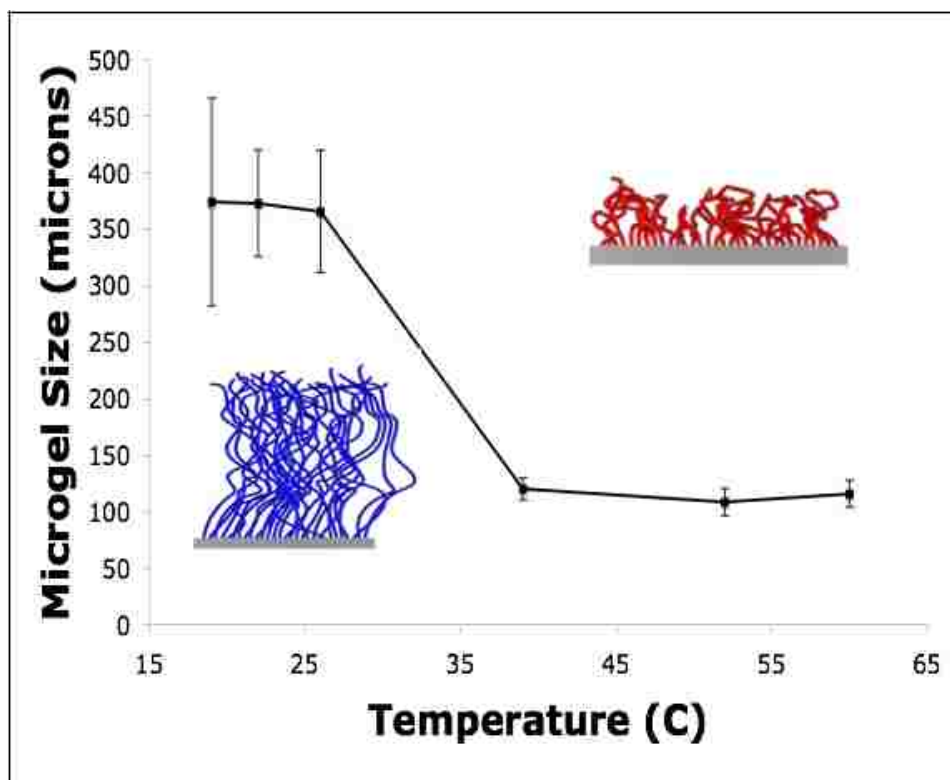


Figure 8.5: Microgels were monitored across the LCST. The gels swelled to 3 times their initial size when the temperature was shifted below the LCST.

8.3.2 Cell response

As it has previously been stated, there is some discussion in the literature as to whether pNIPAM substrates are cytotoxic; of the 5 published papers that demonstrate some apparent cytotoxicity, Neuro2A are cells grown in contact with gels fabricated using an initiator such as polyethylene imine (PEI), which has a similar structure to tetramethylethylenediamine (TEMED), which was used in this study.¹⁰⁸ Therefore, the potential cytotoxicity of the gels was tested to ensure that cells would survive contact with this material. Immediately after making the gels, a biopsy punch was used to create substrates that would fit inside a 96 well plate. These gels were then exposed to media for 24 hours. When this treated media was exposed to healthy 3T3s and EMT6s, cell viability decreased. (See Figure 8.6) If, however, the gels went through 10 cycles above and below the LCST in fresh water prior to making the treated media, cells survived exposure to the treated media. (See Figure 8.7) This indicates that residual NIPAM monomer and TEMED initiator needed to be removed before these substrates were suitable for mammalian cell culture.

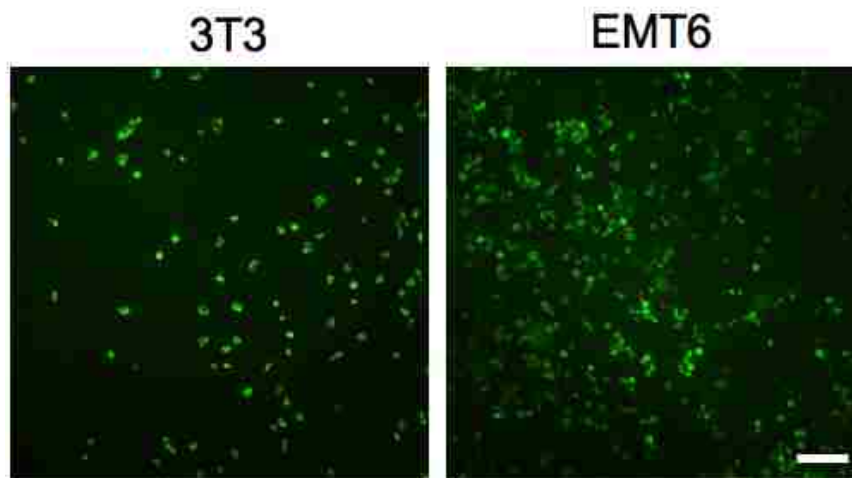


Figure 8.6: Fluorescent microscopy images of 3T3 (left) and EMT6 (right) cells after 24 hours of exposure to media treated with uncleaned hpNIPAM. Scale bar is 100 μm .

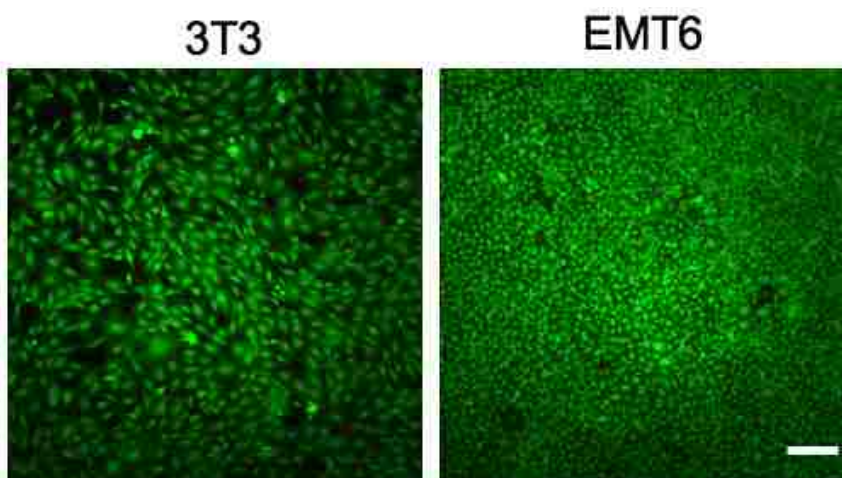


Figure 8.7: Fluorescent microscopy images of 3T3 (left) and EMT6 (right) cells after 24 hours of exposure to media treated with cleaned hpNIPAM. Scale bar is 100 μm .

Using this “clean” hpNIPAM, cells were tagged with Celltracker™ and seeded densely (100,000 cells/well for 3T3s and 50,000 cells/well for EMT6) onto the gels. It was found that the non-cancerous 3T3s were less likely to attach to the gels, instead forming spheroids. (See Figure 8.8) The cancerous EMT6 cells, on

the other hand, readily attached to the gels. These results are consistent with the findings in Chapter 7 that EMT6 cells are more likely to attach and proliferate on pNIPAM films with 3D topography than 3T3s.

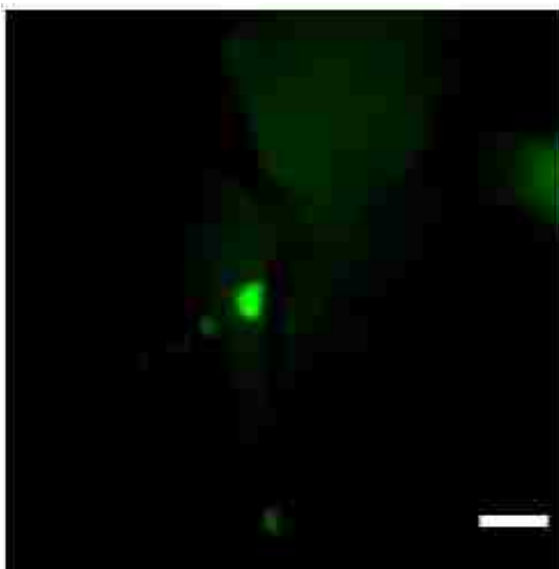


Figure 8.8: Fluorescent microscopy image of CellTracker™ tagged 3T3 cells on a gel. The cells have formed a spheroid on the gel. Scale bar is 100 μm .

8.3.3 Spheroid formation

Before shifting the temperature below the LCST, gels were transferred to PDMS wells, to encourage cell sheets to fold into spheroids as opposed to attaching to the underlying substrate. When the temperature was reduced below the LCST, cells and spheroids detached from the gels, and into the PDMS wells. Trypsinized cells were also seeded into similar PDMS wells to determine if release from hpNIPAM substrates was superior to using PDMS wells alone to form spheroids (as was done by Tekin et al.).⁹ As 3T3s were already spheroids, the EMT6 cell sheets were of primary interest.

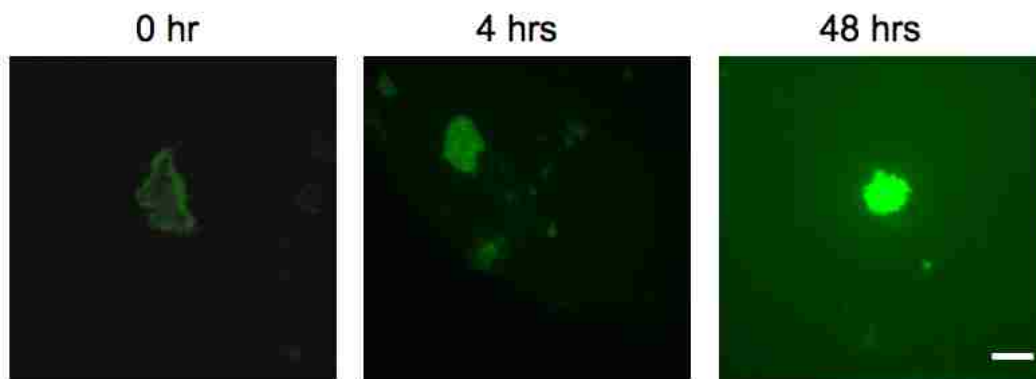


Figure 8.9: Fluorescent microscopy images of CellTracker™ tagged EMT6 cells immediately after (left), 4 hours after (middle), and 48 hours after (left) cell sheet release from hpNIPAM. Scale bar is 100 μm .

Following detachment of the EMT6 cells from the hpNIPAM substrates, the sheets formed a spheroid of $\sim 120 \mu\text{m}$ diameter within 4 hours. (See Figure 8.9) Over the next 20 hours, the spheroid became more compact. The spheroids were monitored over the next 48 hours and measured using Spot Imaging® software. Although the 3T3s formed spheroids directly on the hpNIPAM gels, they were considerably more uniform at $96 \mu\text{m} \pm 28$. The cell sheets that detached were less uniform, resulting in a large standard deviation of resulting spheroid sizes, at $107 \mu\text{m} \pm 69$.

The trypsinized cells, however, did not form spheroids. Instead, the cells attached to the underlying PDMS. (See Figure 8.10)

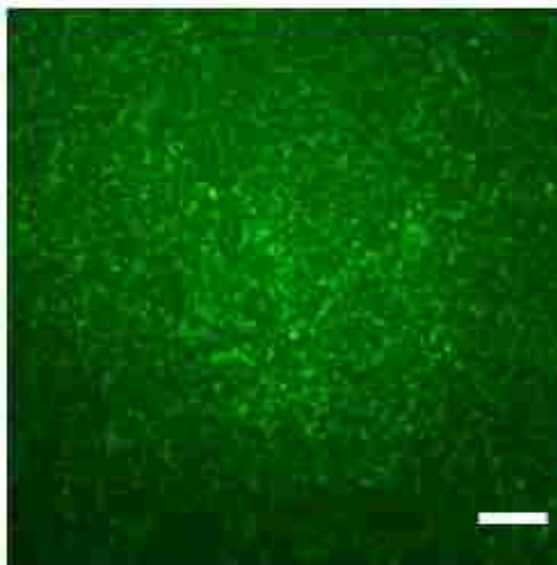


Figure 8.10: Fluorescent microscopy image of CellTracker™ tagged EMT6 cells that were trypsinized and transferred to a PDMS well. Within 4 hours of transfer, the cells had attached to the PDMS.

8.4 Conclusions

In this work, hpNIPAM substrates were characterized and adapted for use as mammalian cell culture platforms. Rapid swelling of the gels as the temperature shifted across the LCST proved useful in producing quick cell detachment. Cells released as spheroids or as cell sheets, depending on cell type. The cancerous (EMT6) cells that released as sheets folded into spheroids within 4 hours of detachment. Regardless of cell type, spheroids were produced within 28 hours of seeding gels. Although, not uniform, with further control over the area on which the cells can attach, rapid production of uniform spheroids of a desired size could be obtainable with this method.

Chapter 9. Conclusions and Future Directions

9.1 Conclusions

PNIPAM has been used for a variety of applications, including tissue engineering,¹ drug delivery,² and biosensing.³ Due to the interest by the biomedical engineering community, there has been a substantial amount of work published. In fact, to date, there are over 500 publications on pNIPAM for bioengineering applications. However, there are many inconsistencies in the literature, including the type and temperature of solution used for cell detachment. In this work, some of the inconsistencies in the literature and challenges that were previously unaddressed when utilizing pNIPAM films are overcome for the purpose of rapid generation of cellular constructs, specifically spheroids.

9.1.1 Optimizing parameters for rapid mammalian cell detachment

Pertinent characteristics of low temperature detachment, including the temperature and type of media used for detachment, were investigated for their effect on the kinetics of cell detachment, as described in Chapter 3. This work presented a study on the effect of the solution and temperature used to initiate cell detachment from pNIPAM on the time required to achieve 100% detachment of cells. The fastest, most reliable release of cells occurred below the LCST of the polymer at 4 °C in serum free media (SFM).

In addition, a novel, inexpensive method for obtaining pNIPAM films for

mammalian cell detachment, combining pNIPAM with a sol-gel, was optimized (described in Chapter 4). A method developed by Rao et al. was successfully adapted for the deposition of pNIPAM for bioengineering applications. Using this pNIPAM in conjunction with a sol-gel was found to be instrumental in maintaining film integrity during experimentation. Determination of the amount of pNIPAM to sol-gel demonstrated that 0.35 wt% spNIPAM surfaces had both the best thermoresponse and cell release. This technique is a simple and affordable alternative to previously described pNIPAM deposition methods for those applications that do not require intact cell sheets, such as protein preconcentration or biofouling release.

9.1.2 Development of novel deposition methods for reliable, controllable cell detachment

Deposition of pNIPAM with a sol-gel was compared to plasma polymerization deposition for use with mammalian cells, as described in Chapter 5. In this work, the differences in surface properties and cellular response of two pNIPAM deposition methods were compared. It was clear that although pNIPAM could be successfully deposited using different techniques and maintain thermoresponse, the deposition method influences coating uniformity and behavior which, in turn, determines which deposition method is appropriate for the desired application.

Furthermore, proper storage conditions (e.g., temperature and relative humidity) for these films were investigated in Chapter 6 to increase stability of the films for using tissue culture conditions. Although it is possible to deposit pNIPAM

using spin coating and plasma deposition that is thermoresponsive, the surfaces clearly are affected by both deposition method and storage conditions. Over time, it was found that the spNIPAM surfaces are unstable, regardless of storage conditions. In contrast, the ppNIPAM surfaces are more stable over time, regardless of the storage conditions, these surfaces encourage more cell attachment and proliferation. Furthermore, ppNIPAM films were demonstrated to be more benign toward cell behavior than alternative pNIPAM films (e.g., reduced cytotoxicity and better biocompatibility). All of these characteristics lead to the conclusion that ppNIPAM surfaces are more useful for cell sheet engineering applications.

9.1.3 Processing pNIPAM for increased mass transfer and accelerated cell detachment

Electrospun mats with a high surface area to volume ratio were utilized to improve cell detachment in Chapter 7. Cells attached to the mats, and would detach within 5 minutes from the mats when the temperature was shifted below the LCST. The espNIPAM mats, with small, dense fibers, are appropriate for cell sheet detachment, with an intact ECM, making these mats ideal for cell sheet engineering.

An alternate substrate for rapid cell release was investigated in Chapter 8. Hydrogel substrates were characterized and adapted for use as mammalian cell culture platforms. Rapid swelling of the gels as the temperature shifted across the LCST proved useful in producing quick cell detachment. The harvested cells

were transferred into PDMS wells, to encourage spheroid formation. Regardless of cell type, spheroids were produced within 28 hours of seeding gels, compared to the 72 hours required for alternative spheroid processing techniques. The result is a platform appropriate for the rapid formation of spheroids.

9.2 Future directions

9.2.1 Rapid formation of uniform and co-cultured spheroids

In Chapter 8, spheroids were obtained rapidly using hpNIPAM. However, the spheroids were not uniform in size, thus requiring a secondary step for relatively homogeneous models. Focusing the size of the hydrogel exposed to the cells will address this drawback. By forcing the cells to only settle in a designated area, the number of cells that will form the resulting cell sheet will be better controlled. One method for doing this is to use a non-fouling “well” (e.g., from PDMS) to encapsulate the gel, exposing only the area of interest to the cells.

The use of PDMS for focusing cell attachment/detachment can also be used with the other methods of pNIPAM deposition discussed, including plasma deposition. However, to increase the rate of cell detachment, porous surfaces as opposed to solid substrates would need to be coated with ppNIPAM, as demonstrated with electron beam ionization by Kwon, et al.

Furthermore, previous work has shown tumorigenic cells affect the proliferation of non-tumorigenic cells. Using either of the above methods, spheroids can be produced to track the cell growth and proliferation over time,

thus allowing the opportunity to study the effect of tumorigenic cells on non-tumorigenic “surrounding tissue.” Spheroids with multiple cell types are typically made by seeding a known mixture of the cells onto surfaces.^{106, 109} This method does not allow for control over the exact proportion of cells in each spheroid. One advantage of using cell sheets harvested from pNIPAM is control over the proportion of cells, since sheets of different cell types can either be layered, or cells can be seeded onto a primary, confluent sheet of cells. This control allows for a more complete understanding of the tumor model, and thus of the relationship between cell behavior and environmental or chemical factors.

9.2.2 Spheroid production and testing within microfluidic devices

Membrane coated ppNIPAM substrates could also be very useful when using microfluidic devices for spheroid formation and testing. Torisawa et al. formed spheroids with a microfluidic device using cell resistant surfaces to force cells to aggregate.⁹⁹ Hsiao et al. has used a similar format to create co-cultured spheroids.¹⁹⁸ If instead, cells were encouraged to attach within the device onto a ppNIPAM-coated membrane, a cell sheet could be detached and fold into a spheroid. This would offer the advantage of rapidly forming more uniform spheroids within the device.

In addition, these spheroids could easily be transferred to a testing platform within the device. Park et al., used the control available within a microfluidic device to control exposure of cells to different environments.¹⁹⁹ The spheroids formed within a device could then be forced into different environments (e.g.,

oxygen enriched vs. oxygen depleted) for more fundamental investigations, or into potential treatments. This platform offers the advantage of utilizing small quantities of the drugs being tested, as well as the ease of testing combinations of drugs at different ratios.²⁰⁰

9.2.3 Thermoresponsive microgels for harvesting individual cells

As mentioned in Chapter 1, EGFR is a transmembrane protein that is upregulated in cancer cells. If the ECM, which will house the extracellular moieties of this protein, is damaged using traditional cell harvesting techniques, it is logical to assume that these proteins are also damaged. This would result in skewed data when these proteins are examined using a technique such as flow cytometry, which requires individual cells in suspension for analysis. Since pNIPAM harvesting results in cells detaching with an intact ECM, individual cell release from these substrates would be necessary for investigating these proteins. One way to obtain individual cells is to create microgels of pNIPAM that are only large enough for a single cell to attach. Once attached, the temperature could be lowered across the LCST, and individual cells would detach with their ECM and transmembrane proteins intact. In addition to cancer research, individual cells with an intact ECM analyzed via flow cytometry could reveal a wealth of information regarding this buried biological interface.

9.2.4 Hydrogels incorporated with fluorescent nanoparticles

Traction force microscopy (TFM) has previously been used as a method for obtaining information about the forces exerted by a cell on a substrate. PNIPAM

hydrogels are perfect platforms for this research, due to their flexibility, which mimics the substrates that are traditionally used for TFM studies (thin silicon films).²⁰¹ These forces could also help explain why cells detach as a sheet from pNIPAM substrates, as the mechanism of detachment is still unknown.

Appendix I

Representative table of deposition methods utilized for mammalian cell culture, showing inconsistencies in literature.

Deposition Method	Cell Type	Cytotoxic	Pop-off Solution	Temperature of Cell Detachment	Form of Cell Detachment
Electron Beam Ionization ¹¹²	Bovine Aortic Endothelial Cells	N/A	Normal Growth Media	10 °C	N/A
Solution Dried on a Substrate ¹⁸³	Hepatocyte	N/A	Normal Growth Media	15 °C	Sheet
Free Radical Polymerization ¹⁹⁷	MC3T3-E1	Yes ²⁰² /No ¹²¹	Normal Growth Media	15 °C	Sheet
UV Polymerization ²⁷	Bovine Carotid Artery Endothelial Cells	N/A	Normal Growth Media	20 °C	Sheet
Plasma Polymerization ¹²⁰	Bovine Aortic Endothelial Cells	No ¹¹⁸	Serum Free Media	25 °C	Sheet
Spun Cast with Sol-Gel ¹²⁰	Bovine Aortic Endothelial Cells	No ¹¹²	Serum Free Media	4 °C	Aggregates

Appendix II

Spheroids formed using pNIPAM substrates.

Cell type	Diameter	Deposition method	Patterning?	Co-culture
Dermal fibroblasts ²⁰³	600 µm	Pour/dry w/collagen	No	No
Human dermal fibroblasts ^{115, 163, 163}	400-1000 µm	Pour/dry w/collagen	Yes/No ¹¹⁵ , UV	No
TIG-7 cells ¹¹⁵	400-950 µm	Pour/dry w/collagen	Yes, UV	No
Human dermal fibroblasts (CCD-922Sk) ¹¹⁵	400-950 µm	Pour/dry w/collagen	Yes, UV	No
IMR-90 cells ¹¹⁵	400-950 µm	Pour/dry w/collagen	Yes, UV	No
Human uterine cervical fibroblasts ¹¹⁵	400-950 µm	Pour/dry w/collagen	Yes, UV	No
Human skin fibroblasts ¹¹⁵	400-950 µm	Pour/dry w/collagen	Yes, UV	No
Human embryo cells ¹¹⁵	400-950 µm	Pour/dry w/collagen	Yes, UV	No
Human dental papilla fibroblastic cells ¹¹⁵	400-950 µm	Pour/dry w/collagen	Yes, UV	No
Rat calvaria osteoblastic cells ¹¹⁵	400-950 µm	Pour/dry w/collagen	Yes, UV	No
MC3T3-E1 cells ¹¹⁵	400-950 µm	Pour/dry w/collagen	Yes, UV	No
Rat mesangial cells ¹¹⁵	400-950 µm	Pour/dry w/collagen	Yes, UV	No
Human aortic intimal smooth muscle cells ¹¹⁵	400-950 µm	Pour/dry w/collagen	Yes, UV	No
Human neonatal medial smooth muscle cells ¹¹⁵	400-950 µm	Pour/dry w/collagen	Yes, UV	No
Rat parenchymal hepatocytes ^{116, 117, 116}	400-1720 µm	Pour/dry w/collagen	Yes/No ¹¹⁵ Yes, UV ¹¹⁷ , etched with a needle ²⁰⁴	Yes
Rat parenchymal hepatocytes ¹¹⁷	1000 µm	ATRP	No	Yes
Rat non-parenchymal hepatocytes ^{116, 116}	570-1720 µm	Pour/dry w/collagen	Yes/No ¹¹⁵ , etched with a needle	Yes
Mouse parenchymal hepatocytes ¹²⁰	400-950 µm	Pour/dry w/collagen	Yes, UV	No

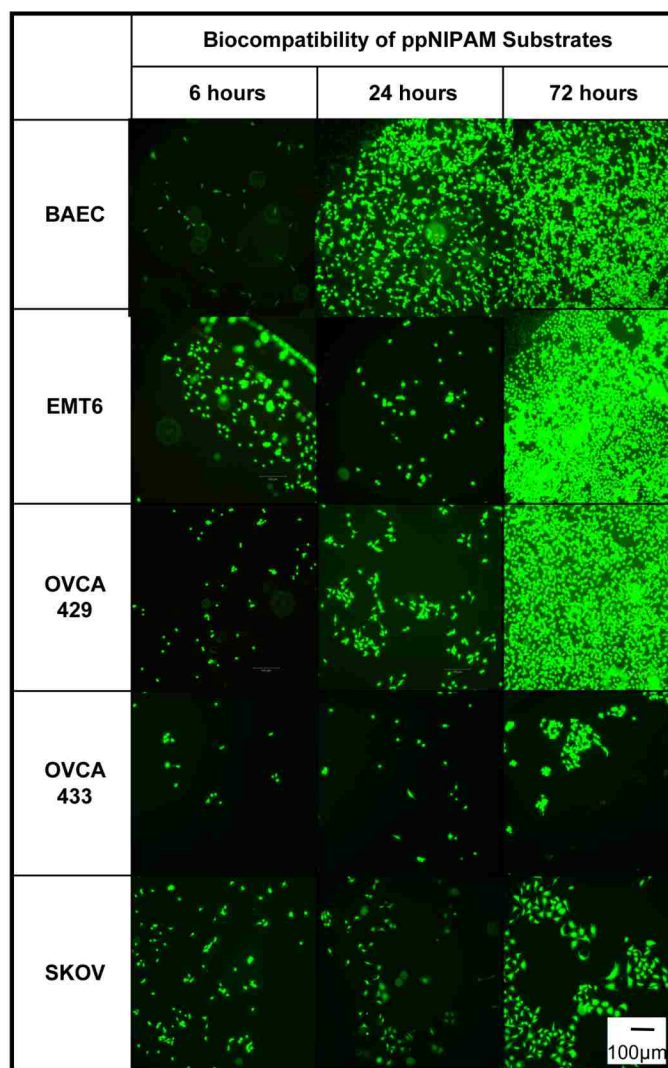
Appendix III

Complete list of cells used in this work.

Cell Name	Source	Cancerous?	Growth Media	Doubling Time (hrs)
Bovine Aortic Endothelial Cells (BAEC)	Cow	No	DMEM	18
MC3T3-E1	Mouse	No	α -MEM	18
EMT6	Rat	Yes	α -MEM	12
OVCA429	Human	Yes	MEM	40
OVCA433	Human	Yes	MEM	40
SKOV	Human	Yes	RPMI	36

Appendix IV

Fluorescent microscopy images of cytotoxicity testing (green=live, red=dead) for BAEC, EMT6, OVCA429, OVCA433, and SKOV cells grown in ppNIPAM treated media.



References

1. Garcia, M.; Jemal, A.; Ward, E.; Center, M.; Hao, Y.; Siegel, R.; Thun, M., *Global Cancer Facts & Figures 2007*. American Cancer Society: Atlanta, GA, 2007.
2. American Cancer Society, *Cancer Facts & Figures 2010*. American Cancer Society: Atlanta, GA, 2010.
3. Gerard, C.; Debruyne, C., Immunotherapy in the landscape of new targeted treatments for non-small cell lung cancer. *Molecular Oncology* **2009**, 3, (5-6), 409-424.
4. Browne, B. C.; O'Brien, N.; Duffy, M. J.; Crown, J.; O'Donovan, N., HER-2 Signaling and Inhibition in Breast Cancer. *Current Cancer Drug Targets* **2009**, 9, (3), 419-438.
5. Ciardello, F.; Tortora, G., EGFR Antagonists in Cancer Treatment. *New England Journal of Medicine* **2008**, 358, (11), 1160-1174.
6. Damia, G.; D'Incalci, M., Contemporary Pre-clinical Development of Anticancer Agents - What are the Optimal Preclinical Models? *European Journal of Cancer* **2009**, 45, (16), 2768-2781.
7. Hynes, N. E.; MacDonald, G., ErbB Receptors and Signaling Pathways in Cancer. *Current Opinion in Cell Biology* **2009**, 21, (2), 177-184.
8. Hynes, N. E.; Lane, H. A., ERBB Receptors and Cancer: The Complexity of Targeted Inhibitors. *Nature Reviews Cancer* **2005**, 5, (7), 341.
9. Friedrich, J.; Ebner, R.; Kunz-Schughart, L. A., Experimental Anti-tumor Therapy in 3-D: Spheroids - Old Hat or New Challenge? *International Journal of Radiation Biology* **2007**, 83, (11-12), 849-871.
10. Shield, K.; Ackland, M. L.; Ahmed, N.; Rice, G. E., Multicellular spheroids in ovarian cancer metastases: Biology and pathology. *Gynecologic Oncology* **2009**, 113, (1), 143-148.
11. Rossi, M. I. D.; Barros, A.; Baptista, L. S.; Garzoni, L. R.; Meirelles, M. N.; Takiya, C. M.; Pascarelli, B. M. O.; Dutra, H. S.; Borojevic, R., Multicellular spheroids of bone marrow stromal cells: a three-dimensional in vitro culture system for the study of hematopoietic cell migration. *Brazilian Journal of Medical and Biological Research* **2005**, 38, (10), 1455-1462.
12. LaRue, K. E. A.; Khalil, M.; Freyer, J. P., Microenvironmental Regulation of Proliferation in Multicellular Spheroids is Mediated Through Differential

Expression of Cyclin-dependent Kinase Inhibitors. *Cancer Research* **2004**, 64, (5), 1621-1631.

13. Corcoran, A.; De Ridder, L. I. F.; Del Duca, D.; Kalala, O. J. P.; Lah, T.; Pilkington, G. J.; Del Maestro, R. F., Evolution of the Brain Tumour Spheroid Model: Transcending Current Model Limitations. *Acta Neurochirurgica* **2003**, 145, (9), 819-824.

14. Kunz-Schughart, L. A.; Freyer, J. P., Phosphorous Metabolites and Steady-state Energetics of Transformed Fibroblasts During Three-dimensional Growth. *American Journal of Physiology-Cell Physiology* **2002**, 283, (4), C1287-C1297.

15. Freyer, J. P., Decreased Mitochondrial Function in Quiescent Cells Isolated from Multicellular Tumor Spheroids. *Journal of Cellular Physiology* **1998**, 176, (1), 138-149.

16. KunzSchughart, L. A.; Habbersett, R. C.; Freyer, J. P., Mitochondrial function in oncogene-transfected rat fibroblasts isolated from multicellular spheroids. *American Journal of Physiology-Cell Physiology* **1997**, 273, (5), C1487-C1495.

17. Marusic, M.; Bajzer, Z.; Vukpavlovic, S.; Freyer, J. P., Tumor-Growth in vivo and as Multicellular Spheroids Compared by Mathematical-models. *Bulletin of Mathematical Biology* **1994**, 56, (4), 617-631.

18. Freyer, J. P.; Schor, P. L.; Jarrett, K. A.; Neeman, M.; Sillerud, L. O., Cellular Energetics Measured by Phosphorus Nuclear-Magnetic-Resonance Spectroscopy are not Correlated with Chronic Nutrient Deficiency in Multicellular Tumor Spheroids .1. *Cancer Research* **1991**, 51, (15), 3831-3837.

19. Holbeck, S. L., Update on NCI in vitro Drug Screen Utilities. *European Journal of Cancer* **2004**, 40, (6), 785-793.

20. Sausville, E. A.; Feigal, E., Evolving approaches to cancer drug discovery and development at the National Cancer Institute, USA. *Annals of Oncology* **1999**, 10, (11), 1287-1291.

21. Burdett, E.; Kasper, F. K.; Mikos, A. G.; Ludwig, J. A., Engineering Tumors: A Tissue Engineering Perspective in Cancer Biology. *Tissue Engineering Part B-Reviews* **2010**, 16, (3), 351-359.

22. Ertel, A.; Verghese, A.; Byers, S.; Ochs, M.; Tozeren, A., Pathway-specific Differences Between Tumor Cell Lines and Normal and Tumor Tissue Cells. *Molecular Cancer* **2006**, 5, (55).

23. van Staveren, W. C. G.; Solis, D. Y. W.; Hebrant, A.; Detours, V.; Dumont, J. E.; Maenhaut, C., Human cancer cell lines: Experimental models for cancer

cells in situ? For cancer stem cells? *Biochimica Et Biophysica Acta-Reviews on Cancer* **2009**, 1795, (2), 92-103.

24. Canavan, H. E.; Cheng, X. H.; Graham, D. J.; Ratner, B. D.; Castner, D. G., Cell Sheet Detachment Affects the Extracellular Matrix: A Surface Science Study Comparing Thermal Liftoff, Enzymatic, and Mechanical methods. *Journal of Biomedical Materials Research Part A* **2005**, 75A, (1), 1-13.

25. Canavan, H. E.; Graham, D. J.; Cheng, X. H.; Ratner, B. D.; Castner, D. G., Comparison of Native Extracellular Matrix with Adsorbed Protein Films using Secondary Ion Mass Spectrometry. *Langmuir* **2007**, 23, (1), 50-56.

26. Canavan, H. E.; Cheng, X. H.; Graham, D. J.; Ratner, B. D.; Castner, D. G., A Plasma-deposited Surface for Cell Sheet Engineering: Advantages Over Mechanical Dissociation of Cells. *Plasma Processes and Polymers* **2006**, 3, (6-7), 516-523.

27. Canavan, H. E.; Cheng, X. H.; Graham, D. J.; Ratner, B. D.; Castner, D. G., Surface Characterization of the Extracellular Matrix Remaining After Cell Detachment from a Thermoresponsive Polymer. *Langmuir* **2005**, 21, (5), 1949-1955.

28. Freshney, R. I., *Culture of Animal Cells. A Manual of Basic Technique*. John Wiley & Sons, Inc.: Hoboken, NJ, 2005; p 360.

29. Bissell, M. J.; Radisky, D., Putting Tumours in Context. *Nature Reviews Cancer* **2001**, 1, (1), 46-54.

30. Jacks, T.; Weinberg, R. A., Taking the Study of Cancer Cell Survival to a New Dimension. *Cell* **2002**, 111, (7), 923-925.

31. Mueller, M. M.; Fusenig, N. E., Friends or Foes - Bipolar Effects of the Tumour Stroma in Cancer. *Nature Reviews Cancer* **2004**, 4, (11), 839-849.

32. Wernert, N., The multiple roles of tumour stroma. *Virchows Archiv-an International Journal of Pathology* **1997**, 430, (6), 433-443.

33. Liotta, L. A.; Kohn, E. C., The Microenvironment of the Tumour-Host Interface. *Nature* **2001**, 411, (6835), 375-379.

34. Milotti, E.; Chignola, R., Emergent Properties of Tumor Microenvironment in a Real-Life Model of Multicell Tumor Spheroids. *Plos One* **2010**, 5, (11), 1-12.

35. Neeman, M.; Jarrett, K. A.; Sillerud, L. O.; Freyer, J. P., Self-diffusion of Water in Multicellular Spheroids Measure by Magnetic-Resonance Microimaging. *Cancer Research* **1991**, 51, (15), 4072-4079.

36. Bortner, C. D.; Cidlowski, J. A., Apoptotic Volume Decrease and the

Incredible Shrinking Cell. *Cell Death and Differentiation* **2002**, 9, (12), 1307-1310.

37. Johnson, J. I.; Decker, S.; Zaharevitz, D.; Rubinstein, L. V.; Venditti, J.; Schepartz, S.; Kalyandrug, S.; Christian, M.; Arbuck, S.; Hollingshead, M.; Sausville, E. A., Relationships Between Drug Activity in NCI Preclinical in vitro and in vivo Models and Early Clinical Trials. *British Journal of Cancer* **2001**, 84, (10), 1424-1431.

38. Shoemaker, R. H., The NCI60 human tumour cell line anticancer drug screen. *Nature Reviews Cancer* **2006**, 6, (10), 813-823.

39. Voskoglou-Nomikos, T.; Pater, J. L.; Seymour, L., Clinical predictive value of the in vitro cell line, human xenograft, and mouse allograft preclinical cancer models. *Clinical Cancer Research* **2003**, 9, (11), 4227-4239.

40. Brody, B., *The Ethics of Biomedical Research: An International Perspective*. Oxford University Press, Inc: New York, NY, 1998.

41. American and Plant Health Inspection Service, Animal Welfare Act. In Agriculture, United States Department of Agriculture, Ed. 1966.

42. Olson, H.; Betton, G.; Robinson, D.; Thomas, K.; Monro, A.; Kolaja, G.; Lilly, P.; Sanders, J.; Sipes, G.; Bracken, W.; Dorato, M.; Van Deun, K.; Smith, P.; Berger, B.; Heller, A., Concordance of the toxicity of pharmaceuticals in humans and in animals. *Regulatory Toxicology and Pharmacology* **2000**, 32, 56-67.

43. Hoffman, M.T., The Escalating Cost of Animal Experimentation: The National Institutes of Health Funding Scandal. In 2001.

44. Dong, X.; Guan, J.; English, J. C.; Flint, J.; Yee, J.; Evans, K.; Murray, N.; MacAulay, C.; Ng, R. T.; Gout, P. W.; Lam, W. L.; Laskin, J.; Ling, V.; Lam, S.; Wang, Y. Z., Patient-Derived First Generation Xenografts of Non-Small Cell Lung Cancers: Promising Tools for Predicting Drug Responses for Personalized Chemotherapy. *Clinical Cancer Research* **2010**, 16, (5), 1442-1451.

45. Peterson, J. K.; Houghton, P. J., Integrating Pharmacology and in vivo Cancer Models in Preclinical and Clinical Drug Development. *European Journal of Cancer* **2004**, 40, (6), 837-844.

46. Robles, A. I.; Varticovski, L., Harnessing genetically engineered mouse models for preclinical testing. *Chemico-Biological Interactions* **2008**, 171, (2), 159-164.

47. Suggitt, M.; Bibby, M. C., 50 years of preclinical anticancer drug screening: Empirical to target-driven approaches. *Clinical Cancer Research* **2005**, 11, (3), 971-981.

48. Directors, S. f. c. T. B. o., The Society for Clinical Trials opposes US legislation to permit marketing of unproven medical therapies for seriously ill patients. *clinical Trials* **2006**, 3, 154-157.
49. Horrobin, D. F., Are Large Clinical Trials in Rapidly Lethal Diseases Usually Unethical? *Lancet* **2003**, 361, (9358), 695-697.
50. Kola, I.; Landis, J., Can the Pharmaceutical Industry Reduce Attrition Rates? *Nature Reviews Drug Discovery* **2004**, 3, (8), 711-715.
51. Sharpless, N. E.; DePinho, R. A., Model organisms - The mighty mouse: genetically engineered mouse models in cancer drug development. *Nature Reviews Drug Discovery* **2006**, 5, (9), 741-754.
52. Sharpless, N. E.; DePinho, R. A., Model Oganisms - The Mighty Mouse: Genetically Engineered Mouse Models in Cancer Drug Development. *Nature Reviews Drug Discovery* **2006**, 5, (9), 741-754.
53. Firestone, B., The challenge of selecting the 'right' in vivo oncology pharmacology model. *Current Opinion in Pharmacology* **2010**, 10, (4), 391-396.
54. Fiebig, H. H.; Maier, A.; Burger, A. M., Clonogenic Assay with Established Human Tumour Xenografts: Correlation of in vitro to in vivo Activity as a Basis for Anticancer Drug Discovery. *European Journal of Cancer* **2004**, 40, (6), 802-820.
55. Boven, E.; Winograd, B.; Berger, D. P.; Dumont, M. P.; Braakhuis, B. J. M.; Fodstad, O.; Langdon, S.; Fiebig, H. H., Phase-II Preclinical Drug Screening in Human Tumore Xenografts- A 1st European Multicenter Collaborative Study. *Cancer Research* **1992**, 52, (21), 5940-5947.
56. Garber, K., Companies Waver in Efforts To Target Transforming Growth Factor beta in Cancer. *Journal of the National Cancer Institute* **2009**, 101, (24), 1664-1666.
57. Abate-Shen, C.; Brown, P. H.; Colburn, N. H.; Gerner, E. W.; Green, J. E.; Lipkin, M.; Nelson, W. G.; Threadgill, D., The Untapped Potential of Genetically Engineered Mouse Models in Chemoprevention Research: Opportunities and Challenges. *Cancer Prevention Research* **2008**, 1, (3), 161-166.
58. DeNardo, D. G.; Coussens, L. M., Inflammation and Breast Cancer - Balancing Immune Response: Crosstalk Between Adaptive and Innate Immune Cells During Breast Cancer Progression. *Breast Cancer Research* **2007**, 9, (4).
59. Garrett, W. S.; Lord, G. M.; Punit, S.; Lugo-Villarino, G.; Mazmanian, S. K.; Ito, S.; Glickman, J. N.; Glimcher, L. H., Communicable Ulcerative Colitis Dnduced by T-bet Deficiency in the Innate Immune System. *Cell* **2007**, 131, (1), 33-45.

60. Nelson, W. G.; DeWeese, T. L.; DeMarzo, A. M., The Diet, Prostate Inflammation, and the Development of Prostate Cancer. *Cancer and Metastasis Reviews* **2002**, 21, (1), 3-16.
61. Varticovski, L.; Hollingshead, M. G.; Robles, A. I.; Wu, X. L.; Cherry, J.; Munroe, D. J.; Lukes, L.; Anver, M. R.; Carter, J. P.; Borgel, S. D.; Stotler, H.; Bonomi, C. A.; Nunez, N. P.; Hursting, S. D.; Qiao, W. H.; Deng, C. X. X.; Green, J. E.; Hunter, K. W.; Merlino, G.; Steeg, P. S.; Wakefield, L. M.; Barrett, J. C., Accelerated preclinical testing using transplanted tumors from genetically engineered mouse breast cancer models. *Clinical Cancer Research* **2007**, 13, (7), 2168-2177.
62. Bhadriraju, K.; Chen, C. S., Engineering Cellular Microenvironments to Cell-based Drug Testing Improve. *Drug Discovery Today* **2002**, 7, (11), 612-620.
63. Casciari, J. J.; Hollingshead, M. G.; Alley, M. C.; Mayo, J. G.; Malspeis, L.; Miyauchi, S.; Grever, M. R.; Weinstein, J. N., Growth and Chemotherapeutic Response of Cells in a Hollow-Fiber In-Vitro Solid Tumor-Model. *Journal of the National Cancer Institute* **1994**, 86, (24), 1846-1852.
64. Chaw, K. C.; Manimaran, M.; Tay, E. H.; Swaminathan, S., Multi-step Microfluidic Device for Studying Cancer Metastasis. *Lab on a Chip* **2007**, 7, (8), 1041-1047.
65. Chaw, K. C.; Manimaran, M.; Tay, F. E. H.; Swaminathan, S., Matrigel Coated Polydimethylsiloxane Based Microfluidic Devices for Studying Metastatic and Non-metastatic Cancer Cell Invasion and Migration. *Biomedical Microdevices* **2007**, 9, (4), 597-602.
66. Debnath, J.; Brugge, J. S., Modelling Glandular Epithelial Cancers in Three-dimensional Cultures. *Nature Reviews Cancer* **2005**, 5, (9), 675-688.
67. Dulong, J. L.; Legallais, C.; Darquy, S.; Reach, G., A Novel Model of Solute Transport in a Hollow-fiber Bioartificial Pancreas Based on a Finite Element Method. *Biotechnology and Bioengineering* **2002**, 78, (5), 576-582.
68. Gillies, R. J.; Galons, J. P.; McGovern, K. A.; Scherer, P. G.; Lien, Y. H.; Job, C.; Ratcliff, R.; Chapa, F.; Cerdan, S.; Dale, B. E., Design and Application of NMR-Compatible Bioreactor Circuits for Extended Perfusion of High-density Mammalian-cell Cultures. *Nmr in Biomedicine* **1993**, 6, (1), 95-104.
69. Hicks, K. O.; Ohms, S. J.; vanZijl, P. L.; Denny, W. A.; Hunter, P. J.; Wilson, W. R., An Experimental and Mathematical Model for the Extravascular Transport of a DNA Intercalator in Tumours. *British Journal of Cancer* **1997**, 76, (7), 894-903.
70. Kim, J. H.; Ahn, S. I.; Zin, W. C., Evaporation of Water Droplets on Polymer Surfaces. *Langmuir* **2007**, 23, (11), 6163-6169.

71. Lee, G. Y.; Kenny, P. A.; Lee, E. H.; Bissell, M. J., Three-dimensional Culture Models of Normal and Malignant Breast Epithelial Cells. *Nature Methods* **2007**, 4, (4), 359-365.
72. Legallais, C.; David, B.; Dore, E., Bioartificial Livers (BAL): Current Technological Aspects and Future Developments. *Journal of Membrane Science* **2001**, 181, (1), 81-95.
73. Muralidhar, R. V.; Jayachandran, G.; Singh, P., Development of High-density Cultivation Systems by Bioencapsulation. *Current Science* **2001**, 81, (3), 263-269.
74. Padron, J. M.; van der Wilt, C. L.; Smid, K.; Smitskamp-Wilms, E.; Backus, H. H. J.; Pizao, P. E.; Giaccone, G.; Peters, G. J., The Multilayered Postconfluent Cell Culture as a Model for Drug Screening. *Critical Reviews in Oncology Hematology* **2000**, 36, (2-3), 141-157.
75. Walker, G. M.; Beebe, D. J., A passive pumping method for microfluidic devices. *Lab on a Chip* **2002**, 2, (3), 131-134.
76. Warrick, J.; Meyvantsson, I.; Ju, J. I.; Beebe, D. J., High-throughput microfluidics: improved sample treatment and washing over standard wells. *Lab on a Chip* **2007**, 7, (3), 316-321.
77. Smalley, K. S. M.; Lioni, M.; Noma, K.; Haass, N. K.; Herlyn, M., In vitro three-dimensional tumor microenvironment models for anticancer drug discovery. *Expert Opinion on Drug Discovery* **2008**, 3, (1), 1-10.
78. Hirschhaeuser, F.; Menne, H.; Dittfeld, C.; West, J.; Mueller-Klieser, W.; Kunz-Schughart, L. A., Multicellular Tumor Spheroids: An Underestimated Tool is Catching Up Again. *Journal of Biotechnology* **2010**, 148, (1), 3-15.
79. Boyd, M.; Mairs, R. J.; Keith, W. N.; Ross, S. C.; Welsh, P.; Akabani, G.; Owens, J.; Vaidyanathan, G.; Carruthers, R.; Dorrens, J.; Zalutsky, M. R., An Efficient Targeted Radiotherapy/Gene Therapy Strategy Utilising Human Tetomerase Promoters and Radioastatine and Harnessing Radiation-mediated Bystander Effects. *Journal of Gene Medicine* **2004**, 6, (8), 937-947.
80. Boyd, M.; Mairs, S. C.; Stevenson, K.; Livingstone, A.; Clark, A. M.; Ross, S. C.; Mairs, R. J., Transfectant Mosaic Spheroids: A New Model for Evaluation of Tumour Cell Killing in Targeted Radiotherapy and Experimental Gene Therapy. *Journal of Gene Medicine* **2002**, 4, (5), 567-576.
81. Djordjevic, B.; Lange, C. S., Cell-cell Interactions in Spheroids Maintained in Suspension. *Acta Oncologica* **2006**, 45, (4), 412-420.
82. Djordjevic, B.; Lange, C. S.; Allison, R. R.; Rotman, M., Response of Primary Colon-cancer Cells in Hybrid Spheroids to 5-Fluorouracil. *Cancer*

Investigation **1993**, 11, (3), 291-298.

83. Djordjevic, B.; Lange, C. S.; Schwartz, M. S.; Rotman, M., Clonogenic Inactivation of Colon Cancer-derived Cells Treated with 5-fluorouracil and Indomethacin in Hybrid Spheroids. *Acta Oncologica* **1998**, 37, (7-8), 735-739.

84. Kunz-Schughart, L. A., Multicellular Tumor Spheroids: Intermediates Between Monolayer Culture and in vivo Tumor. *Cell Biology International* **1999**, 23, (3), 157-161.

85. Vamvakidou, A. P.; Mondrinos, M. J.; Petushi, S. P.; Garcia, F. U.; Lelkes, P. I.; Tozeren, A., Heterogeneous breast tumoroids: An in vitro assay for investigating cellular heterogeneity and drug delivery. *Journal of Biomolecular Screening* **2007**, 12, (1), 13-20.

86. Sutherland, R.; Inch, W. R.; McCredie, J. A., Phytohemagglutinin (Pha)-Induced Transformation of Lymphocytes from Patients with Cancer. *Cancer* **1971**, 27, (3), 574-&.

87. Sutherland, R.; Inch, W. R.; McCredie, J. A.; Kruuv, J., Multi-component Radiation Survival Curve Using an In-Vitro Tumor Model. *International Journal of Radiation Biology and Related Studies in Physics Chemistry and Medicine* **1970**, 18, (5), 491-&.

88. Sutherland, R.; McCredie, J. A.; Inch, W. R., Growth of Multicell Spheroids in Tissue Culture as a Model of Nodular Carcinomas. *Journal of the National Cancer Institute* **1971**, 46, (1), 113-&.

89. Sutherland, R. M., Cell and Environment Interactions in Tumor Microregions- The Multicell Spheroid Model. *Science* **1988**, 240, (4849), 177-184.

90. Olive, P.; Durand, R., Drug and Radiation Resistance in Spheroids: Cell Contact and Kinetics. *Cancer and Metastasis Reviews* **1994**, 13, 121-138.

91. Barbone, D.; Yang, T. M.; Morgan, J. R.; Gaudino, G.; Broaddus, V. C., Mammalian Target of Rapamycin Contributes to the Acquired Apoptotic Resistance of Human Mesothelioma Multicellular Spheroids. *Journal of Biological Chemistry* **2008**, 283, (19), 13021-13030.

92. Dardousis, K.; Voolstra, C.; Roengvoraphoj, M.; Sekandarzad, A.; Mesghenna, S.; Winkler, J.; Ko, Y.; Hescheler, J.; Sachinidis, A., Identification of Differentially Expressed Genes Involved in the Formation of Multicellular Tumor Spheroids by HT-29 Colon Carcinoma Cells. *Molecular Therapy* **2007**, 15, (1), 94-102.

93. Frankel, A.; Man, S.; Elliott, P.; Adams, J.; Kerbel, R. S., Lack of Multicellular Drug Resistance Observed in Human Ovarian and Prostate

Carcinoma Treated with the Proteasome Inhibitor PS-341. *Clinical Cancer Research* **2000**, 6, (9), 3719-3728.

94. Howes, A. L.; Chiang, G. G.; Lang, E. S.; Ho, C. B.; Powis, G.; Vuori, K.; Abraham, R. T., The Phosphatidylinositol 3-kinase Inhibitor, PX-866, is a Potent Inhibitor of Cancer Cell Motility and Growth in Three-dimensional Cultures. *Molecular Cancer Therapeutics* **2007**, 6, (9), 2505-2514.

95. Poland, J.; Sinha, P.; Siegert, A.; Schnolzer, M.; Korf, U.; Hauptmann, S., Comparison of Protein Expression Profiles Between Monolayer and Spheroid Cell Culture of HT-29 Cells Revealed Fragmentation of CK18 in Three-dimensional Cell Culture. *Electrophoresis* **2002**, 23, (7-8), 1174-1184.

96. Kunz-Schughart, L. A.; Freyer, J. P.; Hofstaedter, F.; Ebner, R., The use of 3-D cultures for High-throughput Screening: The Multicellular Spheroid Model. *Journal of Biomolecular Screening* **2004**, 9, (4), 273-285.

97. Ingram, M.; Techy, G. B.; Saroufeem, R.; Yazan, O.; Narayan, K. S.; Goodwin, T. J.; Spaulding, G. F., Three-dimensional Growth Patterns of Various Human Tumor Cell Lines in Simulated Microgravity of a NASA Bioreactor. *In Vitro Cellular & Developmental Biology-Animal* **1997**, 33, (6), 459-466.

98. Frimat, J. P.; Sisnaiske, J.; Subbiah, S.; Menne, H.; Godoy, P.; Lampen, P.; Leist, M.; Franzke, J.; Hengstler, J. G.; van Thriel, C.; West, J., The Network Formation Assay: A Spatially Standardized Neurite Outgrowth Analytical Display for Neurotoxicity Screening. *Lab on a Chip* **2010**, 10, (6), 701-709.

99. Hsiao, A. Y.; Torisawa, Y. S.; Tung, Y. C.; Sud, S.; Taichman, R. S.; Pienta, K. J.; Takayama, S., Microfluidic System for Formation of PC-3 Prostate Cancer Co-culture Spheroids. *Biomaterials* **2009**, 30, (16), 3020-3027.

100. Zhang, M.; Lee, P.; Hung, P.; Johnson, T.; Lee, L.; Mofrad, M., Microfluidic environment for high density hepatocyte culture. *Biomedical Microdevices* **2008**, 10, 117-121.

101. Kojima, R.; Yoshimoto, K.; Takahashi, E.; Ichino, M.; Miyoshi, H.; Nagasaki, Y., Spheroid Array of Fetal Mouse Liver Cells Constructed on a PEG-gel Micropatterned Surface: Upregulation of Hepatic Functions by Co-culture with Nonparenchymal Liver Cells. *Lab on a Chip* **2009**, 9, (14), 1991-1993.

102. Otsuka, H.; Hirano, A.; Nagasaki, Y.; Okano, T.; Horiike, Y.; Kataoka, K., Two-dimensional Multiarray Formation of Hepatocyte Spheroids on a Microfabricated PEG-brush Surface. *Chembiochem* **2004**, 5, (6), 850-855.

103. Powers, M. J.; Domansky, K.; Kaazempur-Mofrad, M. R.; Kalezi, A.; Capitano, A.; Upadhyaya, A.; Kurzawski, P.; Wack, K. E.; Stolz, D. B.; Kamm, R.; Griffith, L. G., A Microfabricated Array Bioreactor for Perfused 3D Liver Culture. *Biotechnology and Bioengineering* **2002**, 78, (3), 257-269.

104. Tamura, T.; Sakai, Y.; Nakazawa, K., Two-dimensional microarray of HepG2 spheroids using collagen/polyethylene glycol micropatterned chip. *Journal of Materials Science-Materials in Medicine* **2008**, 19, (5), 2071-2077.
105. Toh, Y. C.; Zhang, C.; Zhang, J.; Khong, Y. M.; Chang, S.; Samper, V. D.; van Noort, D.; Hutmacher, D. W.; Yu, H. R., A novel 3D mammalian cell perfusion-culture system in microfluidic channels. *Lab on a Chip* **2007**, 7, (3), 302-309.
106. Torisawa, Y. S.; Chueh, B. H.; Huh, D.; Ramamurthy, P.; Roth, T. M.; Barald, K. F.; Takayama, S., Efficient Formation of Uniform-sized Embryoid Bodies Using a Compartmentalized Microchannel Device. *Lab on a Chip* **2007**, 7, (6), 770-776.
107. Nakazawa, K.; Izumi, Y.; Fukuda, J.; Yasuda, T., Hepatocyte Spheroid Culture on a Polydimethylsiloxane Chip Having Microcavities. *Journal of Biomaterial Science Polymer Edition* **2006**, 17, (8), 859-873.
108. Tekin, H.; Anaya, M.; Brigham, M. D.; Nauman, C.; Langer, R.; Khademhosseini, A., Stimuli-responsive Microwells for Formation and Retrieval of Cell Aggregates. *Lab on a Chip* **2010**, 10, 2411-2418.
109. Torisawa, Y. S.; Mosadegh, B.; Cavnar, S. P.; Ho, M.; Takayama, S., Transwells with Microstamped Membranes Produce Micropatterned Two-Dimensional and Three-Dimensional Co-Cultures. *Tissue Engineering Part C* **2011**, 17, (1), 61-67.
110. Ota, H.; Yamamoto, R.; Deguchi, K.; Tanaka, Y.; Kazoe, Y.; Sato, Y.; Miki, N., Three-dimensional Spheroid-forming Lab-on-a-chip Using Micro-rotational Flow. *Sensors and Actuators B* **2010**, 147, 359-365.
111. Reed, J. A.; Lucero, A. E.; Cooperstein, M. A.; Canavan, H. E., The Effect of Cell Culture Parameters on Cell Release Kinetics from Thermoresponsive Surfaces. *Journal of Applied Biomaterials & Biomechanics* **2008**, 6, (2), 81-88.
112. Takezawa, T.; Mori, Y.; Yoshizato, K., Cell-Culture on a Thermoresponsive Polymer Surface. *Bio-Technology* **1990**, 8, (9), 854-856.
113. Nishida, K.; Yamato, M.; Hayashida, Y.; Watanabe, K.; Yamamoto, K.; Adachi, E.; Nagai, S.; Kikuchi, A.; Maeda, N.; Watanabe, H.; Okano, T.; Tano, Y., Corneal Reconstruction with Tissue-engineered Cell Sheets Composed of Autologous Oral Mucosal Epithelium. *New England Journal of Medicine* **2004**, 351, (12), 1187-1196.
114. Shimizu, T.; Yamato, M.; Isoi, Y.; Akutsu, T.; Setomaru, T.; Abe, K.; Kikuchi, A.; Umezu, M.; Okano, T., Fabrication of Pulsatile Cardiac Tissue Grafts Using a Novel 3-dimensional Cell Sheet Manipulation Technique and Temperature-responsive Cell Culture Surfaces. *Circulation Research* **2002**, 90,

(3), E40-E48.

115. Yamazaki, M.; Tsuchida, M.; Kobayashi, K. Y.; Takezawa, T.; Mori, Y., A Novel Method to Prepare Multicellular Spheroids from Varied Cell-Types. *Biotechnology and Bioengineering* **1995**, 48, (1), 17-24.

116. Ueno, K.; Miyashita, A.; Endoh, K.; Takezawa, T.; Yamazaki, M.; Mori, Y.; Satoh, T., Formation of Multicellular Spheroids Composed of Rat Hepatocytes. *Research Communications in Chemical Pathology and Pharmacology* **1992**, 77, (1), 107-120.

117. Endoh, K.; Ueno, K.; Miyashita, A.; Satoh, T., Size-regulation and Biochemical Activities of the Multicellulare Spheroid Composed of Rat-liver Cells. *Research Communications in Chemical Pathology and Pharmacology* **1994**, 83, (3), 317-327.

118. Reed, J. A.; Lucero, A. E.; Hu, S.; Ista, L. K.; Bore, M. T.; Lopez, G. P.; Canavan, H. E., A Low-Cost, Rapid Deposition Method for "Smart" Films: Applications in Mammalian Cell Release. *Acs Applied Materials & Interfaces* **2010**, 2, (4), 1048-1051.

119. Reed, J. A.; Love, S. A.; Lucero, A. E.; Haynes, C. L.; Canavan, H. E., Effect of Polymer Deposition Method on Thermoresponsive Polymer Films and Resulting Cellular Behavior. *Langmuir* **2011**, accepted.

120. Reed, J. A.; Bluestein, B. M.; Canavan, H. E., Effect of Substrate Storage Conditions on the Stability of "Smart" Films Used for Mammalian Cell Applications. *Biomacromolecules* **2011**, submitted.

121. Akiyama, Y.; Kikuchi, A.; Yamato, M.; Okano, T., Ultrathin poly(*N*-isopropylacrylamide) Grafted Layer on Polystyrene Surfaces for Cell Adhesion/Detachment Control. *Langmuir* **2004**, 20, (13), 5506-5511.

122. Cheng, X. H.; Canavan, H. E.; Stein, M. J.; Hull, J. R.; Kveskin, S. J.; Wagner, M. S.; Somorjai, G. A.; Castner, D. G.; Ratner, B. D., Surface Chemical and Mechanical Properties of Plasma-polymerized *N*-isopropylacrylamide. *Langmuir* **2005**, 21, (17), 7833-7841.

123. Pan, Y. V.; Wesley, R. A.; Luginbuhl, R.; Denton, D. D.; Ratner, B. D., Plasma polymerized *N*-isopropylacrylamide: Synthesis and characterization of a smart thermally responsive coating. *Biomacromolecules* **2001**, 2, (1), 32-36.

124. Lucero, A. E. Construction and Characterization of an RF Reactor to Create Plasma Polymerized Thermoresponse Coatings. University of New Mexico, Albuquerque, 2009.

125. Lucero, A. E.; Reed, J. A.; Wu, X.; Canavan, H. E., Fabrication and Characterization of Thermoresponsive Films Deposited by an RF Plasma

Reactor. *Plasma Processes and Polymers* **2010**, 7, (12), 992-1000.

126. Kwon, O. H.; Kikuchi, A.; Yamato, M.; Okano, T., Accelerated Cell Sheet Recovery of Co-grafting of PEG with PIPAAm onto Porous Cell Culture Membranes. *Biomaterials* **2003**, 24, 1223-1232.

127. Garcia, I. L. Polymer Nanofibers: Future Multifunctional Wound Dressing. <http://nanotech.askewmind.com/nanomaterials/polymer-nanofibres-future-multifunctional-wound-dressing/>

128. Cicotte, K. N.; Hedberg-Dirk, E. L.; Dirk, S. M., Synthesis and Electrospun Fiber Mats of Low Tg Poly(propylene fumarate-co-propylene maleate). *Journal of Applied Polymer Science* **2010**, 117, 1984-1991.

129. Shah, R. K.; Kim, J.-W.; Agresti, J. J.; Weitz, D. A.; C., L.-Y., Fabrication of Monodisperse Thermosensitive Microgel and Gel Capsules in Microfluidic Devices. *Soft Matter* **2008**, 4, 2303-2309.

130. Escamilla, R.; Huerta, L., X-ray Photoelectron Spectroscopy Studies of Non-stoichiometric Superconducting NbB_{2+x}. *Superconductor Science & Technology* **2006**, 19, (6), 623-628.

131. Hesse, R.; Chasse, T.; Streubel, P.; Szargan, R., Error Estimation in Peak-shape Analysis of XPS Core-level Spectra using UNIFIT 2003: How Significant are the Results of Peak Fits? *Surface and Interface Analysis* **2004**, 36, (10), 1373-1383.

132. Ratner, B. D.; Castner, D. G., *Electron Spectroscopy for Chemical Analysis*. John Wiley and Sons: Chichester, 1997; p 43-98.

133. Kubo, T.; Fujiwara, S.; Nanao, H.; Minami, I.; Mori, S., TOF-SIMS Analysis of Boundary Films Derived from Calcium Sulfonates. *Tribology Letters* **2006**, 23, (2), 171-176.

134. Artyushkova, K.; Fulghum, J. E., Multivariate Image Analysis Methods Applied to XPS Imaging Data Sets. *Surface and Interface Analysis* **2002**, 33, 185-195.

135. Pei, L.; Jiang, G.; Tyler, B. J.; Baxter, L. L.; Linford, M. R., Time-of-Flight Secondary Ion Mass Spectrometry of a Range of Coal Samples: A Chemometrics (PCA, Cluster, and PLS) Analysis. *Energy Fuels* **2008**, 22, (2), 1059-1072.

136. Cicotte, K. N.; Reed, J. A.; DeLora, J. A.; Canavan, H. E.; Hedberg-Dirk, E. L., Electrospinning pNIPAM for Mammalian Cell Culture Applications. *Journal of Biomedical Materials Research* **2011**, in preparation for submission.

137. Heskins, M.; Guillet, J. E., Solution Properties of Poly(*N*-isopropyl

- acrylamide). *Journal of Macromolecular Science, Part A* **1968**, 2, (8), 1441-1445.
138. Cheng, X. H.; Canavan, H. E.; Graham, D. J.; Castner, D. G.; Ratner, B. D., Temperature Dependent Activity and Structure of Adsorbed Proteins on Plasma Polymerized *N*-isopropyl acrylamide. *Biointerphases* **2006**, 1, (1), 61-72.
139. Okano, T.; Yamada, N.; Okuhara, M.; Sakai, H.; Sakurai, Y., Mechanism of Cell Detachment from Temperature-modulated, Hydrophilic-hydrophobic Polymer Surfaces. *Biomaterials* **1995**, 16, (4), 297-303.
140. Kikuchi, A.; Okuhara, M.; Karikusa, F.; Sakurai, Y.; Okano, T., Two-dimensional Manipulation of Confluently Cultured Vascular Endothelial Cells Using Temperature-responsive poly(*N*-isopropylacrylamide)-grafted Surfaces. *Journal of Biomaterials Science-Polymer Edition* **1998**, 9, 1331-1348.
141. Nandkumar, M. A.; Yamato, M.; Kushida, A.; Konno, C.; Hirose, M.; Kikuchi, A.; Okano, T., Two-dimensional Cell Sheet Manipulation of Heterotypically Co-cultured Lung Cells Utilized Temperature-responsive Culture Dishes Results in Long-term Maintenance of Differentiated Epithelial Cell Functions. *Biomaterials* **2002**, 23, 1121-1130.
142. Rollason, G.; Davies, J. E.; Sefton, M. V., Preliminary-report on Cell-culture on a Thermally Reversible Copolymer. *Biomaterials* **1993**, 14, 153-155.
143. Ito, Y.; Chen, G. P.; Guan, Y. Q.; Imanishi, Y., Patterned Immobilization of Thermoresponsive Polymer. *Langmuir* **1997**, 13, 2756-2759.
144. Ista, L. K.; Mendez, S.; Perez-Luna, V. H.; Lopez, G. P., Synthesis of poly(*N*-isopropylacrylamide) on Initiator-modified Self-assembled Monolayers. *Langmuir* **2001**, 17, 2552-2555.
145. Rao, G. V.; Lopez, G. P., Encapsulation of Poly(*N*-isopropyl acrylamide) in Silica: A Stimuli-responsive Porous Hybrid Material that Incorporates Molecular Nano-valves. *Advanced Materials* **2000**, 12, (22), 1692-1695.
146. Rao, G. V. R.; Krug, M. E.; Balamurugan, S.; Xu, H. F.; Xu, Q.; Lopez, G. P., Synthesis and Characterization of Silica-poly(*N*-isopropylacrylamide) Hybrid Membranes: Switchable Molecular Filters. *Chemistry of Materials* **2002**, 14, (12), 5075-5080.
147. Hybbinette, S.; Bostrom, M.; Lindberg, K., Enzymatic Dissociation of Keratinocytes from Human Skin Biopsies for in vitro Cell Propagation. *Experimental Dermatology* **1999**, 8, 30-38.
148. Tokiwa, T.; Hoshika, T.; Shiraishi, M.; Sato, J., Mechanism of Cell-dissociation with Trypsin and EDTA. *Acta Medica Okayama* **1979**, 33, 1-4.
149. Riikonen, T.; Vihinen, P.; Potila, M.; Rettig, W.; Heino, J., Antibody Against

Human Alpha-1-beta-1 Integrin Inhibits HeLa-cell Adhesion to Laminin and to Type-I, Type-IV, and Type-V Collagens. *Biochemical and Biophysical Research Communications* **1995**, 209, 205-212.

150. Shimizu, Y.; Mobley, J. L., Distinct Divalent-cation Requirements for Integrin-mediated CD4+ T-lymphocyte Adhesion to Icam-1, Fibronectin, Vcam-1, and Invasin. *Journal of Immunology* **1993**, 151, 4106-4115.

151. Ista, L. K.; Perez-Luna, V. H.; Lopez, G. P., Surface-grafted, Environmentally Sensitive Polymers for Biofilm Release. *Applied and Environmental Microbiology* **1999**, 65, (4), 1603-1609.

152. Cunliffe, D.; Alarcon, C. D.; Peters, V.; Smith, J. R.; Alexander, C., Thermoresponsive Surface-grafted poly(*N*-isopropylacrylamide) Copolymers: Effect of Phase Transitions on Protein and Bacterial Attachment. *Langmuir* **2003**, 19, (7), 2888-2899.

153. Okajima, S.; Sakai, Y.; Yamaguchi, T., Development of a Regenerable Cell Culture System that Senses and Releases Dead Cells. *Langmuir* **2005**, 21, (9), 4043-4049.

154. Miyagawa, S.; Sawa, Y.; Sakakida, S.; Taketani, S.; Kondoh, H.; Memon, I. A.; Imanishi, Y.; Shimizu, T.; Okano, T.; Matsuda, H., Tissue Cardiomyoplasty using Bioengineered Contractile Cardiomyocyte Sheets to Repair Damaged Myocardium: Their Integration with Recipient Myocardium. *Transplantation* **2005**, 80, (11), 1586-1595.

155. Chiantore, O.; Guaita, M.; Trossarelli, L., Solution Properties of Poly(*N*-Isopropylacrylamide). *Makromolekulare Chemie-Macromolecular Chemistry and Physics* **1979**, 180, (4), 969-973.

156. Kubota, K.; Fujishige, S.; Ando, I., Single-Chain Transition of Poly(*N*-Isopropylacrylamide) in Water. *Journal of Physical Chemistry* **1990**, 94, (12), 5154-5158.

157. Winnik, F. M.; Ringsdorf, H.; Venzmer, J., Methanol Water as a Co-Nonsolvent System for Poly(*N*-Isopropylacrylamide). *Macromolecules* **1990**, 23, (8), 2415-2416.

158. Otake, K.; Inomata, H.; Konno, M.; Saito, S., Thermal-Analysis of the Volume Phase-Transition with *N*-Isopropylacrylamide Gels. *Macromolecules* **1990**, 23, (1), 283-289.

159. Priest, J. H.; Murray, S. L.; Nelson, R. J.; Hoffman, A. S., Lower Critical Solution Temperatures of Aqueous Copolymers of *N*-Isopropylacrylamide and Other *N*-Substituted Acrylamides. *Acs Symposium Series* **1987**, 350, 255-264.

160. Matyjaszewski, K.; Xia, J. H., Atom Transfer Radical Polymerization.

Chemical Reviews **2001**, 101, (9), 2921-2990.

161. Angiolini, L.; Benelli, T.; Giorgini, L.; Paris, F.; Salatelli, E.; Fontana, M. P.; Camorani, P., Synthesis by ATRP and Effects of Molecular Weight on Photomechanical Properties of Liquid Crystalline Polymers Containing Side-chain Azobenzene Chromophores. *European Polymer Journal* **2008**, 44, (10), 3231-3238.

162. Hennink, W. E.; van Nostrum, C. F., Novel Crosslinking Methods to Design Hydrogels. *Advanced Drug Delivery Reviews* **2002**, 54, (1), 13-36.

163. Takezawa, T.; Yamazaki, M.; Mori, Y.; Yonaha, T.; Yoshizato, K., Morphological and Immuno-cytochemical Characterization of a Hetero-spheroid Composed of Fibroblasts and Hepatocytes. *Journal of Cell Science* **1992**, 101, 495-501.

164. Kanazawa, H.; Yamamoto, K.; Matsushima, Y.; Takai, N.; Kikuchi, A.; Sakurai, Y.; Okano, T., Temperature-responsive Chromatography using Poly(*N*-isopropylacrylamide)-modified Silica. *Analytical Chemistry* **1996**, 68, (1), 100-105.

165. Mizutani, A.; Kikuchi, A.; Yamato, M.; Kanazawa, H.; Okano, T., Preparation of Thermoresponsive Polymer Brush Surfaces and Their Interaction with Cells. *Biomaterials* **2008**, 29, (13), 2073-2081.

166. Da Silva, R. M. P.; Mano, J. F.; Reis, R. L., Smart Thermoresponsive Coatings and Surfaces for Tissue Engineering: Switching Cell-material Boundaries. *Trends in Biotechnology* **2007**, 25, (12), 577-583.

167. Reed, J. A.; Love, S. A.; Lucero, A. E.; Haynes, C. L.; Canavan, H. E., Effect of Polymer Deposition Method on Thermoresponsive Polymer Films and Resulting Cellular Behavior. *Langmuir* **2011**, submitted.

168. Yang, B.; Yang, W., Thermo-sensitive Membranes Regulated by Pore-covering Polymer Brushes. *Journal of Membrane Science* **2003**, 218, 247-255.

169. Yim, H.; Kent, M. S.; Mendez, S.; Lopez, G. P.; Satija, S.; Seo, Y., Effects of Grafting Density and Molecular Weight on the Temperature-dependent Conformational Change of poly(*N*-isopropylacrylamide) Grafted Chains in Water. *Macromolecules* **2006**, 39, (9), 3420-3426.

170. Lu, X. J.; Zhang, L. F.; Meng, L. Z.; Liu, Y. H., Synthesis of poly(*N*-isopropylacrylamide) by ATRP Using a Fluorescein-based Initiator. *Polymer Bulletin* **2007**, 59, (2), 195-206.

171. Davenport, S. G., *Anatomy and Physiology Laboratory Workbook*. 1st ed.; Link Publishing: 2006.

172. Bisht, H. S.; Manickam, D. S.; You, Y. Z.; Oupicky, D., Temperature-controlled Properties of DNA Complexes with poly(ethylenimine)-graft-poly(*N*-isopropylacrylamide). *Biomacromolecules* **2006**, 7, (4), 1169-1178.
173. Cheng, H.; Zhu, J. L.; Sun, Y. X.; Cheng, S. X.; Zhang, X. Z.; Zhuo, R. X., Novel Thermoresponsive Nonviral Gene Vector: P(NIPAAm-co-NDAPM)-b-PEI with Adjustable Gene Transfection Efficiency. *Bioconjugate Chemistry* **2008**, 19, (7), 1368-1374.
174. Francis, M. F.; Dhara, G.; Winnik, F. M.; Leroux, J. C., In Vitro Evaluation of pH-sensitive Polymer/niosome Complexes. *Biomacromolecules* **2001**, 2, (3), 741-749.
175. Hsiue, G. H.; Chang, R. W.; Wang, C. H.; Lee, S. H., Development of In Situ Thermosensitive Drug Vehicles for Glaucoma Therapy. *Biomaterials* **2003**, 24, (13), 2423-2430.
176. Hsiue, G. H.; Hsu, S. H.; Yang, C. C.; Lee, S. H.; Yang, I. K., Preparation of Controlled Release Ophthalmic Drops, for Glaucoma Therapy Using Thermosensitive poly-*N*-isopropylacrylamide. *Biomaterials* **2002**, 23, (2), 457-462.
177. Le Garrec, D.; Taillefer, J.; Van Lier, J. E.; Lenaerts, V.; Leroux, J. C., Optimizing pH-responsive Polymeric Micelles for Drug Delivery in a Cancer Photodynamic Therapy Model. *Journal of Drug Targeting* **2002**, 10, (5), 429-437.
178. Li, Y. Y.; Zhang, X. Z.; Zhu, J. L.; Cheng, H.; Cheng, S. X.; Zhuo, R. X., Self-assembled, Thermoresponsive Micelles Based on Triblock PMMA-b-PNIPAAm-b-PMMA Copolymer for Drug Delivery. *Nanotechnology* **2007**, 18, (21).
179. Lu, H. F.; Targonsky, E. D.; Wheeler, M. B.; Cheng, Y. L., Thermally Induced Gelable Polymer Networks for Living Cell Encapsulation. *Biotechnology and Bioengineering* **2007**, 96, (1), 146-155.
180. Matsumaru, Y.; Hyodo, A.; Nose, T.; Ito, S.; Hirano, T.; Ohashi, S., Application of Thermosensitive Polymers as a New Embolic Material for Intravascular Neurosurgery. *Journal of Biomaterials Science-Polymer Edition* **1996**, 7, (9), 795-804.
181. Ozyurek, Z.; Komber, H.; Gramm, S.; Schmaljohann, D.; Muller, A. H. E.; Voit, B., Thermoresponsive Glycopolymers via Controlled Radical Polymerization. *Macromolecular Chemistry and Physics* **2007**, 208, (10), 1035-1049.
182. Qin, J.; Jo, Y. S.; Ihm, J. E.; Kim, D. K.; Muhammed, M., Thermosensitive Nanospheres with a Gold Layer Revealed as Low-cytotoxic Drug Vehicles. *Langmuir* **2005**, 21, (20), 9346-9351.

183. Reddy, T. T.; Kano, A.; Maruyama, A.; Hadano, M.; Takahara, A., Thermosensitive Transparent Semi-interpenetrating Polymer Networks for Wound Dressing and Cell Adhesion Control. *Biomacromolecules* **2008**, 9, (4), 1313-1321.
184. Vihola, H.; Laukkanen, A.; Valtola, L.; Tenhu, H.; Hirvonen, J., Cytotoxicity of Thermosensitive Polymers poly(*N*-isopropylacrylamide), poly(*N*-vinylcaprolactam) and Amphiphilically Modified poly(*N*-vinylcaprolactam). *Biomaterials* **2005**, 26, (16), 3055-3064.
185. Wadajkar, A. S.; Koppolu, B.; Rahimi, M.; Nguyen, K. T., Cytotoxic Evaluation of *N*-isopropylacrylamide Monomers and Temperature-sensitive poly(*N*-isopropylacrylamide) Nanoparticles. *Journal of Nanoparticle Research* **2009**, 11, (6), 1375-1382.
186. Zhang, H. L.; Iwama, M.; Akaike, T.; Urry, D. W.; Pattanaik, A.; Parker, T. M.; Konishi, I.; Nikaido, T., Human Amniotic Cell Sheet Harvest Using a Novel Temperature-responsive Culture Surface Coated with Protein-based Polymer. *Tissue Engineering* **2006**, 12, (2), 391-401.
187. Zintchenko, A.; Ogris, M.; Wagner, E., Temperature Dependent Gene Expression Induced by PNIPAM-based Copolymers: Potential of Hyperthermia in Gene Transfer. *Bioconjugate Chemistry* **2006**, 17, (3), 766-772.
188. Senden, R. J.; De Jean, P.; McAuley, K. B.; Schreiner, L. J., Polymer Gel Dosimeters with Reduced Toxicity: A Preliminary Investigation of the NMR and Optical Dose-response Using Different Monomers. *Physics in Medicine and Biology* **2006**, 51, (14), 3301-3314.
189. Fu, Q.; Rao, G. V. R.; Ward, T. L.; Lu, Y. F.; Lopez, G. P., Thermoresponsive Transport Through Ordered Mesoporous Silica/PNIPAAm Copolymer Membranes and Microspheres. *Langmuir* **2007**, 23, (1), 170-174.
190. Timmer, M. D.; Shin, H.; Horch, R. A.; Ambrose, C. G.; Mikos, A. G., In Vitro Cytotoxicity of Injectable Biodegradable poly(propylene fumarate)-based networks: Unreacted Macromers, Cross-linked Networks, and Degradation Products. *Biomacromolecules* **2003**, 4, 1026-1033.
191. Nisbet, D. R.; Forsythe, J. S.; Shen, W.; Finkelstein, D. I.; Horne, M. K., A Review of the Cellular Response on Electrospun Nanofibers for Tissue Engineering. *Journal of Biomaterials Applications* **2009**, 24, (7), 7-29.
192. Okuzaki, H.; Kobayashi, K.; Yan, H., Non-woven Fabric of Poly(*N*-isopropyl acrylamide) Nanofibers Fabricated by Electrospinning. *Synthetic Metals* **2009**, 159, 2273-2276.
193. Cui, W.; Zhou, Y.; Chang, J., Electrospun Nanofiberous Materials for Tissue Engineering and Drug Delivery. *Science and Technology of Advanced*

Materials **2010**, 11, 014108.

194. Rockwood, D. N.; Chase, D. B.; Akins, R. E.; Rabolt, J. F., Characterization of Electrospun Poly(*N*-isopropyl acrylamide) Fibers. *Polymer* **2008**, 49, 4025-4032.

195. Bjerkvig, R., *Spheroid Culture in Cancer Research*. CRC Press, Inc: Boca Raton, FL, 1992; p 334.

196. Joseph, N.; Prasad, T.; Raj, V.; Kumar, P. R.; Sreenivasan, K.; Kumary, T. V., A Cytocompatible Poly(*N*-isopropylacrylamide-co-glycidylmethacrylate) Coated Surface as New Substrate for Corneal Tissue Engineering. *Journal of Bioactive and Compatible Polymers* **2010**, 25, (1), 58-74.

197. Meenach, S. A.; Anderson, A. A.; Suthar, M.; Anderson, K. W.; Hilt, J. Z., Biocompatibility Analysis of Magnetic Hydrogel Nanocomposites Based on Poly(*N*-isopropylacrylamide) and Iron Oxide. *Journal of Biomedical Materials Research Part A* **2009**, 91A, (3), 903-909.

198. Park, J. Y.; Takayama, S.; Lee, S. H., Regulating Microenvironmental Stimuli for Stem Cells and Cancer Cells Using Microsystems. *Integrative Biology* **2010**, 2, 229-240.

199. Selimovic, S.; Sim, W. Y.; Kim, S. B.; Jang, Y. H.; Lee, W. G.; Khabiry, M.; Bae, H.; Jambovane, S.; Hong, J. W.; Khademhosseini, A., Generating Nonlinear Concentration Gradients in Microfluidic Devices for Cell Studies. *Analytical Chemistry* **2011**, 83, (6), 2020-2028.

200. Wang, J. H.; Lin, J. S., Cell Traction Force and Measurement Methods. *Biomechanics and Modeling in Mechanobiology* **2007**, 6, (6), 361-371.

201. Okano, T.; Yamada, N.; Sakai, H.; Sakurai, Y., A Novel Recovery-system for Cultured-cell using Plasma-treated Polystyrene Dishes Grafted with Poly(*N*-isopropylacrylamide). *Journal of Biomedical Materials Research* **1993**, 27, (10), 1243-1251.

202. Panayiotou, M.; Freitag, R., Influence of the Synthesis Conditions and Ionic Additives on the Swelling Behaviour of Thermoresponsive Polyalkylacrylamide Hydrogels. *Stimuli Responsive Polymers* **2005**, 46, (18), 6777-6785.

203. Yamazaki, M.; Tsuchida, M.; Kobayashi, K. Y.; Takezawa, T.; Mori, Y., A Novel Method to Prepare Size-Regulated Spheroids Composed of Human Dermal Fibroblasts. *Biotechnology and Bioengineering* **1994**, 44, (1), 38-44.

204. Park, K. H.; Bae, Y. H., Phenotype of Hepatocyte Spheroids in Arg-Gly-Asp (RGD) Containing a Thermo-reversible Extracellular Matrix. *Bioscience, Biotechnology, and Biochemistry* **2002**, 66, (7), 1473-1478.